University of Nevada, Reno

Novel sampling and modeling approaches for studying soils during and after wildfires

A thesis submitted in partial fulfillment of the requirements for the degree of
Master of Science in Natural Resources and Environmental Science

by

Mary K. Brady

Dr. Erin J. Hanan/Thesis Advisor

May 2021

THE GRADUATE SCHOOL

We recommend that the thesis
prepared under our supervision by

Mary K. Brady

entitled

Novel sampling and modeling approaches for studying soils during and after wildfires

be accepted in partial fulfillment of the
requirements for the degree of

Master of Science

Erin Hanan, Ph.D.
Advisor

Dr. Jonathan Greenberg, Ph.D.
Committee Member

Dr. Neil Lareau, Ph.D.
Graduate School Representative

David W. Zeh, Ph.D., Dean
Graduate School

May, 2021

Abstract

Wildfire transforms soil physical, chemical, and biological properties. These changes are integral soil processes in fire-prone terrestrial ecosystems around the world. Although methods for estimating fire energy and impacts aboveground have progressed in recent decades, there remain major challenges in characterizing soil heating and associated effects belowground. Overcoming these challenges is crucial for understanding how fire influences soil carbon storage, biogeochemical cycling, and ecosystem recovery after fires.

The work in chapter one explores nitrogen (N) cycling in soils from a case study on the Walker Fire in Northern California, 2019. Previous work has shown that N cycling is transformed by fire but variability in the magnitude and direction of those changes makes generalizing between and within fires challenging. These studies are often complicated by the lack of prefire samples and verified control areas that did not burn. In this case study, I analyzed N cycling in samples from immediately prefire, immediately postfire, and up to nine months after the fire, in both burned and control areas. The burned sampling locations ranged from low to extreme severity. I found that in this system, fire severity and soil moisture interact to control levels of N cycling and availability. These synergistic effects would have been difficult to discern with traditional sampling designs that rely on postfire measurements and space-for-time substitutions to approximate prefire conditions because of the uncertainties inherent from spatial heterogeneity. This work increases our understanding of factors driving N cycling in Sierra Nevada forests and suggests that, when possible, this sampling design should be employed to study future fires.

Chapter two proposes a model for soil heating during wildfires. Previous work has shown that the extent and duration of soil heating determines the immediate fire effects on soils. However, measuring soil temperatures during fires is logistically complicated. The resulting dearth of temperature data makes elucidating mechanisms and direct relationships between heating and fire effects challenging. In this chapter, I describe and validate a new field method,

called iStakes, that addresses many of the current constraints in measuring soil temperatures. I also explain and validate a modelling framework I designed, called SheFire, which can predict soil temperature over time across soil depths during wildfires. The modeling framework also includes functions to summarize soil heating in a variety of manners and extends soil heating to biological impacts with functions that model soil organism survival at different soil depths. I use data from a case study to demonstrate the utility of iStakes and SheFire. This field method and model make studying the direct effects of fire on soil more streamlined and will help researchers characterize belowground processes that are transformed by fire.

Acknowledgments

I would like to thank my advisor Dr. Erin Hanan for her continuous patience and guidance. I would also like to thank my collaborators Dr. Matthew Dickinson and Dr. Jessica Miesel without whom this project could not have happened. My committee members, Dr. Jonathan Greenberg and Dr. Neil Lareau, provided valuable advice and feedback throughout this work. I would also like to acknowledge Dr. Paul Verberg for his assistance using the LiCOR without which I could not have measured soil microbial biomass. Many thanks to all the people that contributed their time to help me in field and the laboratory. Thank you to all who made this work possible.

Table of Contents

List of Tables

Chapter 1

Chapter 2

List of Figures

Chapter 1

Chapter 2

I. Introduction to thesis research

1. Wildfire and soil

Fire is a key factor shaping the composition and structure of vegetation and soils in semi-arid forests and shrublands (Knelman et al. 2015, Alcañiz et al. 2018). It is well established that wildfires can transform soil biological, chemical, and physical properties which are critical to the functioning of all terrestrial ecosystems (e.g., Giovannini et al. 1990, Neary et al. 1999, Badía-Villas et al. 2014, Doerr et al. 2017). Although fire effects on soil biogeochemistry have been recorded for decades, few generalizations can be made across ecosystems (e.g., Neary et al. 2005, Certini 2005, Hanan et al. 2016, Alcañiz et al. 2018).

It is challenging to generalize how soil properties are transformed by fire because these responses vary with fire severity, preexisting soil characteristics, and time since fire. Therefore, to understand how future fires will influence ecosystem processes, we must consider all these factors, ideally through pre- and postfire samples collected at high temporal resolution. However, doing so can be challenging, in part because access to unplanned wildfires is strictly controlled for safety reasons and prescribed fires, although planned far in advance, are often conducted on short notice.

In the first chapter of my thesis, I use a novel dataset to explore shifts in soil nitrogen (N) cycling following an unplanned wildfire. The dataset includes samples that were collected immediately before and after wildfire, as well as one and a half, six, and nine months later. The areas sampled range from unburned to extreme burn severity. This dataset provides a novel opportunity to analyze the immediate and seasonal changes in N availability and cycling following fire across a range of fire severities.

Even with datasets such as this, it is challenging to extrapolate from one fire to another, or even from one area of a fire to another area due to the high variability in fire behavior and spatially complex soil properties prefire (Ste-Marie and Paré 1999, Busse et al. 2013, Morgan et

al. 2014). Using soil temperatures during fires in a dose-response framework is one possible path to developing a generalizable understanding of how fires transform soils. Linking belowground temperatures to changes in soil properties and processes would provide a more direct link between the fire and its effects on soils than relying on fire severity, assessed through aboveground changes in vegetation. Unfortunately, recording soil temperatures during fires is logistically challenging to implement at a fine spatial scale across soil depth.

In the second chapter of my thesis, I addressed these challenges by developing a new model, Soil Heating in Fire (SheFire), that uses minimal input data collected in the field to predict soil temperature during and after fire, across a range of soil depths. I also explain a new data collection method, iStakes, that eases many of the current constraints on collecting soil temperature data during wildfires.

2. Summary of themes discussed in each chapter

2.1. Effects of wildfire and seasonal changes on N cycling using a novel sampling design

In this chapter, I quantified a variety of soil physical, chemical, and biological processes for soil samples collected immediately before and after wildfire in the Sierra Nevada, as well as seasonally over the first year of recovery. This novel sampling design included locations that did not burn, and locations that burned at varying levels of burn severity – a categorization based on above ground changes to vegetation and soil surface. The novel combination of immediate pre- and postfire sampling, and subsequent seasonal sampling under a range of burn severities enabled me to explore nitrogen cycling at a temporal resolution that is rarely possible with wildfires. It is well established that fires are a key driver of N cycling in fire-prone systems, but the magnitude of those changes can vary substantially with fire severity and time since fire. This variability makes it difficult to predict how fire will influence ecosystem processes. Effects from low severity fires in particular are challenging to predict because in some cases their effects are very

short-lived. However, as fire frequencies increase in many landscapes across the western U.S. (Westerling et al. 2006), these short-term changes may play a larger role in ecosystem N cycling and availability. This study provides a nuanced look at a single fire and how it transformed N cycling across a range of fire severities, at timescales ranging from days to months following fire.

As expected, fire generally enhanced rates of N cycling and N availability. However, the exact changes varied in response to both fire severity and seasonal fluctuations in soil moisture. Areas of higher severity experienced increases in N cycling and availability but N availability crashed after extended periods of high soil water content. Low severity areas did not experience as extreme increases in N availability and cycling but sustained moderately increased levels through periods of high soil water content. Fire effects lasted longer with increasing fire severity, while the areas that did not burn had little to no measurable available nitrogen or nitrogen cycling, regardless of the soil water content.

The sampling design used in this study helped elucidate ephemeral changes in soil biogeochemistry after the fire that would not have been caught without immediate pre- and postfire sampling. While the changes in areas of higher severity fire can last for extended periods of time, this study demonstrates that to understand low severity fires in particular, or the peak changes in higher severity areas, requires studying fires on a temporal scale of days to months, not months to years as has been the case in most previous studies.

2.2. Soil Heating in Fire (SheFire): a model and measurement method for estimating soil heating across depths over time, and belowground responses in wildland fires

The direct impacts of fire on soil occur as a result of the extent and duration of soil heating. However, these data can be challenging to collect on a fine enough temporal and spatial scale to be useful for predicting fire effects or even to compare heating across soil depths. To address this problem, I developed a model in R, called Soil Heating in Fire (SheFire), that predicts soil

heating through time across soil depths. In addition to the model fitting function, the SheFire R package also includes a series of functions that summarize soil heating in variety of manners and a series of response functions that extend the model's predictive scope beyond only soil temperature to include predicted survival for soil organisms. I also tested a new method for collecting soil temperature data, which uses easy to deploy ibutton sensors placed at different soil depths using a wooden stake (i.e., an iStake), rather than thermocouple probes with attached data loggers.

To validate the SheFire model, I designed an experiment that compared predicted temperatures against temperatures recorded at specific depths. Additionally, to demonstrate that the new iStake data collection method is a viable way to record data comparable with traditional methods, I benchmarked ibutton measurements against thermocouple measurements from paired sets of sensors exposed to the same soil heating. I also compared the SheFire model results from each paired set of sensors.

I found that SheFire makes skillful temperature predictions across a range of soil depths. The summary functions provide a variety of ways to compare soil heating across locations, times, and soil depths. The survival response functions, which use temperature and thermal tolerance data to predict organism, tissue, or protein survival over time at a given depth, extend the utility of SheFire to include biological responses to soil heating. SheFire is a powerful tool to help explore soil heating during fires and its direct effects.

For the novel data collection method for recording soil temperatures during fire, I found that iStake recorded temperatures were comparable to those recorded by thermocouples, suggesting that results from studies using thermocouples and studies using ibuttons can reasonably be compared or aggregated. There is no cause for concern that the different sensor types result in sufficiently different temperature readings that they cannot both be used. The

streamlined design of the iStakes offers a viable alternative to time and labor-intensive thermocouple deployment.

The application of iStakes and SheFire to case study data demonstrated the utility of both the field method and the model. The iStakes provided useful soil temperature data from the experimental plots. SheFire was fitted using the data from the iStakes and supplied a valuable way to quantitatively compare the soil heating between plots and predict survival for various organisms and plant tissues in the soil.

Works Cited

Alcañiz, M., L. Outeiro, M. Francos, and X. Úbeda. 2018. Effects of prescribed fires on soil properties: A review. Science of The Total Environment 613–614:944–957.

Badía-Villas, D., J. A. González-Pérez, J. M. Aznar, B. Arjona-Gracia, and C. Martí-Dalmau. 2014. Changes in water repellency, aggregation and organic matter of a mollic horizon burned in laboratory: Soil depth affected by fire. Geoderma 213:400–407.

Busse, M. D., C. J. Shestak, and K. R. Hubbert. 2013. Soil heating during burning of forest slash piles and wood piles. International Journal of Wildland Fire 22:786–796.

Certini, G. 2005. Effects of fire on properties of forest soils: a review. Oecologia 143:1–10.

Doerr, S., C. Santin, J. Reardon, J. Mataix-Solera, C. Stoof, R. Bryant, J. Miesel, and D. Badia. 2017. Soil heating during wildfires and prescribed burns: a global evaluation based on existing and new data 19:17957.

Giovannini, C., S. Lucchesi, and M. Giachetti. 1990. Effects of Heating on Some Chemical Parameters Related to Soil Fertility and Plant Growth. Soil Science 149:344–350.

Hanan, E. J., J. P. Schimel, K. Dowdy, and C. M. D'Antonio. 2016. Effects of substrate supply, pH, and char on net nitrogen mineralization and nitrification along a wildfire-structured age gradient in chaparral. Soil Biology and Biochemistry 95:87–99.

Knelman, J. E., E. B. Graham, N. A. Trahan, S. K. Schmidt, and D. R. Nemergut. 2015. Fire severity shapes plant colonization effects on bacterial community structure, microbial biomass, and soil enzyme activity in secondary succession of a burned forest. Soil Biology and Biochemistry 90:161–168.

Morgan, P., R. E. Keane, G. K. Dillon, T. B. Jain, A. T. Hudak, E. C. Karau, P. G. Sikkink, Z. A. Holden, and E. K. Strand. 2014. Challenges of assessing fire and burn severity using field measures, remote sensing and modelling. International Journal of Wildland Fire 23:1045–1060.

Neary, D. G., C. C. Klopatek, L. F. DeBano, and P. F. Ffolliott. 1999. Fire effects on belowground sustainability: a review and synthesis. Forest Ecology and Management 122:51–71.

Neary, D. G., K. C. Ryan, and L. F. DeBano. 2005. Wildland fire in ecosystems: effects of fire on soils and water. Gen. Tech. Rep. RMRS-GTR-42-vol.4. Ogden, UT: U.S. Department of Agriculture, Forest Service, Rocky Mountain Research Station. 250 p. 042.

Ste-Marie, C., and D. Paré. 1999. Soil, pH and N availability effects on net nitrification in the forest floors of a range of boreal forest stands. Soil Biology and Biochemistry 31:1579–1589.

Westerling, A. L., H. G. Hidalgo, D. R. Cayan, and T. W. Swetnam. 2006. Warming and Earlier Spring Increase Western U.S. Forest Wildfire Activity. Science 313:940–943.

II. Chapter One

Quantifying how wildfire and seasonal fluctuations in the soil environment influence nitrogen cycling using novel timeseries sampling

Mary K. Brady[1], Erin J. Hanan[1], Matthew B. Dickinson[2], Jessica R. Miesel[3], Laura Wade[1], Jonathan Greenberg[1]

[1]Department of Natural Resources and Environmental Science, University of Nevada - Reno, Reno, Nevada, USA

[2]US Forest Service, Northern Research Station, Delaware, Ohio, 43015, USA

[3]Department of Plant, Soil and Microbial Sciences, Michigan State University, East Lansing, Michigan, USA

Abstract

As wildfires become more frequent and severe, it grows increasingly important to understand how they will affect the biogeochemical processes influencing ecosystem recovery. Soil nitrogen (N) cycling is a key process constraining plant productivity and N losses from fire. However, the short-term effects of fire on N cycling, on the scale of days to months, are often overlooked in favor of longer-term studies that examine rates months to decades after fire. This knowledge gap results in part from the fact that many studies rely on space-for-time substitutions to understand fire effects, which generate uncertainty because of differences among sites representing different postfire ages. In addition to these uncertainties, the longer-term focus can limit our ability to quantify shorter-term fire effects, especially for low severity fires, which often have ephemeral responses on N cycling compared to more severe fires. To assess shorter-term N cycling following this fire, this study uses a novel dataset to quantify forest net mineralization and net nitrification rates during the first year of recovery following a wildfire that burned in the Northern Sierra Nevada. Our dataset leverages immediate prefire, immediate postfire, and seasonal soil

samples collected along a gradient of fire severities, including sites that burned at low, high, and extreme severity as well as sites that did not burn in this fire.

We found that immediately after fire, soil pH increased for all severities, but the magnitude and duration of the effect increased with increasing severity. Microbial biomass increased in locations that burned at high severity but decreased in locations that burned at low severity. These differences diminished over time as microbial biomass in the burned sampling sites slowly converged on the control sampling site levels. Nitrogen cycling was affected by both burn severity and soil moisture. Generally, higher burn severity increased net mineralization rates, but they decreased after extended periods with high soil moisture. Low severity samples had lower rates of net mineralization than high severity locations, but they were able to maintain those rates even after periods of high soil moisture. Samples collected from locations that did not burn had the lowest rates of net mineralization. These results suggest that burn severity and seasonal precipitation patterns interact to drive N cycling and availability following this fire. We also found that this sampling design was necessary to help elucidate some of the soil changes postfire and posit mechanisms for differences we observed between severity categories.

1. Introduction

Wildfires shape coniferous forests across the western USA through their effects on forest structure, species composition, and soil chemistry (e.g., Knelman et al. 2015, Alcañiz et al. 2018). Although fire effects on soil chemistry have been recorded for decades, the magnitude and direction of responses can vary, particularly when it comes to nitrogen (N; e.g., Neary et al. 2005, Certini 2005, Hanan et al. 2016b, Alcañiz et al. 2018). However, two trends stand out as particularly robust: increases in pH and increases in net mineralization and nitrification rates following fire. These increases occur across biomes, from forests to savannas, and their magnitude generally grows with burn severity (e.g., Tester 1989, DeLuca et al. 2006, Verma and Jayakumar 2012, Alcañiz et al. 2018, Kranz and Whitman 2019). Other important, although more variable effects of combustion include fluctuations in microbial biomass, and changes in soil moisture and water availability.

There are several interconnected processes that influence N mineralization and nitrification rates after fire. Fire deposits ash and char on soil surfaces, which is rich in ammonium (NH_4^+) and readily decomposable organic N. Ash also contains base-forming cations that can increase soil pH, and fire behavior can further amplify pH increases by destroying organic acids in surface soils (Hanan et al. 2016b). Elevated soil pH increases the ammonia to ammonium ratio in soils (pKa = 10) and because nitrifying bacteria and archaea use ammonia substrate, nitrification increases with higher pH (Prosser 1990, De Boer and Kowalchuk 2001, Hanan et al. 2016b). However, other factors can moderate or counteract increases in N availability. For example, readily decomposable organic materials that are deposited on soil surfaces with ash can stimulate heterotrophic microbial biomass. Increases in microbial biomass, in turn, have been linked with N immobilization in a variety of N-limited ecosystems (Aoyama and Nozawa 1993, Gallardo and Schlesinger 1995). The amount and composition of fire created ash and char can influence which mechanisms dominate, mineralization and nitrification of N or

immobilization by biomass (DeLuca et al. 2006, Hanan et al. 2016b). Additionally, even though fire typically increases immediate N availability, it also oxidizes, volatilizes, and transports large amounts of N away from burned ecosystems, which over longer timescales can reduce the substrate available to heterotrophic microbes and nitrifying bacteria. As a result, N losses due to combustion during the fire and from postfire leaching can outstrip the short term increases in N availability in some areas (Murphy et al. 2006a, Verma and Jayakumar 2012, Alcañiz et al. 2018).

Burn severity can be a key indicator of how these fire and soil processes interact with one another and which dominate in a given location (Neary et al. 1999, González-Pérez et al. 2004, Knicker 2007, Knelman et al. 2015, Whitman et al. 2019). Burn severity is a measure of the extent to which an ecosystem has been transformed by fire (mainly vegetation and surface soils). It can provide a convenient approach for indirectly categorizing how a fire's energy dissipation and residence time has affected an ecosystem, since direct fire characteristics are not as easy to measure across large spatial scales. Energy release rates and totals (which correlate with severity) influence how much ash and char may be deposited, the degree of forest floor combustion, the presence and depth of hydrophobic soil layers, which, along with other factors including plant survival, can change postfire N availability, hydrology, and resulting N losses through leaching. There are both ground-based and remote-sensing approaches to determining severity but, in both cases, as an indirect indicator of fire energy, it is imperfect for quantifying the direct effects of heating belowground (Smith et al. 2016).

Postfire N cycling is regulated by a suite of interacting soil characteristics including soil water content, pH, and microbial biomass (Aoyama and Nozawa 1993, Gallardo and Schlesinger 1995, De Boer and Kowalchuk 2001, Hanan et al. 2016b). In addition to changing how N cycles internally, fires can deposit N rich ash and char on soil surfaces, while simultaneously volatilizing, oxidizing, and transporting N out of a system (DeLuca et al. 2006, Hanan et al. 2016b). Because of varying inputs, outputs, and internal cycling the magnitude of N fluxes can

vary with changes in burn severity (González-Pérez et al. 2004, Knicker 2007, Knelman et al. 2015, Whitman et al. 2019). However, it is extremely challenging to directly link or model relationships between burn severity and belowground N cycling because wildfires are complex and rarely provide an opportunity to compare homologous burned and unburned areas.

Despite the importance of quantifying fire induced transformations for understanding how they affect postfire N dynamics, few studies on wildfires have true prefire samples and instead rely on space-for-time substitutions, which increase uncertainty in a variety of ways. For one, soil properties can vary at fine spatial scales (e.g., less than 30 m; (Campbell 1978, Ste-Marie and Paré 1999, Morgan et al. 2014). Therefore, temporal differences in N cycling that are gleaned from chronosequence measurements (e.g., recently burned, young, and mature stands) can be confounded with spatial differences among stands. The problem is highlighted by studies that have found site heterogeneity has a strong effect on soil processes postfire, sometime even stronger than the fire itself (Santos et al. 2019, Kranz and Whitman 2019). Other studies rely on opportunistic prefire samples, which were initially intended for another use before a study area unexpectedly burned (e.g., Murphy et al. 2006b). However, in many cases, these samples may have been collected weeks, months, or even years before the fire, which can lead to confounding between fire effects and the effects of other environmental drivers such as weather and hydrology, which can change over that time.

In addition to the difficulties with reliable prefire sampling, sampling immediately after wildfire is challenging because of safety constraints and access limitations. As a result, many studies rely on longer postfire time intervals to explore soil biogeochemical changes. The first postfire sampling may not occur until weeks or months after fire, even in the case of prescribed burns (e.g., Stephens et al. 2004, Weber et al. 2014, Kranz and Whitman 2019). Ephemeral changes that occur immediately after fire can be missed if there is a delay in post-fire sampling. However, these ephemeral changes may still influence ecosystem N budgets and postfire

recovery trajectories, particularly in low severity burns, which may have compounding effects as fire frequency is increasing in many ecosystems globally (Pellegrini et al. 2021).

This case study uses a unique sampling approach to circumvent many of the challenges and uncertainties associated with space-for-time substitutions and long time-lags between pre- and postfire sampling. We studied the Walker Fire, which burned in Plumas National Forest, CA in 2019, by sampling within three days before and after the fire, as well as one and a half months, six months, and nine months after fire. We sampled sites that did not burn in the Walker Fire (hereafter referred to as control sites), and sites that burned at low, high, and extreme severity. We measured soil characteristics including pH, microbial biomass, total C:N ratios, fractional water content, NH_4^+, NO_3^-, and net mineralization and nitrification rates to address two questions: (1) how does N cycling change with burn severity in the first year following this fire? And (2) does this sampling design provide unique data to advance methodology for future research, or are long-term studies sufficient?

2. Methods

Traditional fire studies frequently use space-for-time substitutions at one or multiple fires to estimate fire effects over time. In contrast, our study uses repeated sampling through time from before and after one fire in both areas that did and did not burn in this fire (Fig. 1).

2.1. Site and Fire Description

The northern Sierra Nevada experiences a Mediterranean climate and sees more than half of its annual precipitation in January, February, and March when much of it falls as snow (Wagtendonk et al. 2018). Summer precipitation, when it occurs, often comes as afternoon thunderstorms. Average summer high temperatures are approximately 25 °C and winter high temperatures are approximately -5 °C. The portion of Plumas National Forest included in this study is a *Pinus ponderosa* dominated ecosystem with some *Calocedrus decurren*s and occasionally other lower

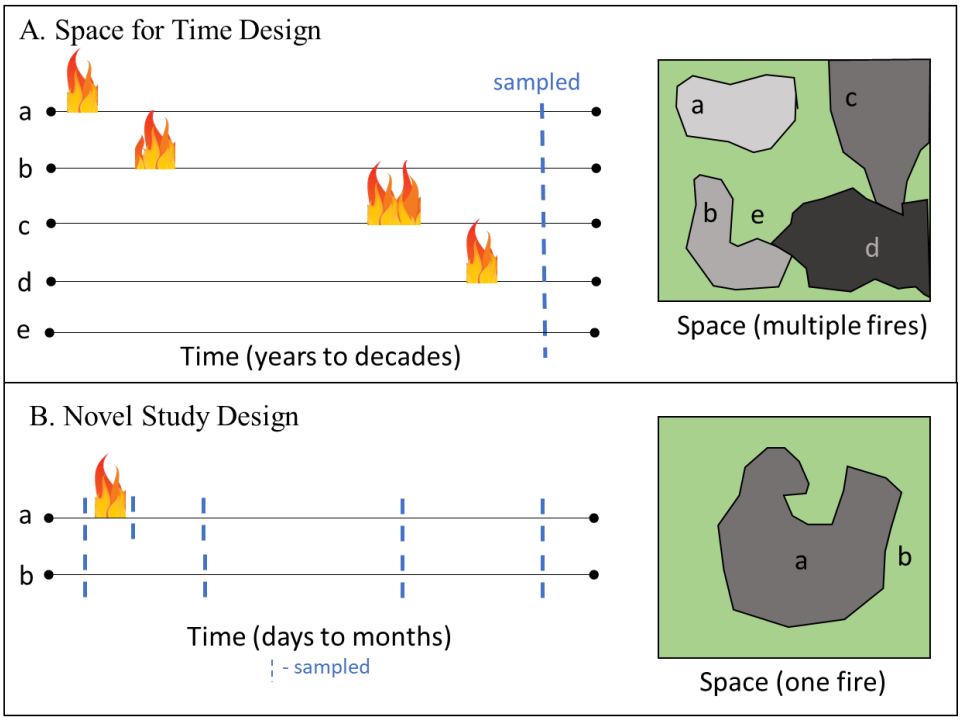

Figure 1. Conceptual diagram comparing A. space for time study designs frequently used to study fire effects and B. the novel study design with repeated sampling at high temporal resolution on one fire used in this research.

montane conifers such as *Pinus lambertiana* (Wagtendonk et al. 2018). Understory vegetation is typically grass and forb dominated with few shrubs. Annual precipitation is approximately 125 cm. The soils are either sandy, mixed, frigid Entic Xerumbrepts (for plots 2 and 3 described below), mixed, frigid Dystric Xeropsamments (for plots 4, 5, and 8), or clayey, smectitic, frigid, shallow Typic Argixerolls (for plots 7 and 9; NRCS and UC Davis 2020). Elevations of sampling locations in this study range from 1650 m to 1700 m above sea level. The local topography at sampling locations is ridges divided by valleys often containing small streams. Site aspect varies and slope ranges from <5° to 17°.

The Walker Fire burned in Plumas National Forest, California in September 2019. It burned approximately 55,000 acres over the course of 12 days, September 4 - 15 (Fig. 2; Dickinson et al. 2019). The fire was actively fought but continued to spread until the morning of

September 16th when there were heavy rains. Fuels, topography, as well as recent fire and management history varied across the area burned. Details can be found in Dickinson et al. 2019.

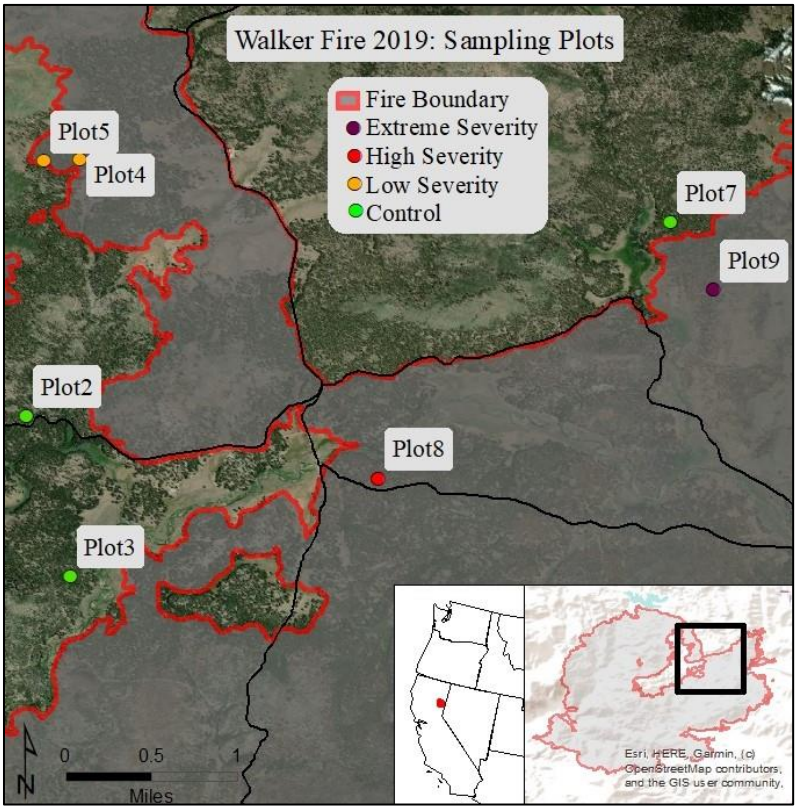

Figure 2. A map showing the plot locations and fire perimeter in the vicinity of Murdoch Crossing Spring. Coordinates for the southwest corner of each plot are given in supplementary Table S1.

2.2 Sampling Design

While the fire was active, the US Forest Service Fire Behavior Assessment Team (FBAT) sampled eight plots prior to fire arrival at those sites. The plot size, 30 m by 30 m, was established for vegetation and fuel surveys in a complimentary study (Greenberg, unpublished). The plots were selected by FBAT members working with the incident command team based on ease of access and a high likelihood of burning within a few days. Plots 4, 5, and 8 burned before rain and burnout operations establishing containment ended active spread (Figure 1; Dickinson et al. 2019). Plots 4 and 5 burned in a surface fire while plot 8 burned in an intense surface fire with

isolated torching. Plot 5 was burned incompletely as rain started to fall. Plots 1, 2, 3, 6, and 7 did not burn (Fig. 2). Plots 1 and 6 were not resampled so they have been excluded from this analysis. For the sake of continuity with the FBAT datasets and report (Dickinson et al. 2019), we did not renumber the plots after removing plots 1 and 6.

We visually assessed burn severity at the plot level based on changes to aboveground vegetation and the forest floor layer of soil. Severity categories were modified slightly from (Turner et al. 2007, Weber et al. 2014) such that complete tree mortality and forest floor combustion was considered high severity while little to no charring on tree boles and incomplete forest floor combustion was considered low severity (Fig. 3). Moderate severity was anything in between those two extremes. Plots 4 and 5 burned at low severity, no plots burned at moderate severity, and plot 8 burned at high severity. Plots 2, 3, and 7 did not burn and will be referred to as control locations.

An additional plot (plot 9) was added in the spring following the fire to have more robust sampling in the high severity category. Plot 9 was set up to be consistent with the size, relative sampling locations, and orientations of the other plots. However, analysis of these samples and continued observation of these sampling locations indicated that the sampling locations in plot 9 were too dissimilar from the high severity locations in plot 8 to reasonably combine the data. They are kept separate in all analyses. Tree mortality in plot 8 was 100% and resulted in postfire needle fall from the trees that did not experience foliage consumption (Fig. 3). Around Plot 8, some trees survived through the study period. Plot 9 had total tree mortality but no postfire needle fall because the canopy needles were entirely consumed in the fire (Fig. 3). While both meet the definition set *a priori* for high severity, for the sake of clarity, the plot 8 sampling locations are called high severity and the plot 9 sampling locations are called extreme severity due to the crown foliage combustion. These two categories are roughly equivalent to severe surface fire and crown fire as described in Turner et al. 2007.

Soil samples were collected in the northeast, southeast, and southwest corners of each plot except for one of the unburned plots which was always sampled in the center of the plot instead of the southeast corner. The precise sampling locations were recorded so that each time a location was re-sampled, the sample was within 1 m of the original, prefire sample but did not overlap with any previous sampling. Plot level data on land-use history, fuel loading, and stand assessments can be found in supplementary tables S2-4.

We chose to focus on mineral soils for these analyses because forest floor consumption was inconsistent, ranging from no combustion in the control locations to almost completely consumed in the high severity sampling locations (which had high forest floor material loadings prefire). The extreme severity sampling locations had no intact forest floor when they were sampled at six and nine months postfire, although there was some ash and char in places. At each sampling location, fifteen 3.5 cm diameter by 5 cm deep mineral soil cores were collected from within a 30 cm diameter ring. Soil samples were brought back to the laboratory for analysis.

Figure 3. From left to right: a low severity, high severity, and extreme severity sampling location. All three photos were taken in June 2020, nine months after the fire.

2.2.1 Field sampling timeline

Prefire and immediate postfire samples were collected over the course of one week. All prefire sampling, in locations that did and did not burn, occurred over the course of four days and

for the locations that burned in this fire, no more than four days prior to fire arrival. Immediately postfire samples were collected within three days of the sampling location burning. Samples were then collected at one and a half months, six months, and nine months postfire at the burned and unburned locations. Samples were kept cool and brough back to the laboratory for immediate processing and analysis.

Table 1. Plots and number of sampling locations per burn severity category and at each sampling event. The sampling timeline covers immediately prefire through nine months after the fire.

Severity category	Plots	Immediately prefire	Immediately postfire	1.5 mo. postfire	6 mo. postfire	9 mo. postfire
Control	2, 3, 7	9	0	9	9	9
Low Severity	4, 5	6	6	6	6	6
High Severity	8	3	3	3	3	3
Extreme Severity	9	0	0	0	3	3

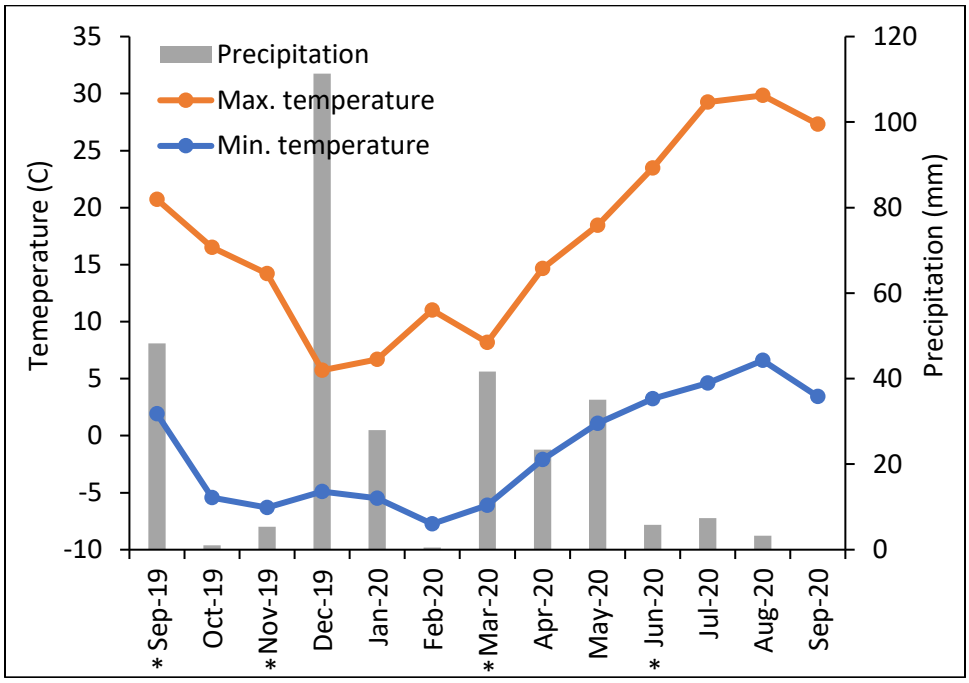

Figure 4. The monthly precipitation and mean maximum and minimum air temperatures from the Coyote, CA Remote Access Weather Station ("RAWS USA Climate Archive" 2020). The timeline covers the Walker Fire (Sep. 2019) and the subsequent year. * indicates months when samples were collected.

Table 2. Sampling events for each soil characteristic. "X" indicates the soil characteristic was measured at the time point. C – control, LS – low severity locations, HS – high severity locations, ES – extreme severity locations.

	Prefire				Immediate Postfire				1.5 mo. Postfire				6 mo. Postfire				9 mo. Postfire			
	C	LS	HS	ES	C	LS	HS	ES	C	LS	HS	ES	C	LS	HS	ES	C	LS	HS	ES
Fractional Water Content	X	X	X			X	X		X	X	X		X	X	X	X	X	X	X	X
pH	X	X	X			X	X		X	X	X		X	X	X	X	X	X	X	X
Microbial Biomass	X	X	X			X	X		X	X	X		X	X	X	X	X	X	X	X
C:N ratio	X	X	X			X	X			X	X					X				X
Available NH_4^+	X	X	X			X	X		X	X	X		X	X	X	X	X	X	X	X
Available NO_3^-	X	X	X			X	X		X	X	X		X	X	X	X	X	X	X	X
Mineralization, Field Moist									X	X	X		X	X	X	X	X	X	X	X
Mineralization, Wetted Wk 1									X	X	X		X	X	X	X	X	X	X	X
Mineralization, Wetted Wk 3									X	X	X		X	X	X	X	X	X	X	X
Nitrification, Field Moist									X	X	X		X	X	X	X	X	X	X	X
Nitrification, Wetted Wk 1									X	X	X		X	X	X	X	X	X	X	X
Nitrification, Wetted Wk 3									X	X	X		X	X	X	X	X	X	X	X

2.3. Lab Analysis

In the laboratory, the mineral soils were run through a 4.7 mm sieve. The soil cores were homogenized by sampling location so that each subsample used for laboratory analysis would be equivalent.

We determined water-holding capacity and fractional water content by weighing 10 g field moist subsamples, then saturating them with water. We dried them at 58 °C for 48 hours. Water-holding capacity was calculated by subtracting the dry soil weight from the saturated weight then dividing by the dry weight. Fractional water content was determined by subtracting dry weight from field wet weight then dividing by field wet weight. Soil pH was measured by adding deionized water to 10 g field moist soil subsamples to create a 1:1 ratio slurry. We recorded pH using a standard electrode.

Microbial biomass was estimated using substrate induced respiration (SIR) in a method adapted from West and Sparling 1986. We used a 3 g glucose to 250 ml deionized water solution and added 1.667 mL of the glucose solution per gram dry weight to the soil subsamples. The CO2 levels were measured immediately after the glucose was added and again after a four-hour incubation. We measured the CO2 concentration in the headspace of the sealed jars by using a glass syringe to extract air samples through the rubber septa in the jar lids and then fed those samples through a LiCOR infrared gas analyzer. The change in CO2 concentration over the four hours was converted to µg carbon per gram of dry soil per hour. Microbial respiration is a reliable index that acts as a proxy for direct microbial biomass measurements (West and Sparling 1986, Beare et al. 1990, Bailey et al. 2002).

Total carbon (C) to N ratios were determined with an elemental analyzer using 0.015 g of ground, homogenized soil. The ratios were measured prefire, immediately postfire, and one and a half months postfire for the low severity and high severity samples. For the extreme severity sampling locations, total C:N ratios were measured at six and nine months postfire because they

were not sampled at the earlier time points. Total C:N in the control samples was only measured prefire because C:N ratios typically change on the scale of decades, not months, without a large disturbance (e.g., Schipper and Sparling 2011, Pellegrini et al. 2018).

In the lab, we incubated sets of soil subsamples, 10 g at field moist weight, for each sampling location. The field-moist incubation was one week long with no added water to approximate field moisture conditions. The second and third incubations, 1-week wetted and 3-week wetted, were incubated at 40 percent water holding capacity for one and three weeks, respectively. When field moisture was above 40 percent water holding capacity, no water was added to the wetted incubations and the soils were incubated at their field moisture. No incubations were conducted for the immediate pre- or postfire samples.

The field-moist incubations provide rates of net mineralization and nitrification at field moisture conditions. The rate from 1-week long wetted incubations provides clues about the soil microbial community composition by removing any water or hydrologic connectivity limitation. The rate for the 3-week long wetted incubations, compared with the 1-week wetted incubations, can provide insights into the population dynamics and resource availability by showing how a prolonged release from water related limitations can affect the NH_4^+ and NO_3^- cycling.

We determined available NH_4^+ and NO_3^- concentrations for all incubated and unincubated (time = 0) samples by extracting the soil samples in 2 M potassium chloride (KCl; 40 mL) for 2 hours then vacuum filtering through a glass fiber filter (Pall Gelmann Type A/E 1.0 lm). The extractants were measured using UV absorbance at 650 nm for NH_4^+ and 540 nm for NO_3^- with a plate reader to determine the amount of NH_4^+ and NO_3^- present. The NH_4^+ and NO_3^- values were adjusted to a µg per g dry soil basis for comparison across samples. Daily net N mineralization rates were calculated as the amount of inorganic N (NH_4^+ and NO_3^-) at the end of a given week minus the amount of inorganic N measured at the end of the week prior, divided by 7. Net nitrification rates were determined analogously but using only NO_3^- concentrations in the

calculation. For week one, the time zero extraction, immediately after collection in the field, was the starting value.

2.4. Statistical Approach

We used each sampling location as a replicate within the burn severity categories and we treated plot as a random effect, because (1) plots were randomly located within each severity level, (2) soil characteristics can vary significantly at distances smaller than the distance between our sampling locations (i.e., 30 m; Campbell 1978, Hudak et al. 2007, Morgan et al. 2014), and (3) plot had no significant effect on any of the soil characteristics we measured before the fire (Table 3). Due to the low sample size, we would not extrapolate these results to other locations, but this approach enables us to assess fire induced changes across burn severity categories on the Walker Fire and the utility of immediate sampling events before and after wildfires.

To examine the extent to which soil characteristics varied among locations that experienced different burn severities, we used linear mixed effects models. For each soil characteristic, we compared (1) between burn severity categories within a sampling event, (2) between sampling events within a burn severity category, and (3) to assessed interactions between burn severity and sampling events. We considered soil characteristic (i.e., pH, fractional water content, etc.) to be the response variable, while burn severity and sampling time were fixed effects and plot was a random effect. Extreme severity was not included in the third analysis due to the short sampling timeline at those sampling locations and the immediately postfire sampling event was excluded because the control sampling locations were not sampled at that time. We used an alpha of 0.1 to determine statistical significance in all analyses to offset the risk of type II errors due to low sample size.

All statistics were run in in R version 4.0.3 (R Core Team 2020), using the following packages: ggplot2 (Wickham 2016), nlme (Pinheiro et al. 2020), car (Fox and Weisberg 2019), lme4 (Bates et al. 2015 p. 4), RLRsim (Scheipl et al. 2008), and multcomp (Hothorn et al. 2008).

Due to the relatively small sample sizes, normality was assessed visually using histograms. Cases where residuals were not normal are marked in the data tables.

3. Results

3.1 Plot level differences

Soil characteristics did not vary significantly with plot before the fire (Table 3). Following fire, plot sometimes affected various soil characteristics, but significant effects were not consistent through time and were confounded with spatial patterns of the fire within the low severity category (Table 3).

	imm. prefire			imm. postfire	1.5 mo. postfire		6 mo. Postfire		9 mo. Postfire	
	All plots	Cont.	Low Sev.	Low Sev.	Cont.	Low Sev.	Cont.	Low Sev.	Cont.	Low Sev.
Water content	0.41	0.34	1.00	0.37	0.25	0.19	0.42	1.00	0.09	0.37
pH	0.42	1.00	1.00	0.24	0.36	0.34	0.02	<0.01	0.10	0.37
Microbial biomass	0.35	0.02	1.00	1.00	0.28	0.34	0.42	1.00	0.07	0.16
NH_4^+	0.34	0.42	1.00	0.36	0.02	0.29	0.42	<0.01	0.28	0.07
NO_3^-	0.31	1.00	NA	1.00	1.00	0.14	0.25	0.14	1.00	0.26

Table 3. P-values for restricted likelihood ratio tests (RLRT) of all prefire samples and the control (cont.) and low severity (low sev.) samples at all sampling events. Control locations were not sampled immediately postfire. Values less than 0.1 indicate that plot was significant for the soil characteristic. Value of 1 indicates that the RLRT statistic was equal to 0 – model fit with the null and alternative hypothesis were indistinguishable. NH_4^+ and NO_3^- refer to the available NH_4^+ and NO_3^- at the time of sample collection. "NA" indicates that all the sample values were 0.

3.1 Fractional water content

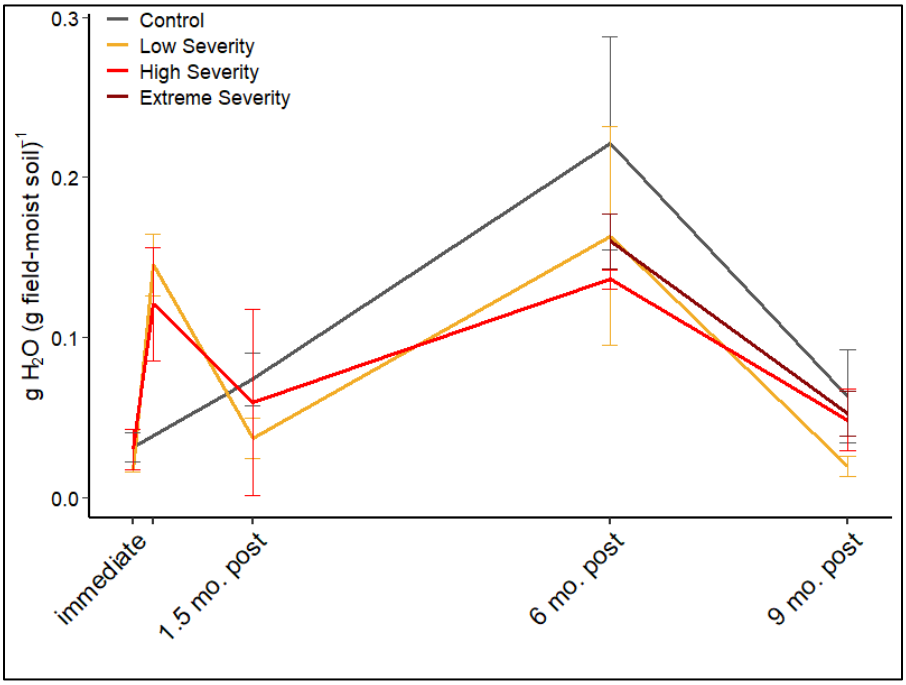

Figure 5. Fractional water content of field-moist soils from the four burn severity categories over time. The x axis is scaled to time. The two tick marks labeled "immediate" are immediately pre- and postfire samples. Control (unburned) sites were not sampled immediately postfire. Error bars show standard deviation within severity categories.

Sampling event had a significant effect on fractional water content (Table S2). Soil fractional water content changed seasonally and with the weather (Fig. 5; Table S9). Immediately postfire, low and high severity sampling locations had high fractional water content following the fire-ending rain. At six months postfire, during the spring thaw, all sampling locations had high soil water content. By nine months postfire, all sampling locations had dried (Fig. 5; Table 9).

3.2 pH

The time (sampling event)- severity interaction had a significant effect on soil pH (Table S2). Soil pH increased immediately after the fire in both low and high severity sampling locations (Fig. 6; Table S9). In high severity sampling locations, pH increased rapidly until one and a half months after the fire while low severity locations leveled off after the immediate postfire sampling event.

Extreme severity had the highest pH of all categories at six and nine months after the fire. The control sampling locations' pH changed less than any of the burned sites (Fig. 6; Table S9).

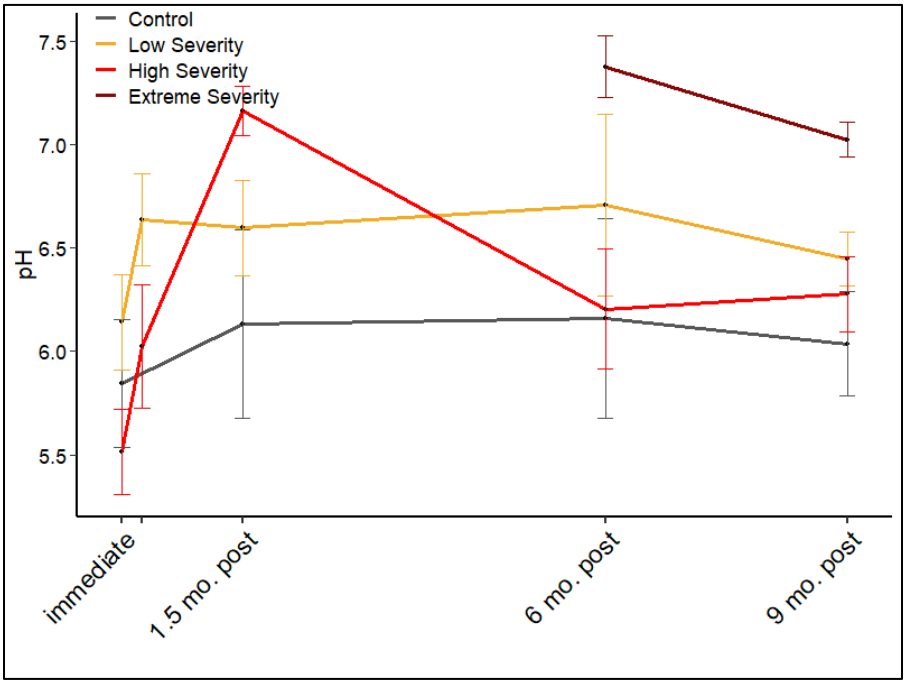

Figure 6. Soil pH values over time from the four burn severity categories. The x as=xis is scaled to time. The two tick marks labeled "immediate" are immediately pre- and postfire samples. Control (unburned) sites were not sampled immediately postfire. Error bars show standard deviation within severity categories.

3.3 Microbial biomass respiration

The time-severity interaction was significant for microbial biomass (Table S2). The control locations had minimal changes in microbial biomass after an initial decrease at one and half months after the fire. Microbial biomass had a non-monotonic response in the burned locations: immediately following fire, microbial biomass decreased in low severity sampling locations while it increased in high severity locations (Fig. 7; Table S9). It continued to increase in high severity locations up to one and a half months postfire then decreased through nine months postfire. After the initial decrease, microbial biomass in low severity locations increased slightly at one and half months postfire and then gradually decreased. At six and nine months after fire, extreme severity locations had the highest microbial biomass of any severity category (Fig. 7; Table S9).

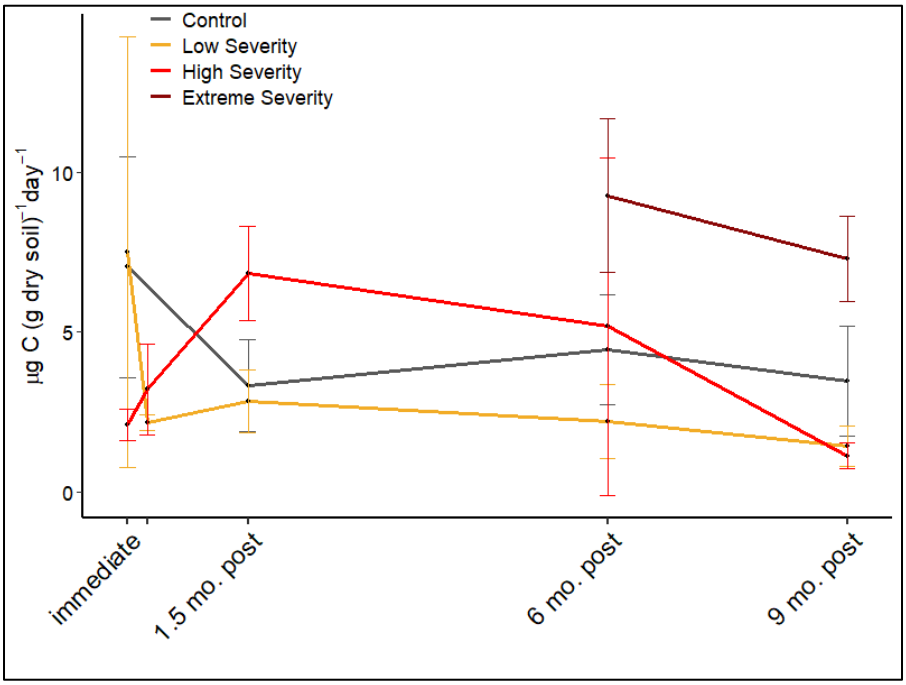

Figure 7. Microbial respiration (µg C per g dry soil per hour), an index for microbial biomass, for the burn severity categories. CO_2 was measured before and after a four-hour incubation with glucose to determine the respiration rate. The x axis is scaled to time. The two tick marks labeled "immediate" are immediately pre- and postfire samples. Control sites were not sampled immediately postfire. Error bars show standard deviation within category.

3.4 Total C:N ratio

Before fire, the control, low severity, and high severity sampling locations all had similar C:N ratios (Table 4). The high severity sampling locations had negligible change after the fire. The low severity sampling locations, on the other hand, decreased immediately after and then increased substantially at one and a half months after fire to more than double the prefire value. However, the variability was high. The C:N ratio had minimal change over that time and the values were lower than the other three severity categories (Table 4).

Table 4. Mean total C:N ratios and standard error for the four burn severity categories over time.

	Immediately Prefire		Immediately Postfire		1.5 mo. Postfire		6 mo. Postfire		9 mo. Postfire	
Severity	Mean	SE	Mean	SE	Mean	SE	Mean	SE	Mean	SE
Control	31.36	0.62	-	-	-	-	-	-	-	-
Low Sev.	40.79	1.03	26.93	0.88	82.89	11.13	-	-	-	-
High Sev.	38.06	2.51	38.29	2.53	35.92	2.66	-	-	-	-

Extreme Sev.	-	-	-	-	-	-	23.91	0.52	22.53	0.18

3.5 Available NH_4^+

The time-severity interaction was significant for available NH_4^+ (Table S2). The available NH_4^+ concentrations were nearly identical among sampling locations before the fire (Fig. 8; Table S9). Immediately after fire, high severity sampling locations had a greater than 40-fold increase, but they dropped by more than 15 µg per g of dry soil from that peak by one and half months after fire and declined only slightly after that. The control and low severity sampling locations had lower values than high severity at all sampling events after the fire. Although the low severity locations had an increase immediately after fire, available NH_4^+ concentrations differed only slightly from the control locations at all subsequent sampling events. Extreme severity had the highest values by a large margin at both six and nine months after fire, although it decreased from six to nine months after fire (Fig. 8; Table S9).

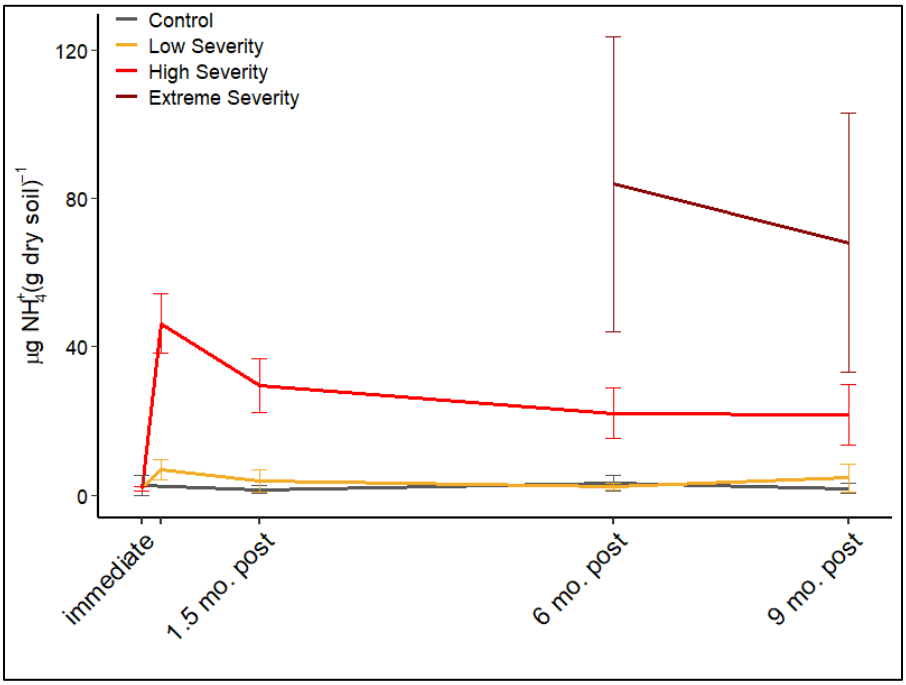

Figure 8. Amount of NH_4^+ per gram of dry soil for the four burn severity categories measured immediately after sample collection. The x axis is scaled to time. The two tick marks labeled "immediate" are immediately pre- and postfire samples. Control (unburned) sites were not sampled immediately postfire. Error bars show standard deviation within severity categories.

3.6 Available NO_3^-

Time, severity, and the time-severity interaction did not significantly affect available NO_3^- (Table S2). Before the fire, only the control locations had measurable NO_3^-, and even those concentrations were low (Fig. 9; Table S9). The control locations were only marginally above 0 at any sampling event. After the fire, low severity maintained the highest available NO_3^- concentrations except for extreme severity at nine months postfire, which had a concentration approximately 30 times higher than any other value. High severity sampling locations were nearly identical to the control locations except at six months after the fire when they had slightly higher available NO_3^- concentrations (Fig. 9; Table S9).

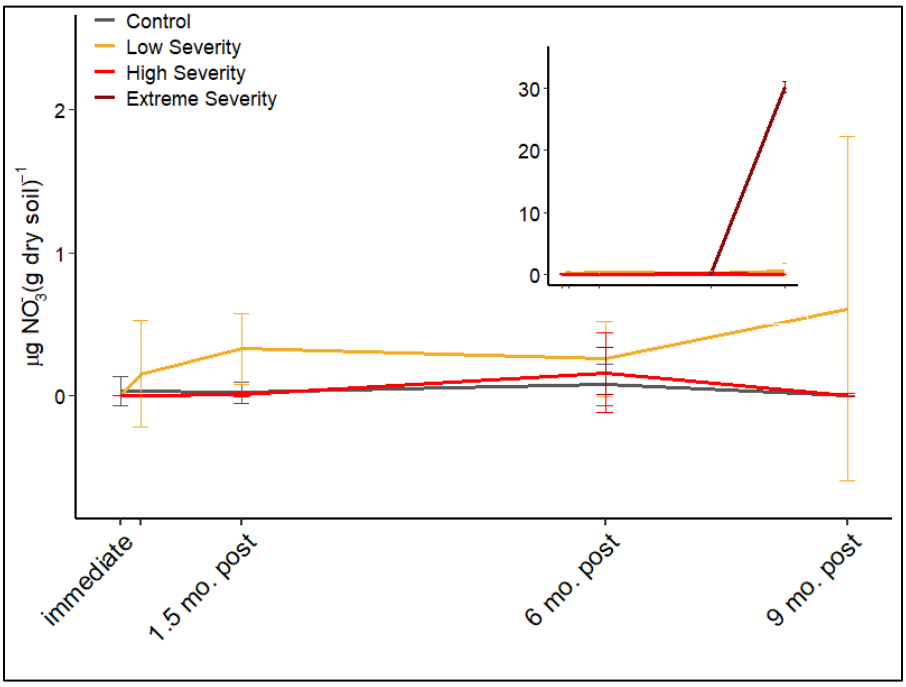

Figure 9. Amount of NO_3^- per g dry soil for the four burn severity categories measured immediately after sample collection. The inset plot shows the data with extreme severity at nine months postfire, the larger plot shows closer view of the data without that point. The x axis is scaled to time. The two tick marks labeled "immediate" are immediately pre- and postfire samples. Control (unburned) sites were not sampled immediately postfire. Error bars show standard deviation within severity categories.

3.7 Daily net mineralization rates

The time-severity interaction significantly influenced rates of net mineralization in the field-moist incubations (Table S2). The field-moist incubations for the control sampling locations had small, negative daily net mineralization rates but they did not substantially differ from zero at any sampling event (Fig. 10; Table S10). The low severity sampling were equivalent to the control locations except at one and half months when the low severity locations had rates slightly lower than control. The high severity locations, on the other hand, had substantially lower net mineralization rates in the field-moist incubations compared to the control and low severity sampling locations although the difference decrease over time as the high severity location rates slowly increased. Extreme severity sampling locations were the only locations to have positive net mineralization rates in the field-moist incubations (Fig. 10; Table S10).

The time-severity interaction significantly influenced the net mineralization rates in the 1-week wetted incubations (Table S2). Mineralization rates in the 1-week wetted incubations for the control locations did not change substantially over time (Fig. 10, Table S10). At one and a half months postfire, high severity sampling locations had the lowest daily net mineralization rate but increased at six months postfire to be roughly equivalent to the control locations and continued to increase through nine months postfire. Low severity soil samples had higher 1- week wetted net mineralization rates than the control locations until nine months postfire when it decreased to around the same rate as the control locations. Extreme severity sampling locations had the highest net mineralization rate for the 1-week wetted incubations at six months postfire but dropped precipitously at nine months postfire to the lowest rate, second only to high severity at one and a half months after the fire (Fig. 10; Table S10). However, rates were extremely variable in soils that burned at extreme severity, which makes robust comparisons challenging. For the 1-week wetted incubations, the daily net mineralization rates were generally higher than the field-moist incubation rates (Fig. 10; Table S10).

Severity significantly influenced the net mineralization rates for the 3-week wetted incubations (Table S2). The control sampling locations had daily net mineralization rates near zero at all points (Fig. 10, Table S10). At all three sampling events, the low severity locations had rates more than double the control rates. The high severity locations, on the other hand, had substantial negative net mineralization rates at all three sampling events with the lowest rate at one and a half months postfire and highest at nine months. The extreme severity sampling locations also had negative net mineralization at one and a half months but by nine months postfire, the extreme severity sampling locations had the highest net mineralization rate for the 3-week wetted incubations. However, net mineralization rates were extremely variable in soils that burned at extreme severity, which makes robust comparison challenging (Fig. 10; Table S10).

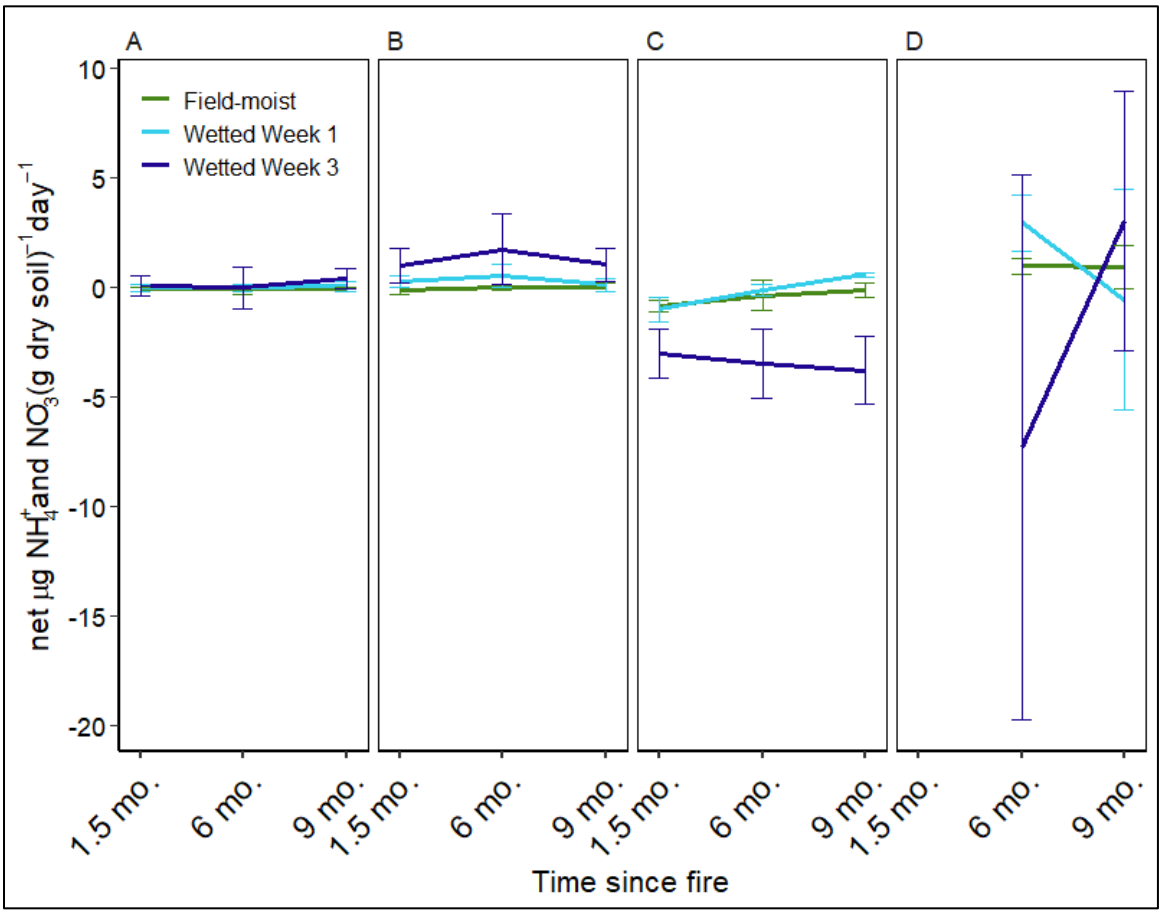

Figure 10. Mean net mineralization (µg NH_4^+ plus NO_3^-) per gram dry soil per day for the weeklong field moist incubations, the 1-week 40% water holding capacity incubations (wetted week one), and the three-

week 40% water holding capacity incubation (wetted week three) for the four burn severity categories. The error bars show standard deviation within the burn severity category. A. Control sampling locations, B. Low severity sampling locations, C. High severity sampling locations, and D. Extreme severity sampling locations.

3.8 Daily net nitrification rates

The time-severity interaction significantly influenced the field-moist incubation net nitrification rates (Table S2). The control sampling locations had no daily net nitrification for the field-moist incubations at one and a half and nine months after fire (Fig. 11; Table S10). At six months, the net nitrification rate was just slightly below zero. The low severity sampling locations had positive rates at one and half and six months postfire, with the highest rate at six months, and a slight negative rate at nine months. The high severity sampling locations had rates close to the control locations except at nine months postfire, when the high severity locations had a marginally higher net nitrification rate. The sampling locations that burned at extreme severity had the highest net nitrification rate for the field-moist incubations at six months postfire and the lowest rate at nine months after the fire (Fig. 11; Table S10).

Time, severity, and the time-severity interaction all were not significant for the 1-week wetted incubation net nitrification rates (Table S2). The control sampling locations had the lowest net nitrification rates for the 1-week wetted incubations: the rates were only slightly higher than zero at nine months after fire (Fig. 11; Table S10). The low severity sampling locations had net nitrification rates roughly five times higher than the control locations at all sampling events for the 1-week wetted incubations. High severity, by contrast, had net nitrification rates slightly lower than the control locations. The extreme severity sampling locations, at six months postfire, had the highest net nitrification rate, however the variability was high. At nine months postfire, the extreme severity sampling locations decrease net nitrification rates to nearly identical to the control location rates (Fig. 11; Table S10).

The time-severity interaction was significant for nitrification rates in the 3-week wetted incubation (Table S2). The control sampling locations had low net nitrification rates at one and a half and nine months postfire but had no net nitrification at six months (Fig. 11; Table S10). Low severity sampling locations had higher net nitrification rates than the control sampling locations at all three points. Both the control locations and low severity locations had their highest net nitrification rates at nine months after fire. The high severity sampling locations had lower rates for the 3-week wetted incubations than both the control and low severity sampling locations. The extreme severity sampling locations had the highest net nitrification rate at six months after the fire but the lowest rate at nine months postfire when the rate was negative (Fig. 11; Table S10).

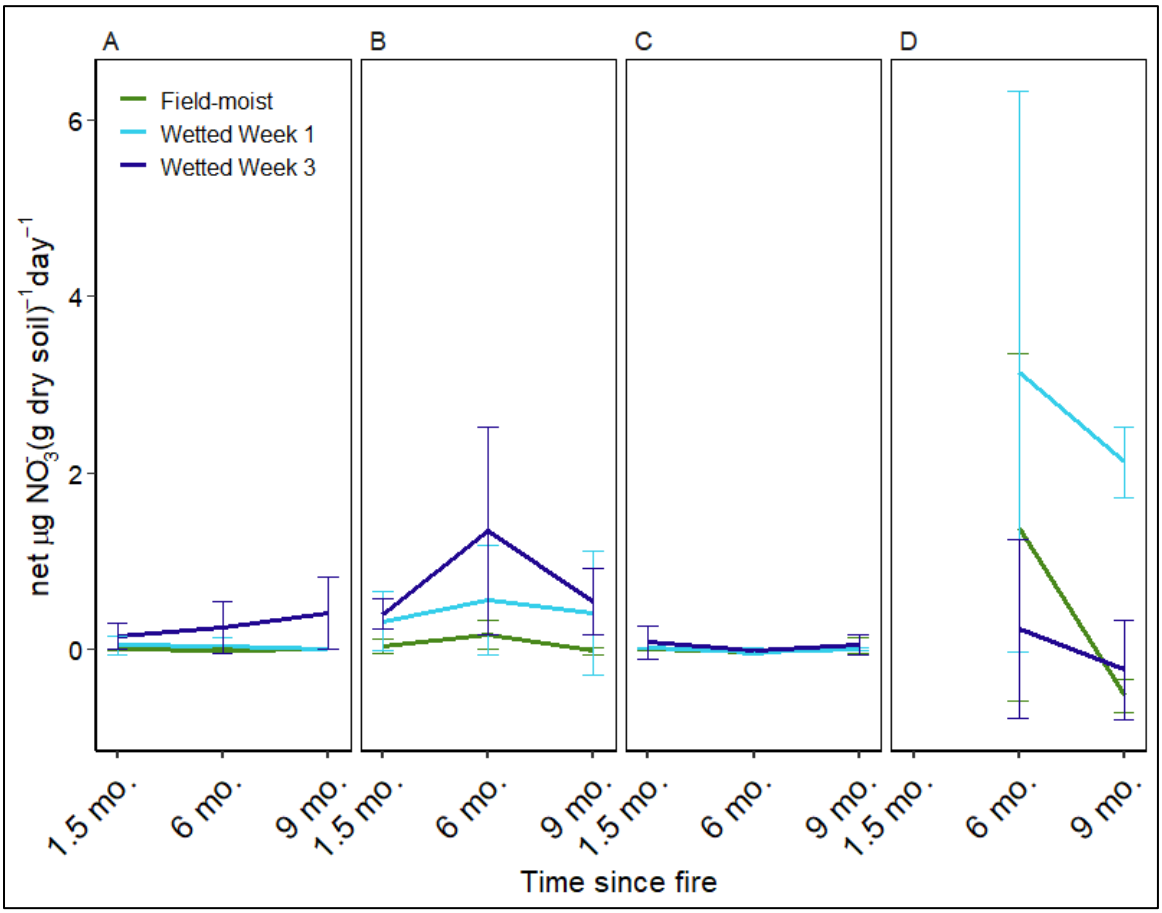

Figure 11. Mean net nitrification (µg NO_3^-) per gram of dry soil per day for the weeklong field-moist incubations, the weeklong 40% water holding capacity incubations (wetted week one), and the three-week long 40% water holding capacity incubation (wetted week three) for the four burn severity categories. The error bars show standard deviation. A. Control sampling locations, B. Low severity sampling locations, C. High severity sampling locations, and D. Extreme severity sampling locations.

4. Discussion

Our novel study design enabled us to examine the immediate and ongoing effects of wildfire on N cycling in a manner that has previously not been feasible. We found that soil water content and burn severity synergistically affect N cycling in this system. Most of the soil characteristics we studied were significantly affected by the burn severity-time interaction (Table S2). Several seasonal variables—such as temperature and plant phenology—can also affect soil properties (e.g., MacDonald et al. 1995, Sierra 1997, Ren et al. 2020). Here, we found that seasonal changes in soil water content play a critical role in postfire N cycling across a range of burn severities after fire. A key strength of this study is that we were able to discern the interactions of fire effects and seasonal effects by comparing burned and unburned sites with pre- and postfire samples collected immediately postfire and through different seasons. We found that N mineralization is enhanced during spring snowmelt in sampling locations that burned and the magnitude of those increases as well as the extent to which mineral N is nitrified is a function of burn severity.

Net Mineralization

We found net immobilization (negative net mineralization) of N in the control, low severity, and high severity sampling locations incubated at field-moist conditions at one and a half, six, and nine months after the fire (Fig. 10). The consistency between the areas that burned, and the control locations suggests that the limitation on net mineralization is not substrate because NH_4^+ is present after the fire in the burned sites (Fig. 10).

The exception to this general pattern is the extreme severity sampling locations which had positive net mineralization rates at field-moist conditions for both six and nine months after the fire (Fig. 10). The extreme severity location results imply that, at these sites, there is enough N rich substrate readily available to sustain positive net mineralization for a prolonged period after the fire. Available NH_4^+ concentrations support this idea. The NH_4^+ concentrations varied

predictably: extreme severity locations had the highest concentrations followed by high severity locations and then the low severity locations, which were only marginally above the control locations (Fig. 10). N oxidation, volatilization of organic matter, and the amounts of readily available N deposited with ash and char can vary in response to the fire type (i.e., smoldering versus crown-fire) as well as the movement of ash by wind and water postfire (Grogan et al. 2000, Neary et al. 2005). So, while the extreme severity sampling locations were not the only sites to receive ash and char from the fire, it is possible that they received more N rich substrate than the other sampling locations, which is what supported their increased net mineralization rates for months after the fire.

Net Nitrification

The net nitrification rates in the field-moist incubations followed the same pattern as net mineralization but were slightly higher (Fig. 8, 9), revealing that, following fire in these sites, NH_4^+ is simultaneously being immobilized in some microsites, while being nitrified in others. This process can occur in locations where N-cycling is relatively tight (Schimel and Bennett 2004).

The extreme severity sampling locations at six months postfire followed the same pattern as other locations, but the magnitude was larger. At nine months postfire, NO_3^- concentrations were 30 times higher in sampling locations that burned at extreme severity than in any other burn severity at any sampling event (Fig. 9), however, we did not observe increases in net nitrification for this sampling event in our laboratory incubations (Fig. 11). While this appears paradoxical, a potential explanation comes from the plant community. Although not quantified, we anecdotally observed that the extreme severity sampling locations had far more forbs at nine months postfire that any other sampling location or sampling time (see Fig. 3 for photographs). One of the common forbs was

Lupinus spp., which are known to be symbiotic N-fixers and can increase mineral N concentrations in soil (Goergen and Chambers 2009, Che et al. 2018). Other forbs present, such as *Achillea millefolium* (yarrow), may also contribute mineral N to the soils (Haahtela et al. 1981). Therefore, there may have been substantial nitrification occurring in the soils at the extreme severity sampling locations that our laboratory analyses would not have measured because it was happening in close proximity to live plant roots, which were not present in the soil incubations. This suggestion is further supported by other studies that have found herbaceous plant cover postfire increases soil NO_3^- concentration (Driscoll et al. 1999).

Microbial biomass controls on N cycling

Despite net immobilization in the field-moist incubations, the sampling locations that burned at high severity had consistently higher background NH_4^+ concentrations—five times the concentration of the control and low severity sampling locations (Fig. 8). Microbial biomass was likely the cause of this unexpected juxtaposition. The high severity sampling locations had higher microbial biomass than the control and low severity locations at one and half and six months after the fire (Fig. 7). The higher microbial biomass would have increased the demand for N and the microbial immobilization of N would reduce net mineralization rates even if NH_4^+ was still being produced. Although we did not measure gross mineralization, these results suggest that there may have been accelerated N cycling occurring in the high severity sampling locations, with simultaneously elevated rates of net immobilization. This is consistent with tight N cycling and simultaneous mineralization-immobilization occurring in N-rich and N-poor microsites, respectively. Our results support other work that has also found there are strong microbial controls on N availability in fire dominated coniferous forests (Vitousek and Melillo 1979, Turner et al. 2007).

The extreme severity sampling locations had more microbial biomass than the high severity locations and higher net mineralization rates (Fig. 7, 8). This apparent contradiction, given the microbially dominated mechanism proposed for the high severity locations, can be resolved by looking at available NH_4^+ concentrations which were substantially higher in the extreme severity sampling locations compared to high severity. This difference suggests that there is sufficient N available in the extreme severity locations to sustain both a large microbial biomass community and high net mineralization rates. The source of that additional N in those locations may be from a combination of ash and char deposition and the N fixing plant community discussed above.

Soil pH

Soil pH frequently increases as a result of fire (Certini 2005, Alcañiz et al. 2018), which is important because no single soil characteristic is as influential as soil pH (Thomas 1996, Lauber et al. 2009, Rousk et al. 2010). In our study, soil pH in the low and high severity sampling locations both increased by approximately the same amount immediately postfire—about half a pH unit (Fig. 6). This increase could be due to organic acid consumption during the fire and the deposition of base-forming cations (Certini 2005). We found the pH increases in soils that burned at low severity were short-lived (Fig. 6) because soil can act as a strong pH buffer and base forming cations like potassium (K) and sodium (Na) compounds formed in the fire may not persist for long (Certini 2005). Unlike our results, not all studies have found a pH change in mineral soil after low severity fires (e.g., Murphy et al. 2006a, Knicker 2007, Alcañiz et al. 2018). However, these studies sampled soils weeks to months after fire, which means they could have missed pH changes that may have occurred over shorter timescales. In our sampling locations that burned at high severity on the other hand, pH remained high for much longer (Fig. 6), perhaps because fire deposited more ash and char, which contain base-rich cations. Also, because the high severity fire consumed more forest floor and led to greater plant mortality, it may have taken

longer for organic acids to reaccumulate in those locations. Increases in pH were further intensified in soils that burned at extreme severity (Fig. 6) likely due to similar mechanisms. Similarly, Hanan et al. 2016a found prolonged pH increases in chaparral ecosystems that burn under a stand-replacing fire regime and many studies corroborate increased magnitude of pH change with increasing burn severity (e.g., Certini 2005, Alcañiz et al. 2018).

These differences in pH are critical for understanding N cycling because pH regulates the conversion of ammonium to ammonia: a one unit increase in pH leads to a ten-fold increase in the ammonia (NH3-) to ammonium (NH_4^+) ratio (De Boer and Kowalchuk 2001, Hanan et al. 2016b). Ammonia is the preferred substrate for nitrifying bacteria (Watson et al. 1989, Prosser 1990). Therefore, we would expect to see higher net nitrification rates when soil pH is higher, even if the NH_4^+ availability is the same. Although N cycling was tight in all locations except those that burned at extreme severity, we did observe this pattern at six months after the fire. Additionally, the sampling locations that burned at extreme severity had the highest pH and their net nitrification rates were significantly higher than the other severity categories (Fig. 6, 11). This suggests the microbial controls discussed above may be strong enough to outstrip pH-driven increases in net nitrification.

Moisture controls on N cycling

The wetted incubations remove water and hydrologic connectivity limitations on mineralization and nitrification. They allow us to infer certain aspects of N cycling that could occur with the soil microbial communities present in the field following rain and snow melt events. The control locations demonstrate almost no response to increased water availability. This was surprising because dry soils are known to have lower nitrification rates (Booth et al. 2005). These findings imply extremely tight N cycling and/or N limitation in mature stands in this system. Similar patterns have also been observed in other conifer forests (Vitousek et al. 1979, Turner et al. 2007).

Following fire, N cycling was not as tight as in unburned locations. While the field-moist net mineralization rates did not differ substantially between the low, high, and extreme severity sampling locations across time, the addition of water caused different reactions. The low severity sampling locations responded with increased net mineralization in the 1-week long wetted incubations for each sampling time up to six months after the fire and increased net nitrification up to nine months after the fire. However, at nine months, the magnitude of the increases appeared to decrease compared to six months after the fire. These findings align with previous work that show fire effects on mineralization decrease with time postfire (Turner et al. 2007, Sharma et al. 2017) but that effects on NO_3^- persist longer than effects on NH_4^+ (Wan et al. 2001).

Because the high severity sampling locations were more transformed by the fire, it is not surprising that the changes to net mineralization lasted longer at these locations. In the high severity locations, the addition of water increased net mineralization. However, in the 3-week long wetted incubations, net mineralization rates dropped below zero. This may have been due to immobilization by the microbial biomass, which likely increased over the course of the 3-week wetted incubations. The growth of microbial biomass, and subsequent N immobilization, is most apparent in the samples from sites that burned at high severity perhaps because those sampling locations were already primed with relatively high microbial biomass (Fig. 7).

Microbial immobilization is also likely responsible for the surprisingly low net nitrification rates observed in the high severity sampling locations: all net nitrification rates were within 0.1 μg NO_3^- per g dry soil per day for all incubation types at all sampling events, which was even lower than nitrification rates in the control locations. If the relatively high heterotrophic microbial biomass is immobilizing NH_4^+, then there would be very little leftover for the nitrifiers to convert to NO_3^-, which could explain the low net nitrification. Extreme severity sampling locations, which also has high microbial biomass, responded more like the low severity locations than high severity locations with increased net nitrification after the addition of water. Here,

unlike high severity, it appears there was enough substrate for the nitrifiers to convert some NH_4^+ to NO_3^- despite probable high demand from the rest of the microbial biomass. There also may be differences in the microbial community composition due to the different burn severities, which could also play a role in how NH_4^+ is immobilized postfire (Weber et al. 2014). Further work is needed to explore the microbial community composition in these sites, but it offers a path for understanding the mechanisms behind these nonmonotonic responses in net mineralization and nitrification to the addition of water across a gradient of burn severity.

The effects of water addition were not apparent in the areas that did not burn but lasted for months in areas that did, and their magnitude increased with increasing burn severity. These patterns of low net mineralization and nitrification rates (and in some cases net immobilization) at field-moist conditions but higher rates after the addition of water suggest that, following fires in this system, N cycling in the soil is driven by occasional periods of increased cycling after rain that build up the soil NH_4^+ and NO_3^- pools followed by periods of reduced cycling when the microbes must draw on those pools for their N requirements. This reliance on water further corroborates our finding that there is a strong microbial control over N cycling. Additionally, these periods of increased N cycling after rain are reminiscent of effects seen in arid systems where there are periods of intense microbial activity following wetting events (i.e., the Birch effect; Birch 1958, Unger et al. 2010). The Birch effect can help explain how periods of net immobilization balance with periods of high net mineralization when soils are moist. Thus, fires may play a critical role in soil N cycling in this system by facilitating mineralization and nitrification pulses with rain and seasonal soil wetting. Because climate change is increasing fire activity and burn severity (Westerling et al. 2006, Mantgem et al. 2013) and altering winter snowpack and precipitation (Howat and Tulaczyk 2005, Hatchett et al. 2017), understanding these postfire N cycling patterns is critical for predicting forest health and resilience in the Sierra Nevada, across western North America, and in other fire-prone forests globally.

5. Conclusion

We found that changes in soil N cycling postfire are not only an effect of burn severity; they are also attenuated by soil aridity. Soil water interacts with burn severity to heighten fire effects on N cycling. These changes are particularly noteworthy juxtaposed against the control sampling locations, which show minimal changes through time for any soil characteristic other than water content. While not all soil characteristics could be assessed before the fire, the consistency through time in the control sites, along with the minimal prefire differences between any of the sampled areas lend additional credence to our findings that fire, both alone and through interactions with soil water content, is a major driver of N cycling in this system.

The importance of rain on N cycling postfire has long been established in the literature (Neary et al. 1999, Grogan et al. 2000, Certini 2005). However, in this system, N cycling appears to be extremely tight—there is almost no net mineralization or nitrification without recent fire. In this scenario, the importance of rain and seasonal snowmelt postfire is heightened because it increases N cycling and makes larger pools of available soil N. These finding also support the hypothesis that fire has a stronger effect on N cycling than atmospheric deposition and leaching in semi-arid systems (Johnson et al. 1998, 2009).

Our findings highlight the need for further research on biogeochemical cycling using immediate pre- and postfire samples, as well as follow up sampling across seasons. There are numerous studies that investigate N cycling postfire but most studies focus on year and decadal scales postfire, not day to months (e.g., DeLuca and Sala 2006, Turner et al. 2007, 2019). These studies have found increases in N pools and cycling up to decades after wildfire. Our study extends these findings to include ephemeral and short-term seasonal changes in soil biogeochemistry, especially following low severity fires. Quantifying short-term responses is a critical step towards projecting how future, compounding fire events or increases in fire size and severity will affect ecosystem N budgets. Our results provide insight into how fire can affect

short-term and seasonal N cycling. The challenges of interpreting the trends in the extreme severity locations, compared to the other sampling locations that were sampled immediately before and after the fire, emphasizes the utility of those samples in understanding both short- and longer-term trends in soil processes after fire. While the studies that look years-to-decades after fire offer valuable information about long-term recovery, this study elucidates short-term responses and how low severity burns in particular can still shape biogeochemical cycling of a forest system. This knowledge will improve our understanding of how fire and fuel management will interact as we face increasing fire activity and more arid conditions across our landscapes (Lentile et al. 2007).

Acknowledgements

The Fire Behavior Assessment Team (https://www.frames.gov/fbat/home) collected the data on the Walker Fire that made this paper possible, team members included Matthew Dickinson, Lisa Loncar, Alicia Reiner, Scott Dailey, Jerry Bednarczyk, Cedar Drake, Jarred Gordon, Maryjane Heckel, Barry Kleckler, Jessica Miesel, and Laura Wade while Carol Ewell made sure equipment and transport were ready for the assignment. The FBAT thanks incident staff and others for their support (please see the Walker Fire report: Dickinson et al. 2019: https://www.frames.gov/sites/default/files/FBAT/reports/Walker-Fire-2019_FBAT-report_20191011.pdf).

Works Cited

Alcañiz, M., L. Outeiro, M. Francos, and X. Úbeda. 2018. Effects of prescribed fires on soil properties: A review. Science of The Total Environment 613–614:944–957.

Aoyama, M., and T. Nozawa. 1993. Microbial biomass nitrogen and mineralization-immobilization processes of nitrogen in soils incubated with various organic materials. Soil Science and Plant Nutrition 39:23–32.

Bailey, V. L., A. D. Peacock, J. L. Smith, and H. Bolton. 2002. Relationships between soil microbial biomass determined by chloroform fumigation–extraction, substrate-induced

respiration, and phospholipid fatty acid analysis. Soil Biology and Biochemistry 34:1385–1389.

Bates, D., M. Maechler, B. Bolker, and S. Walker. 2015. Fitting Linear Mixed-Effects Models Using lme4. Journal of Statistical Software 67:1–48.

Beare, M. H., C. L. Neely, D. C. Coleman, and W. L. Hargrove. 1990. A substrate-induced respiration (SIR) method for measurement of fungal and bacterial biomass on plant residues. Soil Biology and Biochemistry 22:585–594.

Birch, H. F. 1958. The effect of soil drying on humus decomposition and nitrogen availability. Plant and Soil 10:9–31.

Booth, M. S., J. M. Stark, and E. Rastetter. 2005. Controls on Nitrogen Cycling in Terrestrial Ecosystems: A Synthetic Analysis of Literature Data. Ecological Monographs 75:139–157.

Campbell, J. B. 1978. Spatial Variation of Sand Content and pH Within Single Contiguous Delineations of Two Soil Mapping Units. Soil Science Society of America Journal 42:460–464.

Certini, G. 2005. Effects of fire on properties of forest soils: a review. Oecologia 143:1–10.

Che, X., J. L. Moir, A. D. Black, H. Sheng, and X. Li. 2018. Effects of perennial Russell lupins on soil nitrogen and carbon in acid high-country soils. Journal of New Zealand Grasslands:67–72.

De Boer, W., and G. A. Kowalchuk. 2001. Nitrification in acid soils: micro-organisms and mechanisms. Soil Biology and Biochemistry 33:853–866.

DeLuca, T. H., M. D. MacKenzie, M. J. Gundale, and W. E. Holben. 2006. Wildfire-Produced Charcoal Directly Influences Nitrogen Cycling in Ponderosa Pine Forests. Soil Science Society of America Journal 70:448–453.

DeLuca, T. H., and A. Sala. 2006. Frequent Fire Alters Nitrogen Transformations in Ponderosa Pine Stands of the Inland Northwest. Ecology 87:2511–2522.

Dickinson, M., L. Loncar, A. Reiner, S. Dailey, J. Bednarczyk, C. Drake, J. Gordon, M. Heckel, B. Kleckler, J. Miesel, and L. Wade. 2019. 2019 Walker Fire, Plumas National Forest, Fire Behavior Assessment Team (FBAT) Report. US Forest Service: 34.

Driscoll, K. G., J. M. Arocena, and H. B. Massicotte. 1999. Post-fire soil nitrogen content and vegetation composition in Sub-Boreal spruce forests of British Columbia's central interior, Canada. Forest Ecology and Management 121:227–237.

Fox, J., and S. Weisberg. 2019. An R Companion to Applied Regression, Third Edition. Thousand Oaks CA.

Gallardo, A., and W. H. Schlesinger. 1995. Factors determining soil microbial biomass and nutrient immobilization in desert soils. Biogeochemistry 28:55–68.

Goergen, E. M., and J. C. Chambers. 2009. Influence of a native legume on soil N and plant response following prescribed fire in sagebrush steppe. International Journal of Wildland Fire 18:665.

González-Pérez, J. A., F. J. González-Vila, G. Almendros, and H. Knicker. 2004. The effect of fire on soil organic matter—a review. Environment International 30:855–870.

Grogan, P., T. D. Burns, and F. S. Chapin III. 2000. Fire effects on ecosystem nitrogen cycling in a Californian bishop pine forest. Oecologia 122:537–544.

Haahtela, K., T. Wartiovaara, V. Sundman, and J. Skujiņš. 1981. Root-Associated N2 Fixation (Acetylene Reduction) by Enterobacteriaceae and Azospirillum Strains in Cold-Climate Spodosols. Applied and Environmental Microbiology 41:203–206.

Hanan, E. J., C. M. D'Antonio, D. A. Roberts, and J. P. Schimel. 2016a. Factors Regulating Nitrogen Retention During the Early Stages of Recovery from Fire in Coastal Chaparral Ecosystems. Ecosystems 19:910–926.

Hanan, E. J., J. P. Schimel, K. Dowdy, and C. M. D'Antonio. 2016b. Effects of substrate supply, pH, and char on net nitrogen mineralization and nitrification along a wildfire-structured age gradient in chaparral. Soil Biology and Biochemistry 95:87–99.

Hatchett, B. J., B. Daudert, C. B. Garner, N. S. Oakley, A. E. Putnam, and A. B. White. 2017. Winter Snow Level Rise in the Northern Sierra Nevada from 2008 to 2017. Water 9:899.

Hothorn, T., F. Bretz, and P. Westfall. 2008. Simultaneous Inference in General Parametric Models. Biometrical Journal 50:346–363.

Howat, I. M., and S. Tulaczyk. 2005. Climate sensitivity of spring snowpack in the Sierra Nevada. Journal of Geophysical Research: Earth Surface 110.

Hudak, A. T., P. Morgan, M. J. Bobbitt, A. M. S. Smith, S. A. Lewis, L. B. Lentile, P. R. Robichaud, J. T. Clark, and R. A. McKinley. 2007. The Relationship of Multispectral Satellite Imagery to Immediate Fire Effects. Fire Ecology 3:64–90.

Johnson, D. W., W. W. Miller, R. B. Susfalk, J. D. Murphy, R. A. Dahlgren, and D. W. Glass. 2009. Biogeochemical cycling in forest soils of the eastern Sierra Nevada Mountains, USA. Forest Ecology and Management 258:2249–2260.

Johnson, D. W., R. B. Susfalk, R. A. Dahlgren, and J. M. Klopatek. 1998. Fire is more important than water for nitrogen fluxes in semi-arid forests. Environmental Science & Policy 1:79–86.

Keeley, J. E. 2009. Fire intensity, burn severity and burn severity: a brief review and suggested usage. International Journal of Wildland Fire 18:116–126.

Knelman, J. E., E. B. Graham, N. A. Trahan, S. K. Schmidt, and D. R. Nemergut. 2015. Burn severity shapes plant colonization effects on bacterial community structure, microbial biomass, and soil enzyme activity in secondary succession of a burned forest. Soil Biology and Biochemistry 90:161–168.

Knicker, H. 2007. How does fire affect the nature and stability of soil organic nitrogen and carbon? A review. Biogeochemistry 85:91–118.

Kranz, C., and T. Whitman. 2019. Short communication: Surface charring from prescribed burning has minimal effects on soil bacterial community composition two weeks post-fire in jack pine barrens. Applied Soil Ecology 144:134–138.

Lauber, C. L., M. Hamady, R. Knight, and N. Fierer. 2009. Pyrosequencing-Based Assessment of Soil pH as a Predictor of Soil Bacterial Community Structure at the Continental Scale. Applied and Environmental Microbiology 75:5111–5120.

Lentile, L. B., P. Morgan, C. Hardy, A. T. Hudak, R. Means, R. Ottmar, P. Robichaud, E. Sutherland, F. Way, and S. Lewis. 2007. Lessons Learned From Rapid Response Research on Wildland Fires. U.S. Department of Agriculture: Forest Service - National Agroforestry Center:10.

MacDonald, N. W., D. R. Zak, and K. S. Pregitzer. 1995. Temperature Effects on Kinetics of Microbial Respiration and Net Nitrogen and Sulfur Mineralization. Soil Science Society of America Journal 59:233–240.

Mantgem, P. J. van, J. C. B. Nesmith, M. Keifer, E. E. Knapp, A. Flint, and L. Flint. 2013. Climatic stress increases forest burn severity across the western United States. Ecology Letters 16:1151–1156.

Morgan, P., R. E. Keane, G. K. Dillon, T. B. Jain, A. T. Hudak, E. C. Karau, P. G. Sikkink, Z. A. Holden, and E. K. Strand. 2014. Challenges of assessing fire and burn severity using field measures, remote sensing and modelling. International Journal of Wildland Fire 23:1045–1060.

Murphy, J. D., D. W. Johnson, W. W. Miller, R. F. Walker, and R. R. Blank. 2006a. PRESCRIBED FIRE EFFECTS ON FOREST FLOOR AND SOIL NUTRIENTS IN A SIERRA NEVADA FOREST: Soil Science 171:181–199.

Murphy, J. D., D. W. Johnson, W. W. Miller, R. F. Walker, E. F. Carroll, and R. R. Blank. 2006b. Wildfire effects on soil nutrients and leaching in a Tahoe Basin Watershed. Journal of environmental quality.

Neary, D. G., C. C. Klopatek, L. F. DeBano, and P. F. Ffolliott. 1999. Fire effects on belowground sustainability: a review and synthesis. Forest Ecology and Management 122:51–71.

Neary, D. G., K. C. Ryan, and L. F. DeBano. 2005. Wildland fire in ecosystems: effects of fire on soils and water. Gen. Tech. Rep. RMRS-GTR-42-vol.4. Ogden, UT: U.S. Department of Agriculture, Forest Service, Rocky Mountain Research Station. 250 p. 042.

NRCS, and UC Davis. 2020. Soil Web. California Soil Resources Lab.

Pellegrini, A. F. A., A. Ahlström, S. E. Hobbie, P. B. Reich, L. P. Nieradzik, A. C. Staver, B. C. Scharenbroch, A. Jumpponen, W. R. L. Anderegg, J. T. Randerson, and R. B. Jackson. 2018. Fire frequency drives decadal changes in soil carbon and nitrogen and ecosystem productivity. Nature 553:194–198.

Pellegrini, A. F. A., A. C. Caprio, K. Georgiou, C. Finnegan, S. E. Hobbie, J. A. Hatten, and R. B. Jackson. 2021. Low-intensity frequent fires in coniferous forests transform soil organic matter in ways that may offset ecosystem carbon losses. Global Change Biology in press.

Pinheiro, J., D. Bates, S. DebRoy, D. Sarkar, and R Core Team. 2020. nlme: Linear and Nonlinear Mixed Effects Models.

Prosser, J. I. 1990. Autotrophic Nitrification in Bacteria. Pages 125–181 *in* A. H. Rose and D. W. Tempest, editors. Advances in Microbial Physiology. Academic Press.

R Core Team. 2020. R: A language and environment for statistical computing. R Foundation for Staistical Computing, Vienna, Austria.

RAWS USA Climate Archive. 2020. . Western Regional Climate Center Coyote, CA.

Ren, G., M. He, G. Li, A. Anandkumar, Z. Dai, C. B. Zou, Z. Hu, Q. Ran, and D. Du. 2020. Effects of Solidago canadensis Invasion and Climate Warming on Soil Net N Mineralization. Polish Journal of Environmental Studies 29:3285–3294.

Rousk, J., E. Bååth, P. C. Brookes, C. L. Lauber, C. Lozupone, J. G. Caporaso, R. Knight, and N. Fierer. 2010. Soil bacterial and fungal communities across a pH gradient in an arable soil. The ISME Journal 4:1340–1351.

Santos, F., A. S. Wymore, B. K. Jackson, S. M. P. Sullivan, W. H. McDowell, and A. A. Berhe. 2019. Burn severity, time since fire, and site-level characteristics influence streamwater chemistry at baseflow conditions in catchments of the Sierra Nevada, California, USA. Fire Ecology 15:3.

Scheipl, F., S. Greven, and H. Kuechenfoff. 2008. Size and power of tests for a zero random effect variance or polynomial regression in additive and linear mixed models. Computational Statistics & Data Analysis 52:3283–3299.

Schipper, L. A., and G. P. Sparling. 2011. Accumulation of soil organic C and change in C:N ratio after establishment of pastures on reverted scrubland in New Zealand. Biogeochemistry 104:49–58.

Sharma, U., Garima, J. C. Sharma, and M. Devi. 2017. Effect of Forest fire on soil nitrogen mineralization and microbial biomass: A review. Journal of Pharmacognosy and Phytochemistry 6:682–685.

Sierra, J. 1997. Temperature and soil moisture dependence of N mineralization in intact soil cores. Soil Biology and Biochemistry 29:1557–1563.

Smith, A. M. S., A. M. Sparks, C. A. Kolden, J. T. Abatzoglou, A. F. Talhelm, D. M. Johnson, L. Boschetti, J. A. Lutz, K. G. Apostol, K. M. Yedinak, W. T. Tinkham, and R. J. Kremens. 2016. Towards a new paradigm in burn severity research using dose–response experiments. International Journal of Wildland Fire 25:158.

Ste-Marie, C., and D. Paré. 1999. Soil, pH and N availability effects on net nitrification in the forest floors of a range of boreal forest stands. Soil Biology and Biochemistry 31:1579–1589.

Stephens, S. L., T. Meixner, M. Poth, B. McGurk, and D. Payne. 2004. Prescribed fire, soils, and stream water chemistry in a watershed in the Lake Tahoe Basin, California. International Journal of Wildland Fire 13:27–35.

Tester, J. R. 1989. Effects of Fire Frequency on Oak Savanna in East-Central Minnesota. Bulletin of the Torrey Botanical Club 116:134–144.

Thomas, G. W. 1996. Soil pH and soil acidity.

Turner, M. G., E. A. H. Smithwick, K. L. Metzger, D. B. Tinker, and W. H. Romme. 2007. Inorganic nitrogen availability after severe stand-replacing fire in the Greater Yellowstone ecosystem. Proceedings of the National Academy of Sciences 104:4782–4789.

Turner, M. G., T. G. Whitby, and W. H. Romme. 2019. Feast not famine: Nitrogen pools recover rapidly in 25-yr-old postfire lodgepole pine. Ecology 100:e02626.

Unger, S., C. Máguas, J. S. Pereira, T. S. David, and C. Werner. 2010. The influence of precipitation pulses on soil respiration – Assessing the "Birch effect" by stable carbon isotopes. Soil Biology and Biochemistry 42:1800–1810.

U.S. Forest Service. 2021, March 3. FSGeodata Clearinghouse.

U.S. Geological Survey. 2019, March 21. Wildland Fire Decision Support System.

Verma, S., and S. Jayakumar. 2012. Impact of forest fire on physical, chemical and biological properties of soil: A review.

Vitousek, P. M., J. R. Gosz, C. C. Grier, J. M. Melillo, W. A. Reiners, and R. L. Todd. 1979. Nitrate Losses from Disturbed Ecosystems. Science 204:469–474.

Vitousek, P. M., and J. M. Melillo. 1979. Nitrate Losses From Disturbed Forests: Patterns and Mechanisms. Forest Science 25:605–619.

Wagtendonk, J. W. van, J. A. Fites-Kaufman, H. D. Safford, M. P. North, and B. Collins. 2018. Sierra Nevada Bioregion. Fire in California's Ecosystems:249–279.

Wan, S., D. Hui, and Y. Luo. 2001. Fire Effects on Nitrogen Pools and Dynamics in Terrestrial Ecosystems: A Meta-Analysis. Ecological Applications 11:1349–1365.

Watson, S. W., E. Bock, H. Harms, H. P. Koops, and A. B. Hooper. 1989. Nitrifying bacteria. Pages 1808–1834 Bergey's Manual of Systematic Bacteriology. The Williams and Wilkins Co., Baltimore, MD.

Weber, C. F., J. S. Lockhart, E. Charaska, K. Aho, and K. A. Lohse. 2014. Bacterial composition of soils in ponderosa pine and mixed conifer forests exposed to different wildfire burn severity. Soil Biology and Biochemistry 69:242–250.

West, A. W., and G. P. Sparling. 1986. Modifications to the substrate-induced respiration method to permit measurement of microbial biomass in soils of differing water contents. Journal of Microbiological Methods 5:177–189.

Westerling, A. L., H. G. Hidalgo, D. R. Cayan, and T. W. Swetnam. 2006. Warming and Earlier Spring Increase Western U.S. Forest Wildfire Activity. Science 313:940–943.

Whitman, T., E. Whitman, J. Woolet, M. D. Flannigan, D. K. Thompson, and M.-A. Parisien. 2019. Soil bacterial and fungal response to wildfires in the Canadian boreal forest across a burn severity gradient. Soil Biology and Biochemistry 138:107571.

Wickham, H. 2016. ggplot2: Elegant Graphics for Data Analysis. Springer-Verlag New York.

Supplementary Information

S1. Plot level data:

Table S1. The coordinates for the southwest corners of each plot. Coordinates use NAD83.

Plot	Latitude	Longitude
2	40.121722	-120.559139
3	40.108233	-120.555500
4	40.143311	-120.554603
5	40.143147	-120.557666
7	40.137983	-120.504950
8	40.116517	-120.529500
9	40.132514	-120.501463

Table S2. Site description from the FBAT report for plots 2, 3, 4, 5, 7, and 8 (Dickinson et al. 2019). Additional data added for plot 9. Silvicultural and hazardous fuels treatment history was determined from the Forest Service data clearinghouse ((U.S. Forest Service 2021)). Treatments were performed over areas much larger than FBAT plots and, as such, conditions within plots may not always represent average treatment conditions. Wildfire history was determined from perimeters available in the Wildland Fire Decision Support System (WFDSS; (U.S. Geological Survey 2019).

Plot	Treatment history	Wildfire history	Walker Fire	Slope (%)	Aspect	Elev. (m)
2	2008 salvage cut borders the plot	Low severity in 2007 Wheeler Fire	Did not burn	14	S	1656
3	Plot near a 1982 sanitation cut, and near a 2002 precommercial thin in the same area	None recorded	Did not burn	8	N	1680
4	1996 commercial & precommercial thin	Low severity in 2007 Wheeler Fire	Low severity	7	W	1672
5	1996 commercial & precommercial thin	Low severity in 2007 Wheeler Fire	Low severity	9	W	1736

7	1975 cut, 1994 commercial & precommercial thin, 2003 precommercial thin	Bore charring consistent with burning in 2007 Wheeler Fire but outside official perimeter	Did not burn	3	N	1704
8	None recorded	None recorded	High severity	7	NE	1694
9	2003 precommercial thin, planned salvage cut 2020	None recorded	Extreme severity	17	SW	1704

Table S3. Canopy characteristics from the FBAT report for plots 2, 3, 4, 5, 7, and 8 (Dickinson et al. 2019). Plot 9 was not surveyed by FBAT before the fire. Canopy height and cover are estimated directly from plot data. Canopy height is the average across all overstory trees in the sample. QMD, tree density, basal area, canopy base height, and canopy bulk density are FVS outputs based on plot data

Plot	Overstory density (trees ≥ 6 in DBH/acre)	Pole density (trees < 6 in DBH/acre)	Quadratic mean diameter (cm)	Basal area (m2/hectare)	Canopy Cover (%)	Canopy height (m)	Canopy base height (m)	Canopy bulk density (kg/m2)
2	242.17	0	40.64	33.06	62	20.73	7.01	0.07
3	219.93	0	40.64	28.70	31	23.17	9.14	0.05
4	210.04	0	48.26	36.73	23	23.47	7.32	0.05
5	486.81	0	35.56	45.69	46	20.12	5.79	0.08
7	212.51	0	50.8	41.09	31	27.13	12.19	0.04
8	1025.51	1423.35	22.86	107.44	62	21.64	1.83	0.27

Table S4. Surface fuels and fuel bed depths for plots 2, 3, 4, 5, 7, and 8 from the FBAT report (Dickinson et al. 2019). Plot 9 was not surveyed by FBAT before the fire.

	Mean fuel loading (tons/hectare)									Fuel Bed Depth (cm)
Plot	Duff	Litter	1-hr	10-hr	100-hr	1000-hr	Forb & grass	Shrub & seedling	total	
2	15.32	5.77	0.48	1.93	4.27	0.00	<0.01	0.89	19.33	58.85
3	25.86	8.03	0.38	1.41	1.83	0.68	<0.01	0.12	37.66	21.16
4	6.28	8.03	0.23	0.35	0	0.00	0.14	0.49	15.32	13.13
5	2.76	5.52	0.10	1.23	0.93	9.59	0.03	0.36	17.07	24.56

7	8.54	5.52	0.05	0.35	0	0.68	<0.01	0.07	14.56	13.54
8	50.97	5.27	0.23	1.58	0	0.00	<0.01	0.01	58.00	20.32

S2. Detailed Statistical Results

Table S5. Statistical results for significant factors affecting each soil characteristic. Time refers to the sampling event, severity refers to the burn severity category, and interaction refers to the time-severity interaction. The extreme severity samples and the immediate post-fire sampling event are not considered in this analysis due to a shortened timeline and a lack of immediate post-fire samples in control plots, respectively. $^{+}$ indicates the results from linear mixed effects models that had non-normal residuals.

	category	Chi^2	df	p value
pH	time	5.81	3	0.12
	severity	4.94	2	0.08
	interaction	27.83	6	<0.01
Microbial Biomass	time	11.9	3	0.01
	severity	7.96	2	0.02
	interaction	18.77	6	<0.01
Fractional Water	time	150.21^{+}	3^{+}	$<0.01^{+}$
Content	severity	0.66^{+}	2^{+}	0.72^{+}
	interaction	8.81^{+}	6^{+}	0.18^{+}
Available NH_4^+	time	1.63	3	0.65
	severity	0.37	2	0.83
	interaction	120.71	6	<0.01
Available NO_3^-	time	0.24^{+}	3^{+}	0.97^{+}
	severity	0.03^{+}	2^{+}	0.99^{+}
	interaction	7.16^{+}	6^{+}	0.31^{+}
Net Mineralization	time	0.32	2	0.85
Field-moist	severity	28.13	2	<0.01
incubation	interaction	11.27	4	0.02
Net Mineralization	time	0.21	2	0.9
1-week wetted	severity	26.34	2	<0.01
incubation	interaction	50.68	4	<0.01
Net Mineralization	time	1.23	2	0.54

3-week wetted	severity	20.22	2	<0.01
incubation	interaction	5.17	4	0.27
Net Nitrification	time	0.15	2	0.93
Field-moist	severity	0.56	2	0.75
incubation	interaction	30.4	4	<0.01
Net Nitrification	time	0.18	2	0.91
1-week wetted	severity	1.11	2	0.57
incubation	interaction	1.91	4	0.75
Net Nitrification	time	1.88	2	0.39
3-week wetted	severity	0.68	2	0.71
incubation	interaction	13.95	4	0.01

Table S6. Statistical results from multiple comparisons of the burn severity category means in the linear mixed effects models for soil incubations within a sampling event. $^{+}$ indicates the results from linear mixed effects models that had non-normal residuals

		1.5 months Postfire		6 months Postfire		9 months Postfire	
Characteristic	Comparison	z score	p value	z score	p value	z score	p value
Mineralization	Control/Low	-0.44	0.90	0.49	0.96	0.13^{+}	1.00^{+}
Field-moist	Control/High	-5.42	<0.01	-1.36	0.52	-0.43^{+}	0.97^{+}
	Control/Extreme	-	-	4.98	<0.01	3.82^{+}	$<0.01^{+}$
	Low/High	-4.79	<0.01	-1.65	0.35	-0.50^{+}	0.96^{+}
	Low/Extreme	-	-	4.33	<0.01	3.50^{+}	0.00^{+}
	High/Extreme	-	-	5.18	<0.01	3.47^{+}	0.00^{+}
Mineralization	Control/Low	1.94	0.13	1.64	0.35	0.07	1.00
1-week wetted	Control/High	-5.35	<0.01	-0.28	0.99	0.45	0.97
	Control/Extreme	-	-	6.68	<0.01	-0.53	0.95
	Low/High	-6.48	<0.01	-1.48	0.44	0.37	0.98
	Low/Extreme	-	-	5.07	<0.01	-0.55	0.95
	High/Extreme	-	-	5.68	<0.01	-0.80	0.85
Mineralization	Control/Low	1.72^{+}	0.20^{+}	0.75	0.87	0.54	0.95
3-week wetted	Control/High	-4.71^{+}	$<0.01^{+}$	-1.18	0.64	-2.92	0.02
	Control/Extreme	-	-	-2.46	0.06	1.79	0.27

	Low/High	-5.72^{+}	<0.01^{+}	-1.67	0.34	-3.15	0.01
	Low/Extreme	-	-	-2.88	0.02	1.29	0.56
	High/Extreme	-	-	-1.05	0.72	3.85	<0.01
Nitrification	Control/Low	1.04	0.55	0.51	0.96	-0.52	0.95
Field-moist	Control/High	0.08	1.00	-0.03	1.00	1.01	0.74
	Control/Extreme	-	-	3.07	0.01	-10.76	<0.01
	Low/High	-0.69	0.77	-0.40	0.98	1.34	0.54
	Low/Extreme	-	-	2.52	0.06	-9.76	<0.01
	High/Extreme	-	-	2.53	0.05	-9.61	<0.01
Nitrification	Control/Low	1.59	0.25	0.86	0.82	1.60^{+}	0.37^{+}
1-week wetted	Control/High	-0.17	0.98	-0.09	1.00	0.01^{+}	1.00^{+}
	Control/Extreme	-	-	4.08	<0.01	6.59^{+}	<0.01^{+}
	Low/High	-1.35	0.37	-0.72	0.89	-1.18^{+}	0.63^{+}
	Low/Extreme	-	-	3.20	0.01	5.02^{+}	<0.01^{+}
	High/Extreme	-	-	3.40	0.00	5.37^{+}	<0.01^{+}
Nitrification	Control/Low	2.37	0.05	1.39^{+}	0.50^{+}	0.61	0.93
3-week wetted	Control/High	-0.54	0.85	-0.25^{+}	0.99^{+}	-1.33	0.54
	Control/Extreme	-	-	-0.02^{+}	1.00^{+}	-2.42	0.07
	Low/High	-2.27	0.06	-1.27^{+}	0.58^{+}	-1.71	0.31
	Low/Extreme	-	-	-1.05^{+}	0.72^{+}	-2.74	0.03
	High/Extreme	-	-	0.19^{+}	1.00^{+}	-0.89	0.81

Table S7. Statistical results from multiple comparisons of the burn severity category means in the linear mixed effects models for each soil characteristic within a sampling event. $^{+}$ indicates the results from linear mixed effects models that had non-normal residuals.

		Immediately Prefire		Immediately Postfire		1.5 mo. Postfire		6 mo. Postfire		9 mo. Postfire	
Characteristic	Comparison	z score	p value	z score	p value	z score	p value	z score	p value	z score	p value
Fractional	Control/Low	-3.39^{+}	0.00^{+}	-	-	-2.76^{+}	0.02^{+}	-1.86^{+}	0.24^{+}	-2.33	0.09
Water	Control/High	-0.17^{+}	0.98^{+}	-	-	-0.85^{+}	0.67^{+}	-2.16^{+}	0.13^{+}	-0.62	0.92
Content	Control/Extreme	-	-	-	-	-	-	-1.56^{+}	0.40^{+}	-0.45	0.97

	Low/High	2.37^{+}	0.05^{+}	-1.39^{+}	0.16^{+}	1.25^{+}	0.42^{+}	-0.65^{+}	0.91^{+}	1.15	0.65
	Low/Extreme	-	-	-	-	-	-	-0.08^{+}	1.00^{+}	1.31	0.55
	High/Extreme	-	-	-	-	-	-	0.49^{+}	0.96^{+}	0.14	1.00
pH	Control/Low	2.06	0.10	-	-	2.09	0.09	2.56	0.05	2.56	0.05
	Control/High	-1.80	0.17	-	-	3.66	<0.01	1.18	0.63	1.18	0.63
	Control/Extreme	-	-	-	-	-	-	4.85	<0.01	4.85	<0.01
	Low/High	-3.23	0.00	-3.09^{+}	0.00^{+}	1.89	0.14	-0.80	0.85	-0.80	0.85
	Low/Extreme	-	-	-	-	-	-	2.66	0.04	2.66	0.04
	High/Extreme	-	-	-	-	-	-	2.99	0.01	2.99	0.01
Microbial	Control/Low	0.25	0.97	-	-	-0.62	0.81	-2.61	0.04	-1.73	0.30
Biomass	Control/High	-1.48	0.30	-	-	3.44	0.00	-1.73	0.30	-1.58	0.39
	Control/Extreme	-	-	-	-	-	-	4.43	<0.01	2.86	0.02
	Low/High	-1.58	0.25	3.12	0.00	3.70	0.00	0.32	0.99	-0.19	1.00
	Low/Extreme	-	-	-	-	-	-	6.13	<0.01	3.99	<0.01
	High/Extreme	-	-	-	-	-	-	5.03	<0.01	3.63	0.00
C:N ratio	Control/Low	2.95	0.01	-	-	-	-	-	-	-	-
	Control/High	1.66	0.22	-	-	-	-	-	-	-	-
	Control/Extreme	-	-	-	-	-	-	-	-	-	-
	Low/High	-0.64	0.80	2.67^{+}	0.01^{+}	-1.17^{+}	0.24^{+}	-	-	-	-
	Low/Extreme	-	-	-	-	-	-	-	-	-	-
	High/Extreme	-	-	-	-	-	-	-	-	-	-
Available	Control/Low	-0.81^{+}	0.70^{+}	-	-	1.31	0.39	-0.10	1.00	0.43	0.97
NH_4^+	Control/High	-0.72^{+}	0.75^{+}	-	-	13.08	<0.01	2.04	0.17	2.37	0.08
	Control/Extreme	-	-	-	-	-	-	8.71	<0.01	7.93	<0.01
	Low/High	-0.08^{+}	1.00^{+}	11.61	<0.01	11.35	<0.01	2.00	0.19	1.92	0.21
	Low/Extreme	-	-	-	-	-	-	8.29	<0.01	7.16	<0.01
	High/Extreme	-	-	-	-	-	-	5.45	<0.01	4.54	<0.01
Available	Control/Low	-0.78^{+}	0.72^{+}	-	-	2.53	0.03	1.26^{+}	0.58^{+}	1.34^{+}	0.53^{+}
NO_3^-	Control/High	-0.61^{+}	0.81^{+}	-	-	-0.10	0.99	0.45^{+}	0.97^{+}	0.01^{+}	1.00^{+}
	Control/Extreme	-	-	-	-	-	-	0.52^{+}	0.95^{+}	52.63^{+}	<0.01^{+}
	Low/High	0.00^{+}	1.00^{+}	-0.58^{+}	0.56^{+}	-1.98	0.11	-0.52^{+}	0.96^{+}	-0.99^{+}	0.75^{+}

	Low/Extreme	-	-	-	-	-	-	-0.46^{+}	0.97^{+}	48.62^{+}	<0.01^{+}
	High/Extreme	-	-	-	-	-	-	0.05^{+}	1.00^{+}	42.96^{+}	<0.01^{+}

Table S8. Statistical results from multiple comparisons of the mean values within a burn severity category in the linear mixed effects models for each soil characteristic across sampling events. $^{+}$ indicates the results from linear mixed effects models that had non-normal residuals.

		Control		Low Severity		High Severity		Extreme Severity	
Characteristic	Comparison	z score	p value	z score	p value	z score	p value	z score	p value
pH	Prefire/imm. Postfire	-	-	3.288^{+}	0.01^{+}	3.277^{+}	0.01^{+}	-	-
	Prefire/1.5 mo.	1.666	0.34	3.023^{+}	0.02^{+}	10.649^{+}	<0.01^{+}	-	-
	Prefire/6 mo.	1.826	0.26	3.751^{+}	<0.01^{+}	3.514^{+}	<0.01^{+}	-	-
	Prefire/9 mo.	1.108	0.68	2.03^{+}	0.25^{+}	4.915^{+}	<0.01^{+}	-	-
	imm. Postfire/1.5 mo.	-	-	-0.265^{+}	1.00^{+}	7.372^{+}	<0.01^{+}	-	-
	imm. Postfire/6 mo.	-	-	0.463^{+}	0.99^{+}	0.237^{+}	1.00^{+}	-	-
	imm. Postfire/9 mo.	-	-	-1.258^{+}	0.72^{+}	1.638^{+}	0.47^{+}	-	-
	1.5 mo./6 mo.	0.16	1.00	0.728^{+}	0.95^{+}	-7.135^{+}	<0.01^{+}	-	-
	1.5 mo./9 mo.	-0.557	0.95	-0.993^{+}	0.86^{+}	-5.734^{+}	<0.01^{+}	-	-
	6 mo./9 mo.	-0.718	0.89	-1.721^{+}	0.42^{+}	1.401^{+}	0.63^{+}	-3.596	<0.01
Microbial	Prefire/imm. Postfire	-	-	-3.17^{+}	0.01^{+}	1.736^{+}	0.41^{+}	-	-
Biomass	Prefire/1.5 mo.	-3.88	< 0.01	-2.681^{+}	0.06^{+}	5.828^{+}	<0.01^{+}	-	-
	Prefire/6 mo.	-2.67	0.04	-3.026^{+}	0.02^{+}	0.656^{+}	0.97^{+}	-	-
	Prefire/9 mo.	-3.722	0.01	-3.46^{+}	<0.01^{+}	-1.109^{+}	0.80^{+}	-	-
	imm. Postfire/1.5 mo.	-	-	0.489^{+}	0.99^{+}	4.092^{+}	<0.01^{+}	-	-
	imm. Postfire/6 mo.	-	-	0.144^{+}	1.00^{+}	-1.08^{+}	0.82^{+}	-	-
	imm. Postfire/9 mo.	-	-	-0.346^{+}	1.00^{+}	-2.845^{+}	0.04^{+}	-	-
	1.5 mo./6 mo.	1.21	0.62	-0.346^{+}	1.00^{+}	-5.172^{+}	<0.01^{+}	-	-
	1.5 mo./9 mo.	0.159	1.00	-0.779^{+}	0.94^{+}	-6.937^{+}	<0.01^{+}	-	-
	6 mo./9 mo.	-1.052	0.72	-0.434^{+}	0.99^{+}	-1.764^{+}	0.39^{+}	-0.912	0.36
C:N ratio	Prefire/imm. Postfire	-	-	-0.618^{+}	0.81^{+}	0.038^{+}	1.00^{+}	-	-
	Prefire/1.5 mo.	-	-	1.877^{+}	0.15^{+}	-0.34^{+}	0.94^{+}	-	-
	Prefire/6 mo.	-	-	2.495^{+}	0.03^{+}	-0.377^{+}	0.92^{+}	-	-

	6 mo./9 mo.	-	-	-	-	-	-	-1.452	0.15
Available NH_4^+	Prefire/imm. Postfire	-	-	4.007^+	$<0.01^+$	8.099^+	$<0.01^+$	-	-
	Prefire/1.5 mo.	-1.352	0.53	1.573^+	0.52^+	5.065^+	$<0.01^+$	-	-
	Prefire/6 mo.	0.556	0.95	0.515^+	0.99^+	3.698^+	$<0.01^+$	-	-
	Prefire/9 mo.	-0.967	0.77	2.288^+	0.15^+	3.634^+	$<0.01^+$	-	-
	imm. Postfire/1.5 mo.	-	-	-2.434^+	0.11^+	-3.034^+	0.02^+	-	-
	imm. Postfire/6 mo.	-	-	-3.492^+	$<0.01^+$	-4.401^+	$<0.01^+$	-	-
	imm. Postfire/9 mo.	-	-	-1.719^+	0.42^+	-4.465^+	$<0.01^+$	-	-
	1.5 mo./6 mo.	1.907	0.23	-1.057^+	0.83^+	-1.367^+	0.65^+	-	-
	1.5 mo./9 mo.	0.385	0.98	0.715^+	0.95^+	-1.431^+	0.61^+	-	-
	6 mo./9 mo.	-1.523	0.42	1.772^+	0.39^+	-0.064^+	1.00^+	-0.517	0.61
Available NO_3^-	Prefire/imm. Postfire	-	-	0.461^+	0.99^+	0.000^+	1.00^+	-	-
	Prefire/1.5 mo.	-0.226^+	1.00^+	0.992^+	0.86^+	0.090^+	1.00^+	-	-
	Prefire/6 mo.	1.055^+	0.72^+	0.784^+	0.94^+	1.578^+	0.51^+	-	-
	Prefire/9 mo.	-0.821^+	0.85^+	1.844^+	0.35^+	0.053^+	1.00^+	-	-
	imm. Postfire/1.5 mo.	-	-	0.532^+	0.98^+	0.090^+	1.00^+	-	-
	imm. Postfire/6 mo.	-	-	0.323^+	1.00^+	1.578^+	0.51	-	-
	imm. Postfire/9 mo.	-	-	1.383^+	0.64^+	0.053^+	1.00^+	-	-
	1.5 mo./6 mo.	1.281^+	0.58^+	-0.209^+	1.00^+	1.488^+	0.57^+	-	-
	1.5 mo./9 mo.	-0.594^+	0.93^+	0.852^+	0.91^+	-0.037^+	1.00^+	-	-
	6 mo./9 mo.	-1.875^+	0.24^+	1.061^+	0.83^+	-1.525^+	0.55^+	59.03	<0.01
Mineralization	1.5 mo./6 mo.	0.128	0.99	1.369^+	0.36^+	1.317	0.39	-	-
Field-moist	1.5 mo./9 mo.	0.922	0.63	1.297^+	0.40^+	1.919	0.13	-	-
incubation	6 mo./9 mo.	0.795	0.71	-0.072^+	1.00^+	0.602	0.82	-0.057^+	0.96^+
Mineralization	1.5 mo./6 mo.	-0.054^+	1.00^+	1.387^+	0.35^+	2.959^+	0.01^+	-	-
1-week wetted	1.5 mo./9 mo.	0.656^+	0.79^+	-0.835^+	0.68^+	5.342^+	$<0.01^+$	-	-
incubation	6 mo./9 mo.	0.71^+	0.76^+	-2.222^+	0.07^+	2.383^+	0.05^+	-1.168^+	0.24^+
Mineralization	1.5 mo./6 mo.	-0.292	0.95	1.598	0.25	-0.39^+	0.92^+	-	-
3-week wetted	1.5 mo./9 mo.	1.101	0.51	0.113	0.99	-0.657^+	0.79^+	-	-
incubation	6 mo./9 mo.	1.393	0.35	-1.486	0.30	-0.267^+	0.96^+	1.292^+	0.20^+
Nitrification	1.5 mo./6 mo.	-1.489	0.30	2.56^+	0.03^+	-0.578	0.83	-	-

Field-moist	1.5 mo./9 mo.	0.044	1.00	-1.016^{+}	0.57^{+}	1.011	0.57	-	-
incubation	6 mo./9 mo.	1.534	0.28	-3.576^{+}	<0.01^{+}	1.589	0.25	-1.672^{+}	0.09^{+}
Nitrification	1.5 mo./6 mo.	-0.29^{+}	0.96^{+}	0.912	0.63	-1.912^{+}	0.14^{+}	-	-
1-week wetted	1.5 mo./9 mo.	-1.546^{+}	0.27^{+}	0.332	0.94	-0.482^{+}	0.88^{+}	-	-
incubation	6 mo./9 mo.	-1.256^{+}	0.42^{+}	-0.58	0.83	1.431^{+}	0.33^{+}	-0.552	0.58
Nitrification	1.5 mo./6 mo.	0.773	0.72	2.647	0.02	-0.827^{+}	0.69^{+}	-	-
3-week wetted	1.5 mo./9 mo.	2.054	0.10	0.392	0.92	-0.187^{+}	0.98^{+}	-	-
incubation	6 mo./9 mo.	1.282	0.41	-2.255	0.06	0.639^{+}	0.80^{+}	-0.693^{+}	0.49^{+}

Table S9. Mean and standard error for the soil characteristics measured at all sampling events.

		Immediately Prefire		Immediately Postfire		1.5 mo. Postfire		6 mo. Postfire		9 mo. Postfire	
Characteristic	Severity	Mean	SE	Mean	SE	Mean	SE	Mean	SE	Mean	SE
Fractional Water	Control	0.03	0.00	-	-	0.07	0.00	0.22	0.01	0.06	0.00
Content	Low severity	0.02	0.00	0.15	0.00	0.04	0.00	0.16	0.01	0.02	0.00
(g H_2O per g field-	High severity	0.03	0.00	0.12	0.01	0.06	0.02	0.14	0.00	0.05	0.01
moist soil)	Extreme severity	-	-	-	-	-	-	0.16	0.01	0.05	0.00
pH	Control	5.84	0.03	-	-	6.13	0.05	6.16	0.05	6.04	0.03
	Low severity	6.14	0.04	6.64	0.04	6.60	0.04	6.71	0.07	6.45	0.02
	High severity	5.52	0.07	6.02	0.10	7.16	0.04	6.06	0.01	6.28	0.06
	Extreme severity	-	-	-	-	-	-	7.38	0.05	7.02	0.03
Microbial Biomass	Control	6.95	0.39	-	-	3.32	0.16	4.45	0.19	3.47	0.19
(µg C per g dry soil	Low severity	7.62	1.12	1.95	0.07	2.82	0.16	2.21	0.20	1.43	0.10
per hour)	High severity	2.04	0.16	3.46	0.36	6.83	0.49	2.58	0.38	1.13	0.14
	Extreme severity	-	-	-	-	-	-	9.27	0.81	7.73	0.55
C:N ratio	Control	31.36	0.62	-	-	-	-	-	-	-	-
	Low severity	40.79	1.03	26.93	0.88	82.89	11.13	-	-	-	-
	High severity	38.06	2.51	38.29	2.53	35.92	2.66	-	-	-	-
	Extreme severity	-	-	-	-	-	-	23.91	0.52	0.05	0.00
Available NH_4^+	Control	2.63	0.29	-	-	1.48	0.11	3.10	0.23	1.81	0.14

(µg NH_4^+ per g dry soil)	Low severity	1.71	0.09	6.80	0.44	3.71	0.50	2.36	0.15	4.62	0.64
	High severity	1.59	0.19	46.26	2.65	29.53	2.39	21.99	2.26	21.63	2.73
	Extreme severity	-	-	-	-	-	-	83.85	13.24	68.04	11.66
Available NO_3^- (µg NO_3^- per g dry soil)	Control	0.03	0.01	-	-	0.02	0.01	0.08	0.02	0.00	0.00
	Low severity	0.00	0.00	0.15	0.06	0.33	0.04	0.26	0.04	0.61	0.20
	High severity	0.00	0.00	0.00	0.00	0.01	0.01	0.16	0.09	0.01	0.00
	Extreme severity	-	-	-	-	-	-	0.17	0.06	30.20	0.29

Table S10. Mean daily net mineralization (µg of NH_4^+ plus NO_3^- per g dry soil per day) and nitrification rates (µg NO_3^- per g dry soil per day) with standard error for soil incubations. Wetted incubations were at 40% soil water holding capacity. The field-moist incubation was one week.

		1.5 mo. Postfire		6 mo. Postfire		9 mo. Postfire	
Incubation	Severity	Mean	SE	Mean	SE	Mean	SE
Mineralization: Field-moist	Control	-0.11	0.01	-0.10	0.02	-0.05	0.01
	Low severity	-0.16	0.03	-0.02	0.03	-0.03	0.03
	High severity	-0.87	0.09	-0.38	0.22	-0.16	0.11
	Extreme Severity	-	-	0.94	0.12	0.90	0.33
Mineralization: 1-week wetted	Control	-0.03	0.02	-0.03	0.02	0.02	0.03
	Low severity	0.26	0.04	0.54	0.09	0.09	0.05
	High severity	-1.02	0.19	-0.15	0.08	0.54	0.02
	Extreme Severity	-	-	2.91	0.44	-0.59	1.67
Mineralization: 3-week wetted	Control	0.06	0.05	-0.03	0.11	0.40	0.05
	Low severity	0.95	0.13	1.72	0.26	1.01	0.13
	High severity	-3.05	0.37	-3.51	0.53	-3.82	0.51
	Extreme Severity	-	-	-7.30	4.15	2.98	1.97
Nitrification Field-moist	Control	0.00	0.00	-0.01	0.00	0.00	0.00
	Low severity	0.03	0.01	0.17	0.03	-0.02	0.01
	High severity	0.00	0.00	-0.02	0.01	0.05	0.03
	Extreme Severity	-	-	1.38	0.65	-0.52	0.06
Nitrification 1-week wetted	Control	0.05	0.01	0.04	0.01	0.25	0.03
	Low severity	0.32	0.06	0.56	0.10	1.35	0.20
	High severity	0.01	0.00	-0.02	0.01	0.00	0.00
	Extreme Severity	-	-	3.14	1.06	0.23	0.34
Nitrification 3-week wetted	Control	0.15	0.02	0.00	0.00	0.41	0.05
	Low severity	0.40	0.03	0.41	0.12	0.54	0.06
	High severity	0.08	0.06	0.00	0.00	0.06	0.04
	Extreme Severity	-	-	2.12	0.13	-0.23	0.19

Supplementary Works Cited

Dickinson, M., L. Loncar, A. Reiner, S. Dailey, J. Bednarczyk, C. Drake, J. Gordon, M. Heckel, B. Kleckler, J. Miesel, and L. Wade. 2019. Fire Behavior Assessment Team (FBAT) Report. US Forest Service: 34.

U.S. Forest Service. 2021, March 3. FSGeodata Clearinghouse.

U.S. Geological Survey. 2019, March 21. Wildland Fire Decision Support System.

III. Chapter Two

Soil Heating in Fire (SheFire): a model and measurement method for characterizing soil heating and associated belowground responses in wildland fires

Mary K. Brady[1], Matthew B. Dickinson[2], Jessica R. Miesel[3], Carissa L. Wonkka[4], Kathleen L. Kavanagh[5], Alexandra G. Lodge[6], William E. Rogers[6], Heath D. Starns[7], Doug R. Tolleson[7], Morgan L. Treadwell[8], Dirac Twidwell[9], Erin J. Hanan[1]

[1]Department of Natural Resources and Environmental Science, University of Nevada - Reno, Reno, Nevada, USA

[2]US Forest Service, Northern Research Station, Delaware, Ohio, 43015, USA

[3]Department of Plant, Soil and Microbial Sciences, Michigan State University, East Lansing, Michigan, USA

[4]USDA, ARS, Northern Plains Agricultural Research Laboratory, Sidney, Montana, 59270

[5]College of Forestry, Oregon State University, Corvallis, Oregon, 97331, USA

[6]Department of Ecosystem Science and Management, Texas A&M University, College Station, Texas, 77843, USA

[7]Department of Ecosystem Science and Management, Texas A&M AgriLife Research, Sonora, Texas, 76950, USA

[8]Department of Rangeland, Wildlife and Fisheries Management Ecosystem Science and Management, Texas A&M AgriLife Extension Service, San Angelo, Texas, 76901, USA

[9]Department of Agronomy and Horticulture, University of Nebraska at Lincoln, Lincoln, Nebraska, 68588, USA

Abstract

Fire has transformative effects on soil physical, chemical, and biological properties in terrestrial ecosystems around the world. While methods for estimating fire characteristics and associated effects aboveground have progressed in recent decades, there remain major challenges in characterizing soil heating and associated effects belowground. Overcoming these challenges is crucial for understanding how fire influences soil carbon storage, biogeochemical cycling, and ecosystem recovery post fire. In this paper we present a novel framework for characterizing belowground heating and effects. The framework includes (1) an open-source model to estimate fire-driven soil heating, cooling, and the effects of heating across depths and over time (Soil Heating in Fire model; SheFire), and (2) a simple field method for recording soil temperatures at multiple depths using iButton sensors, self-contained temperature sensor and data loggers, installed along a wooden stake inserted into the soil (i.e., an iStake). The iStake overcomes many logistical challenges associated with obtaining temperature profiles with thermocouples. Heating measurements provide inputs to the SheFire model and modeled soil heating can then be used to derive ecosystem response functions, such as heating effects on microorganisms and tissues. To validate SheFire estimates, we conducted an experiment using a burn table where iStakes recorded temperatures that were used to fit the SheFire model. We then compared SheFire predicted temperatures against measured temperatures at other soil depths. To benchmark iStake measurements against those recorded by thermocouples, we co-located both types of sensors in the burn table experiment. We found that SheFire demonstrated skill in interpolating and extrapolating soil temperatures, with the largest errors occurring at the shallowest depths. We also found that iButton sensors are comparable to thermocouples for recording soil temperatures during fires. Finally, we present a case study using SheFire and iStakes to estimate soil heating during a prescribed fire. We predict how that heating would have influenced *Chamaecrista*

nictitans seed and tree root vascular cambium survival at different soil depths. This measurement-modeling framework provides a cutting-edge approach for estimating how fire energy transfers through a soil profile and predicting biological responses.

1. Introduction

Wildfires can transform soil biological, chemical, and physical properties which are critical to terrestrial ecosystem functioning (e.g., Giovannini et al. 1990, Neary et al. 1999, Robichaud 2000, Badía-Villas et al. 2014, Doerr et al. 2017). However, soil temperatures can vary by hundreds of degrees C within a given fire (Busse et al. 2013), which makes it challenging to generalize how soil properties may be transformed. Estimating belowground heat and mass transport, with associated temperature regimes, is essential to understanding how ecosystem services and processes, including carbon storage, primary production, and biogeochemical cycling, are changing across spatially complex fire footprints. Many effects of interest, such as effects on soil biota, occur as temperature-dependent rate processes (e.g., Rosenberg 1971) and, as such, characterizing temperature regimes is central to understanding fire effects on soils.

Several tools have been used to estimate fire effects, both above- and belowground. For example, some models have been developed to predict specific fire effects belowground given simulated, not measured, fire conditions. However, these models (e.g., Choczynska and Johnson 2009), though promising, are difficult to apply broadly given the range of required inputs. Further, the underlying soil heating models and associated software systems (e.g., FOFEM in Lutes 2017) have not been evaluated for use outside of the laboratory. Alternatively, remote sensing indices such as the difference normalized burn severity index (dNBR) can provide \ estimates of aboveground fire severity across ecosystems and landscapes. However, using these indices to assess belowground effects can have extremely high uncertainty because (1)

belowground fire effects do not always track predictably with fire energy (Hartford and Frandsen 1992) and aboveground changes such as vegetation mortality and charring of the soil surface (Hudak et al. 2007, Murphy et al. 2008), and (2) there can be large scaling mismatches between a remote sensing pixel (e.g., 30-m for Landsat) and processes that occur at the scale of microns to centimeters (Massman et al. 2010, Morgan et al. 2014, Regan et al. 2017, Ramcharan et al. 2018, Zhang et al. 2020). To address the first issue, some studies have used other remote sensing techniques, such as hyperspectral and multispectral imaging, which can be more sensitive to soil-specific changes (e.g., ash deposition and areas of bare ground; Kokaly et al. 2007). However, this is an imperfect solution because even soil-specific metrics are still derived from changes occurring at the surface and do not take into account belowground soil properties such as soil organic matter, which can influence how heat propagates through a soil profile (Morgan et al. 2014). While ground based (finer-scale) measurements of burn severity can help address scaling mismatches that occur with satellite data (issue 2 above), local severity estimates still lack mechanistic connections between the fire processes or properties and their effects belowground (Smith et al. 2016a).

Using direct measurements of fire behavior and energy to infer belowground responses is likely to be much more powerful than indirectly inferring belowground effects from coarse estimates of aboveground changes (Kreye et al. 2013, Quigley et al. 2019, Kreye et al. 2020). However, collecting direct measurements for fire energy and soil heating is challenging. For one, soil heating through time cannot be measured from satellite imagery and therefore, we need tools on the ground for quantifying heating during a fire (Morgan et al. 2014).

Given limited development of most of these measurement methods and logistical challenges associated with their use in the field, there remains a dearth of data on soils during fires. For unplanned fires, wildfires, access is often a primary limitation. Prescribed fires on the

other hand, are typically planned for years but are still often conducted on short notice when conditions are appropriate which can complicate sampling and site instrumentation. Considerably more attention has been paid to fire measurement than soil measurement development (see reviews in Kremens et al. 2010, Ichoku et al. 2012, Moran et al. 2019) and instrumenting a burn, whether planned or unplanned, can be equipment and time intensive (Ottmar et al. 2016). Finally, fire effects are highly spatially variable so it can be misleading to extrapolate data gathered in one area to try to understand another (Busse et al. 2013, Morgan et al. 2014, Smith et al. 2016b).

Thermocouples are the current standard for logging temperature measurements and have been used for decades (e.g., Iverson et al. 2004, Kennard et al. 2005, Bova and Dickinson 2008, Pereira et al. 2019). They record point-specific temperatures at discrete time intervals and can be placed at any soil depth of interest (Busse et al. 2010, Kreye et al. 2013, Kreye et al. 2020). However, using thermocouples for soil measurement can be time consuming as they require precision work to install in the field—a major drawback when attempting to install them under time constraints, such as instrumenting an advancing wildfire. Additionally, disturbing soil structure, as occurs with thermocouple installation, alters soil heating dynamics (Busse et al. 2010). The standard techniques for thermocouple installation reduce soil disturbance directly around the tip of the thermocouple by installing them through the side of an excavated hole and into the soil (e.g., Robichaud and Brown 2019), but these methods do not mitigate disturbance in close proximity to the sensor which can influence lateral heat transfer. Further, the canister designed by Robichaud and Brown (2019), that allows for ease of deployment, is constructed of metal, which may increase heat transfer into the soil along the can. Inserting insulated rods vertically into the soil with thermocouples exposed at specified depths (Kreye et al. 2020) offers promise, yet challenges in fire-hardening the system during intense fires remain. In this paper, we explore the use of iButtons exposed along wooden stakes (iStakes) as a way to minimize soil

disturbance, better match soil thermal properties, protect measurement devices from excessive heating, and increase efficiency of use for measuring soil heating during wildland fires. iButtons are integrated sensors and data loggers so there is no need to protect any additional equipment from heat (Maxim Integrated 2002).

Regardless of how the temperature data are collected, we need tools for applying them. Attempts to understand how fire-induced heating affects soil properties must take soil depth into account—because in addition to heating, soil properties such as microbial processes, biogeochemical cycling, and soil organic matter also vary with depth (e.g., Achat et al. 2012, Balesdent et al. 2018, Kramer et al. 2017). Physical models of soil heating have potential to characterize soil heating and mass transport at high depth resolution (e.g., Campbell et al. 1997, Massman et al. 2010) but they require much more development for practical use. Alternatively, instrumenting every possible soil depth of interest to directly record temperatures in the field is not feasible either. In order to quantify fire effects on soil properties and biota, as well as to provide validation data for physical models, we need a statistical model that can interpolate and extrapolate temperature regimes to a depth of interest based on a limited set of measurements taken at discrete soil depths.

Thus, the goals of this paper are twofold: to present an open-source modeling tool to understand soil heating and heating effects across depths over time (Soil Heating in Fire; SheFire), and to demonstrate a novel data collection method which minimizes soil disturbance and installation time (iStakes). To support this measurement-modeling framework, we describe a burn table experiment used to validate SheFire temperature estimates at different soil depths and to benchmark our iStake method against thermocouple readings. Finally, we present a case study using iStakes and SheFire to estimate soil heating during a prescribed fire and predict how heating may influence seed and root survival at different soil depths using a thermal tolerance

model (Dickinson et al. 2004). The thermal tolerance model is based on a temperature-dependent rate process and associated data. It offers a way to clarify the effects of the highly variable temperature regimes to which soil biota are exposed.

2. Methods

Below, we describe the SheFire modeling framework (section 2.1), and a measurement method, iStakes, which provides one way to easily collect the data needed as input to fit the SheFire model (section 2.2). All soil depths discussed in this paper refer to the depth below the mineral soil surface as the forest floor can combust during fires.

2.1. SheFire model description

SheFire is a modeling framework for elucidating mineral soil temperatures during fire across a range of soil depths. It also enables researchers to predict biological responses to soil heating. Fitting the SheFire model requires temperature measurements over time from three different soil depths at the same location. The model then interpolates and extrapolates from those data to estimate temperature time series across a range of depths. Using those estimates, functions in the model framework can then be used to explore the nuances of the soil heating and biological responses. The current response functions focus on organismal thermal tolerance but the SheFire modeling framework can readily be expanded in a modular fashion to incorporate additional response functions that are of interest to model users. The different components of the modeling framework are described in the following sections. The modeling framework is contained in an R package, called SheFire, comprised of the model building function (*shefire*), and a series of summary and response functions that evaluate and apply the SheFire model object to understand soil heating and its effects.

2.1.1 Fitting the model

Input Data

Heat transfer through a soil profile is both soil- and fire-specific (Abu-Hamdeh and Reeder 2000, Abu-Hamdeh 2003, Kreye et al. 2013, Busse et al. 2013, Smith et al. 2016b, Pereira et al. 2019). As a result, the SheFire model must be fit separately for each location from measured temperature data. The model is fit using the *shefire* function in the R package. The inputs to this function are the temperature data and a series of parameters that allow for model fine tuning. The parameters are described in detail in supplementary Table S1. The model requires temperature recordings from three soil depths which can be measured with thermocouples, iButtons, or any other temperature sensor that records a time stamp with each temperature reading. The input data can have any data logging rate, but the three sensors must log at the same rate.

Data Trimming

The input temperature data do not need to be manually cleaned or trimmed to the beginning and end of the fire effects prior to building the model, however, they must all start at the same point in time. The function is designed to extract the fire induced heating and subsequent cooling period from data sets that may contain measurements collected prior to the arrival of the flaming front and after complete soil cooling. With default settings, the prefire data (i.e., everything up to 30 minutes preceding the initiation of soil heating) is removed. Initiation is defined as the last time that the temperature rate of change between two sequential measurements was zero before the maximum temperature was reached. The end of the data is determined by the first of the following events: a temperature rise after soil cooling has begun, a user-determined cut off time, or the end of the data set. All three temperature recordings must cover the same time period so the shallow sensor is used to set the start and end points, as it will be the first to heat, then the data from the deeper two sensors are trimmed to match.

Fitting BFD curves to input data

The base equation of the model is a "Temperature - Time Curve of Complete Process of Fire Development", also known as a BFD curve, which was developed for studying compartment fires in buildings (Barnett 2002) but has been used in other studies of fire and soils (Adie et al. 2011, Grau-Andrés et al. 2017, Massman 2021). BFD curves calculate temperature at a given time. Note that the nomenclature from here on follows that used in the SheFire R package for reasons of clarity.

A BFD equation has four terms that correspond to: initial temperature before the arrival of the flaming front (*InitTemp*), maximum temperature reached (*MaxTemp*), time the maximum was reached after heating began (*TimeAtMax*), and a shape parameter that determines the overall shape of the curve (*Shape*; equation 1 in Barnett 2002):

$$Temperature = InitTemp + MaxTemp \text{ x } e^{-z} \quad (1)$$

where *e* is Euler's number and the exponent (*z*) is further defined as:

$$z = \left(ln(time) - ln(TimeAtMax)\right)^2 \Big/ Shape. \quad (1a)$$

BFD equations are fit to each of the three trimmed input temperature recordings. We designed SheFire to use a nonlinear least squares approach to determine the best fit.

Fitting parameter-depth regressions

We then have SheFire extract the four BFD parameters (*InitTemp*, *MaxTemp*, *TimeAtMax*, and *Shape*) from each of the three fitted equations. Using the three values for each parameter, one from each input sensor depth, SheFire fits separate regression equations to estimate each parameter value for given soil depths, using the following equations:

$$InitTemp = A \text{ x } depth^{-B} \quad (2)$$

$$MaxTemp = e^{C} \text{ x } depth^{D} \quad (3)$$

$$TimeAtMax = F + G \text{ x } depth \quad (4)$$

$$Shape = H \text{ x } depth^{-1} \quad (5)$$

where *depth* is the soil depth for which the BFD equation parameter will be calculated (equations 2-5). These regression equations allow a BFD parameter to be estimated for any input soil depth.

Equations 3 and 4 are fit using a simple linear model and subsequently evaluated for model performance by calculating R^2, the coefficient of determination. The data for equation 3 are log transformed before fitting. Equations 2 and 5 are fit using a nonlinear least squares approach. They are subsequently evaluated with a Pearson correlation coefficient comparing the BFD parameter values from the equations fit to the input data against the parameter values calculated by the regression equations for the same soil depths as the input data.

Once the regression equations have been fit, the model can estimate each of the four BFD parameters for a given soil depth and thus can model temperature over time at any depth.

Setting model constraints

The final portion of model development sets constraints for the model. The time range that the model covers is equal to the time range of the trimmed input data. This may not be the full length of the input data sets if they covered prefire or post-cooling periods. SheFire also extracts the timestamp associated with the model start and end points from the input data to allow model-time to real-time conversions. To avoid mathematical problems associated with zero values, model time starts at 0.0001 minutes. SheFire sets the shallowest depth for which the model can predict temperatures as the depth for which the *TimeAtMax* parameter is 1. That is to say, the soil depth that reaches its peak temperature one minute after the beginning of model time is the shallowest depth that the model can calculate. A time cut off is used to set the shallowest depth because increasingly shallow depths have increasingly early peak temperatures. See supplementary section S1: *Model implementation* for comments on the issues concerning this approach. There is no deepest depth limit but the summary and response functions in SheFire will

print a warning for soil depths more than 5 cm deeper than the deepest sensor used to build the model because deep predictions have not yet been experimentally validated.

Model output

The *shefire* function outputs a list of the various equations, values, and constraints that comprise the model (Table 1). The summary and response functions included in the SheFire modeling framework can be applied to this output to explore soil heating, cooling, and biological responses. Users can also build custom functions that interact with the model to address specific research questions. Further details are in supplementary section S1: *Model implementation*.

Table 1. Names and descriptions of *shefire* function outputs. These are needed to run the summary and response functions included in the SheFire modeling framework.

Name	Description
BFDEquation	Function to calculate temperature over time given values for the four BFD parameters
MaxTemp.reg	Function to calculate MaxTemp parameter for a given soil depth
TimeAtMax.reg	Function to calculate TimeAtMax parameter for a given soil depth
Shape.reg	Function to calculate Shape parameter for a given soil depth
InitTemp.reg	Function to calculate InitTemp parameter for a given soil depth
MaxTemp.coeffs	Coefficient values for the MaxTemp.reg function
TimeAtMax.coeffs	Coefficient values for the TimeAtMax.reg function
Shape.coeffs	Coefficient values for the Shape.reg function
InitTemp.coeffs	Coefficient values for the InitTemp.reg function
InitTemp.byDepth	An additional parameter needed for InitTemp.reg function – a list of InitTemp values calculated for the input temperature data
sensorDepths	An additional parameter needed for InitTemp.reg function – a list of sensor depths
Shallowest	The shallowest depth (in cm) for which the model will calculate temperature over time
FullTime	Duration (min.) that the model covers
StartTime	Timestamp at the beginning of the model time range
EndTime	Timestamp at the end of the model time range

2.1.2 Heating summary functions

The SheFire modeling framework includes a set of functions to summarize different aspects of soil heating and cooling (Table 2). The most basic function is *temp_over_time*, which calculates temperature at a given depth at a specified time resolution. This function is called in all other

summary and response functions. More details about specific summary functions and their implementation can be found Table 2.

Table 2. The summary functions included in the SheFire modeling framework. The function name, description, and output are included.

Function Name	Description	Output
temp_over_time	Calculates temperature over time for a specified soil depth, time range and resolution (i.e., temperature at every 1 minute)	A list of the temperature values at each time increment
time_above	Calculates the duration of time at or above a chosen temperature threshold, for a specified soil depth	Duration in minutes
heating	For a specified soil depth, isolates the portion of the model time range that the soil is heating	A list of temperatures at the specified time resolution for the soil depth from the point that it began to warm through the time when it reaches its maximum temperature
cooling	For a specified soil depth, isolates the portion of the model time range that the soil is cooling	A list of temperatures at the specified time resolution for the soil depth from the point it began to cool through the end of model time range
time_temp_ranges	Calculates the time spent in different temperature ranges for a specified soil depth. The breadth of the temperature ranges, but not the boundary temperatures dividing the ranges, is set by the user	A data frame of the temperature boundary values and the time spent in each temperature range
set_temp_ranges	Calculates the time spent in different temperature ranges for specified soil depth(s). User sets the boundaries for the temperature ranges	A data frame of the temperature boundary values and the time spent in each temperature range (for each specified depth)
depth_for_temp	Calculates the deepest soil depth that reaches a specified temperature	The soil depth (cm)
summ_depth_range	Calculates the mean, standard deviation, median, and maximum temperature at each time point for a specified portion of the soil profile	A data frame containing those statistics for the depth range at each time point

2.1.3 Heating response functions

The SheFire modeling framework currently includes two response functions (*survival_percent* and *survival_depth*) that use soil heating to estimate survival. *Survival_percent* calculates the percent survival at the user specified depth. *Survival_depth* determines the soil depth at which a user specified percent survival will occur. For example, *survival_percent* could determine the percent survival for a particular species of seed at 5 cm depth, while *survival_depth* could be used to find the soil depth where 85% of those seeds survived. We demonstrate these functions in the case study by estimating survival of seeds and vascular cambium cells from soil temperature regimes in a prescribed fire.

The two functions rely on a thermal tolerance model for estimating survival (Dickinson et al. 2004). Survival can be thought of as a general dimensionless effects variable where response to heating is quantified relative to pre-fire condition. Thermal tolerance is based on temperature-dependent rate processes, the kinetics of which have been quantified in various ways for different biological systems, including by tissue respiration (Caldwell 1993, Dickinson et al. 2005), protein denaturation (Rosenberg et al. 1971), cell survival (Lorenz 1939, Dickinson and Johnson 2004), tissue survival from visual inspection or vital staining (Lorenz 1939, Nelson 1952), and organismal survival (Martin et al. 1969).

The thermal tolerance model is solved numerically in two parts: determining the rate of impact and accumulating that impact over time. We determine the rate of impact from a temperature-dependent first-order rate process equation, termed the “absolute rate theory equation” by Rosenberg et al. (1971). This equation has two parameters that must be estimated for each unique biological system: activation entropy (*deltaS*), and activation enthalpy (*deltaH*). These parameters are determined statistically from thermal tolerance data (Dickinson and Johnson 2004). If needed, a user could incorporate a simpler, single-parameter rate equation (the

Arrhenius equation) into SheFire, opening up more sources of rate process information (Dickinson et al. 2005). The rate of impact increases exponentially with temperature:

$$k = \frac{kBoltz\ T}{hPlanck} \text{ x } e^{\left(\frac{deltaS}{RGas}\right)} \text{ x } e^{\left(\frac{-deltaH}{RGas\ T}\right)} \quad (6)$$

where *k* is the rate parameter (s^{-1}), *kBoltz* is the Boltzman constant ($J*K^{-1}$), *T* refers to soil temperature in Kelvin, *hPlanck* is Planck's constant ($J*s^{-1}$), and *RGas* is the universal gas constant ($J*K^{-1}*mol^{-1}$). The accumulation of the temperature effects is assumed to be additive with no effect reversal (see Dickinson and Johnson 2004)). Thus, survival is recursively decremented at each timestep at a temperature dependent rate. Survival begins at 100 percent:

$$S_{current} = S_{previous} - k \text{ x } t_{length} \text{ x } S_{previous} \quad (7)$$

where $S_{current}$ is survival up through the current time step, $S_{previous}$ is survival up through the preceding time step, and t_{length} is the length of the time step in seconds. Survival is not decremented at temperatures below the user specified threshold. The temperature threshold is the lowest temperature at which there would be a temperature effect on survival for the biological system of interest.

2.2 iStake description

iButton sensors are small, cylindrical devices approximately 1.5 cm in diameter and 0.5 cm width that measure and record temperature. There are a few different models but the two relevant here are the high temperature iButtons (Thermochron 8K High) and the low temperature iButtons (Thermochron, 4K). High temperature iButtons will record temperatures when the sensor is between 0 °C and 125 °C while the low temperature iButton will record when it is between -40 °C and 85 °C.

The iStakes are composed of a simple wooden stake with iButton temperature sensors installed across their width such that the iButtons surfaces are flush with the outside of the stake to provide thermal contact with the soil (Figure 1). Therefore, with a single stake inserted into the

ground, temperatures at multiple soil depths can be measured simultaneously with minimal soil disturbance (Figure 2A). A full description of iStake construction and field deployment is in supplementary section S2: *iStake construction and field deployment*.

It is important to benchmark iButtons against thermocouples because different devices deployed in different ways can result in different temperature measurements because the temperature recorded is the temperature of the device (Kennard et al. 2005, Bova and Dickinson 2008). A key advantage of measuring temperatures in soils is that, as long as there is good thermal contact between the device and the soil, the device temperature should faithfully reflect soil temperature. Thin thermocouples or thin thermocouple probes (a thermocouple sheathed in, typically, stainless steel) maximize thermal contact with soil and provide a point measurement. A disadvantage of an iButton is that it is in contact with soil over both its front and back surfaces and will not be a point measurement. Instead, given the high thermal conductivity of its metal case, its temperature will average over 1.5 cm of the soil column which could lead to different readings than thermocouples. Further, an iButton has more thermal inertia than a thin thermocouple or thermocouple probe and may heat and cool more slowly.

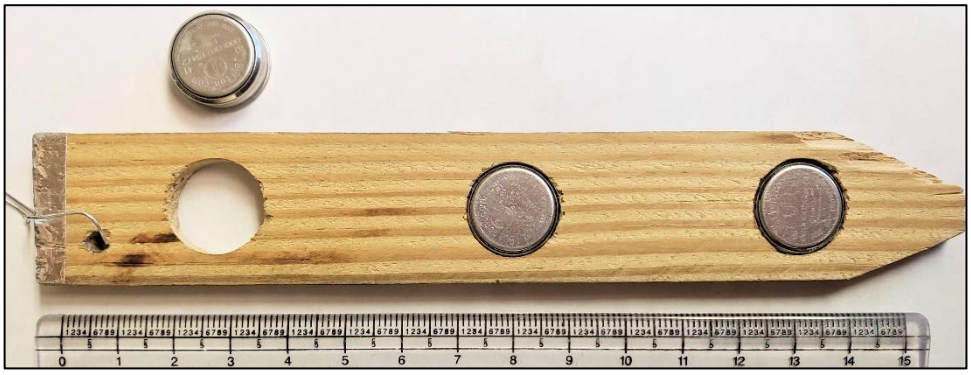

Figure 1. A complete iButton stake that will measure soil depths 5, 10, and 15 cm when installed with the top of the stake (picture left) 2 cm below the soil surface.

2.3 Validation and benchmarking

To validate the SheFire model and benchmark iButton readings against thermocouple readings, we conducted instrumented test burns. The test burns used a burn table set-up that consisted of a metal frame that held ceramic fiber boards flush with the top of 20 cm tall, 10 cm diameter cans filled with soil (Miesel, unpublished; Figure 2B and 2C). We drilled 10 cm diameter holes in the ceramic board using a circular drill bit such that four cans fit in each ceramic board. The open tops of the cans sat flush with the top surface of the board and the sides of the cans were flush against the inside of the holes in the board so there was no gap between the edge of the board and the sides of the can. The top of the soil, inside the cans, was continuous with the top surface of the ceramic board.

The cans, below the ceramic board, were wrapped in ceramic fiber insulation and a layer of fire-shelter insulating material. The insulation was designed to minimize lateral heat gain or loss from the soil so that heat transfer was primarily vertical through the soil. This was designed to mimic soil in situ, which would not be isolated in columns and would heat and cool with the surrounding soil. The cans of soil, while not perfect facsimiles of a continuous soil bed, enabled reliable, precise sensor installation with minimal soil disturbance around the thermocouples.

Once the cans were situated in the burn table, we installed the temperature sensors. For the model validation experiment described in section *3.2.1.* we installed one iStake with iButtons at 5, 10, and 15 cm below the soil surface and one iStake with iButtons at 4, 7, and 12 cm deep per can. There were nine cans and thus nine replicate paired iStakes. High temperature iButtons were used at 4 and 5 cm depths, while low temperature iButtons were used at all other depths. For the benchmarking experiment described in *3.2.2.* we installed an iStake in each can with iButtons at 5, 10, and 15 cm below the soil surface and we installed thermocouples at the same depths

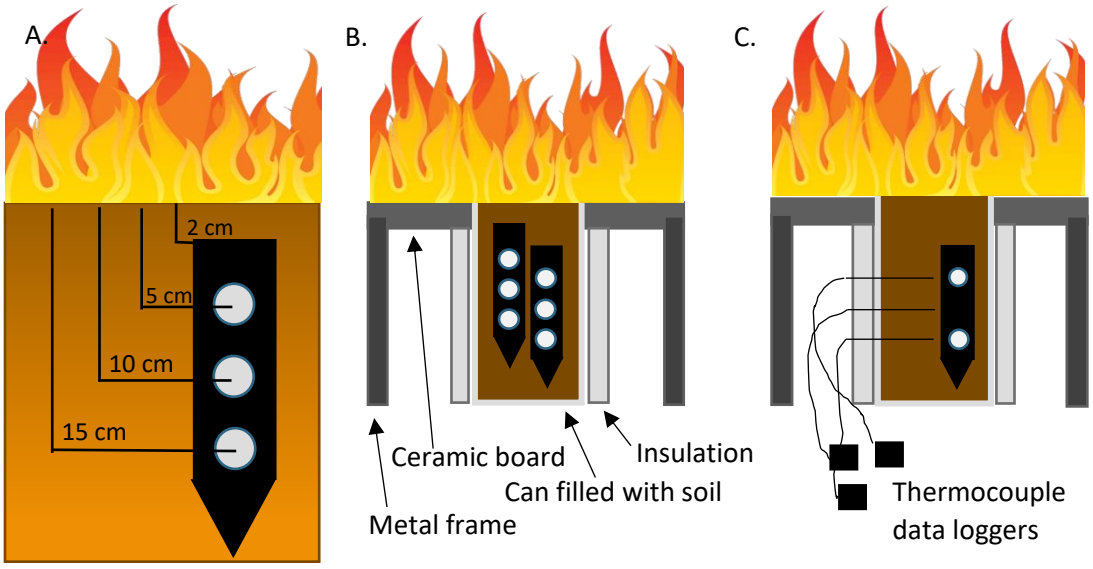

Figure 2. A. Diagram of standard iButton stake deployment in the field and within the soil cans. B. Diagram of experimental set up for comparing model predictions against measured temperatures. C. Diagram of experimental set up for comparing iButtons against thermocouples. Diagrams are not to scale.

through small holes drilled in the sides of the can. There were 15 cans prepared in this manner. All thermocouples used were type K (Omega Engineering, Norwalk, CT) thermocouple probes (1.6 mm diameter) and thermocouple data loggers were Madge Tech TC101A (Madge Tech, Warner, NH). High temperature iButtons were used at 5 cm deep, low temperature iButtons were used at 10 and 15 cm deep.

After we instrumented the insulated, soil-filled cans, we placed a fuel bed, containing a mixture of dry pine needles, woodchips, and small twigs (less than 2 cm diameter), loosely stacked on top of the soil and ceramic boards. For each of the experiments described in *2.3.1*. and *2.3.2*, we ignited the fuel bed and supplied additional fuels as needed to maintain active flames for approximately 10 minutes and then allowed the fire to reach extinction, and the soils to cool for several hours so that the entire recorded dataset (starting 10 minutes prior to ignition) was 350 minutes long. The burns were conducted over the course of three days in October 2020.

2.3.1 SheFire validation

For each replicate of paired iStakes, we used the data recorded at 5, 10, and 15 cm deep to fit the SheFire model. We then used the model to predict soil temperatures at 4, 7, and 12 cm deep and compared those predictions against the temperatures recorded at those depths. We compared model predictions against the recorded temperatures using Pearson correlation coefficient, R^2, and root mean square error (RMSE). The 4, 7, and 12 cm comparisons were all analyzed separately in order to determine how the model performed at different depths. Due to sensor malfunctions, we only tested the 4 cm deep predictions in four of the nine replicates.

While the insulation surrounding the cans mitigated the heat transfer between the soil and air, it did not eliminate it and the soil slowly heated throughout the day in a manner that is inconsistent with soil temperatures recorded in situ during wildfires. This was evident from the soil cooling pattern postfire (supplementary Figure S1). To account for this shifting temperature baseline, we adjusted the data used to build and test the model by fitting a linear regression line between the soil temperature before ignition and the soil temperature at the end of the cool down period and then subtracting the value on the regression line from the temperature recorded at each time step. Then, we added 5 °C to the temperatures to ensure final adjusted temperatures were > 0. See supplementary Figure S1 for a comparison of adjusted and unadjusted temperatures over time from one replicate.

2.3.2 Sensor benchmarking

To benchmark iButtons against thermocouples we had 15 replicates of iStakes paired with sets of thermocouples (Figure 2C). In each replicate, we used both iStakes and thermocouples to record temperatures at 5, 10, and 15 cm depths. For analysis, the readings at 10 cm and 15 cm were combined because they were both measured with low temperature iButtons. The 5 cm readings were analyzed separately because they were recorded using high temperature iButtons. Due to sensor malfunctions, the 5 cm comparisons were included in 14 of the 15 replicates. Thus, there

were 30 paired low temperature iButtons and thermocouple comparisons and 14 paired high temperature iButtons and thermocouple comparisons.

The thermocouple and iButton readings were compared at each timestep within each iButton – thermocouple pair using Pearson correlation coefficient, R^2, and RMSE. While each sensor pair is independent, the temperature points within a paired set of sensors are not. To address this, we also fit BFD equations to the data from each sensor. Then the BFD equation parameters were compared between the paired iButtons and thermocouples to measure how the recorded temperatures differed as a set and not just at individual time steps. In order to fit the BFD equations with the *shefire* function, both the iButton data and the thermocouple data were adjusted using the method described in *2.3.1.* to account for the solar heating that occurred over the course of the experiment. We ran *shefire* function with the *reg* parameter set to False so that it only fit the BFD equations and used the *override.clip* option for both iButton data and thermocouple data which prevents the model from shortening the data set based on rising temperatures after the maximum temperature is reached. This *override.clip* option was necessary because some of the thermocouple data were noisy enough that the model attempted to clip those datasets shorter than the iButton data. Details on the model fitting parameters can be found in supplementary Table S1.

3. Results

3.1. SheFire validation

The SheFire predictions at 12 cm were more accurate than at 7 cm and 4 cm, however, model predictions at both 7 and 12 cm demonstrated a high level of skill (Table 3; Figure 3). The 4 cm predictions fared the worst of the three but the Pearson correlation coefficient and R^2 were still high at above 0.9 (Table 3). The RMSE was highest for 4 cm at 3.6 °C and lowest for 12 cm at

0.7 °C (Table 3). The predicted temperatures do not differ consistently from measured temperatures across depth: the times (i.e., heating, peak temperature, cooling, etc.) and characteristics (i.e., earlier, later, warmer, cooler) in which they differ are a result of the subtle variations between each temperature record and not a systemic difference between predictions and measurements (Figure 3). Additional information on results by replicate, calculated with both the unadjusted and adjusted temperatures, is provided in supplementary Table S2.

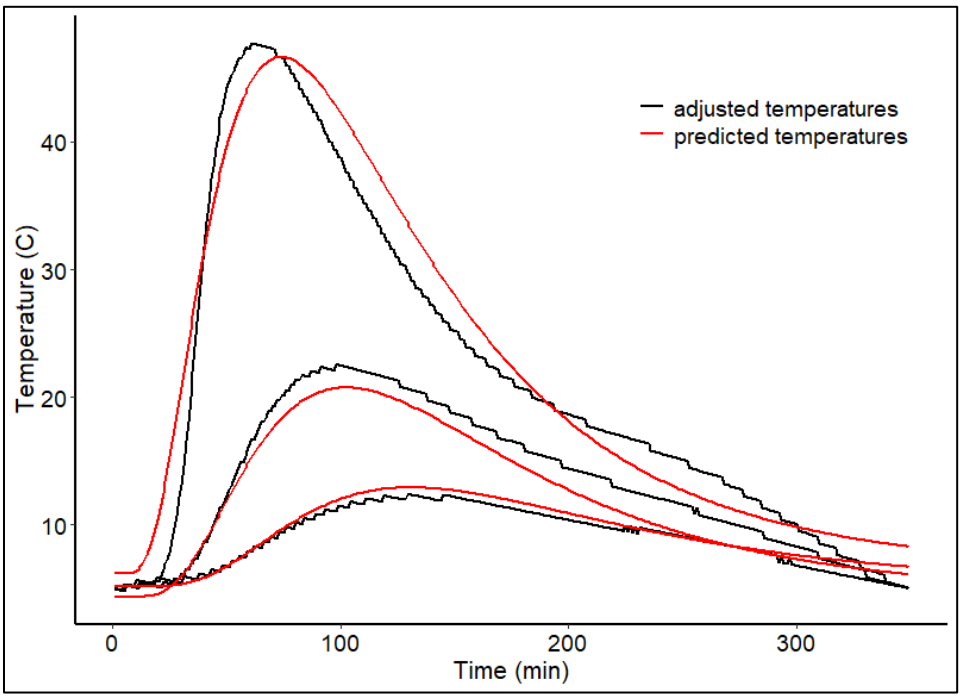

Figure 3. Adjusted temperature measurements (black) and model predictions (red) for soil depths 5, 10, and 15 cm deep from an example replicate. The topmost pair of curves are 5 cm, the middle pair are 10 cm, and the bottom pair are 15 cm depth.

Table 3. A summary of the model predictions compared against actual measurements showing the Pearson correlation coefficient, R^2, and the RMSE. The mean value and standard error are given for each statistic within each depth category.

	12 cm (N = 9)			7 cm (N = 9)			4 cm (N = 4)		
	Pearson	R^2	RMSE	Pearson	R^2	RMSE	Pearson	R^2	RMSE
Mean	0.98	0.97	0.66	0.98	0.96	1.50	0.96	0.92	3.56
Stnd Error	<0.01	<0.01	0.09	0.01	0.01	0.15	0.01	0.01	0.51

3.2. Benchmarking

The high temperature iButtons did not match thermocouples quite as tightly as the low temperature iButtons (Table 4; Figure 4A). The high temperature iButtons and the thermocouples had mean RMSE of 2.1 °C and the low temperature iButtons and the thermocouples had a mean RMSE of 0.9 °C (Table 4). While the high temperature iButton readings did differ more from thermocouples than the low temperature iButton readings, the difference was small and both types of iButtons recorded temperatures that were in close agreement to thermocouples. A full list of comparisons for each sensor pair can be found in supplementary Table S3.

Table 4. Statistical comparisons of thermocouple versus iButton readings on a point-by-point basis. The mean value and standard error is shown for each statistic in the two sensor categories. A table containing the statistics for each replicate can be found in Appendix S4: Table S2.

	low temperature iButtons vs thermocouples: 30 trials	high temperature iButtons vs thermocouples: 14 trials
Pearson	0.98 +/- <0.01	0.97 +/- 0.01
R^2	0.97 +/- 0.01	0.94 +/- 0.02
RMSE	0.87 +/- 0.08	2.11 +/- 0.32

When comparing iButton vs. thermocouple timeseries estimates, we subtracted the iButton BFD parameter values from the thermocouple BFD parameters to quantify the difference between the two. *Shape* was the parameter with the smallest difference for both low and high temperature thermocouples (Table 5). The BFD parameters fit to the iButton and thermocouple data matched well for *InitTemp* where the mean difference was smaller than 0.6 °C for both iButton types (Figure 4B). The *MaxTemp* parameters had slightly larger differences. Here the larger difference was for the high temperature iButtons which had a 4.2 °C higher *MaxTemp* parameter, on average, than the BFD curves fit to the thermocouple readings. Thermocouples had *TimeAtMax* values 3.3 minutes later than the low temperature iButtons and 7.6 minutes later than the high temperature iButtons. The list of all BFD parameters fit to each sensor, organized by both depth and by thermocouple - iButton pairs, can be found in supplementary Table S4.

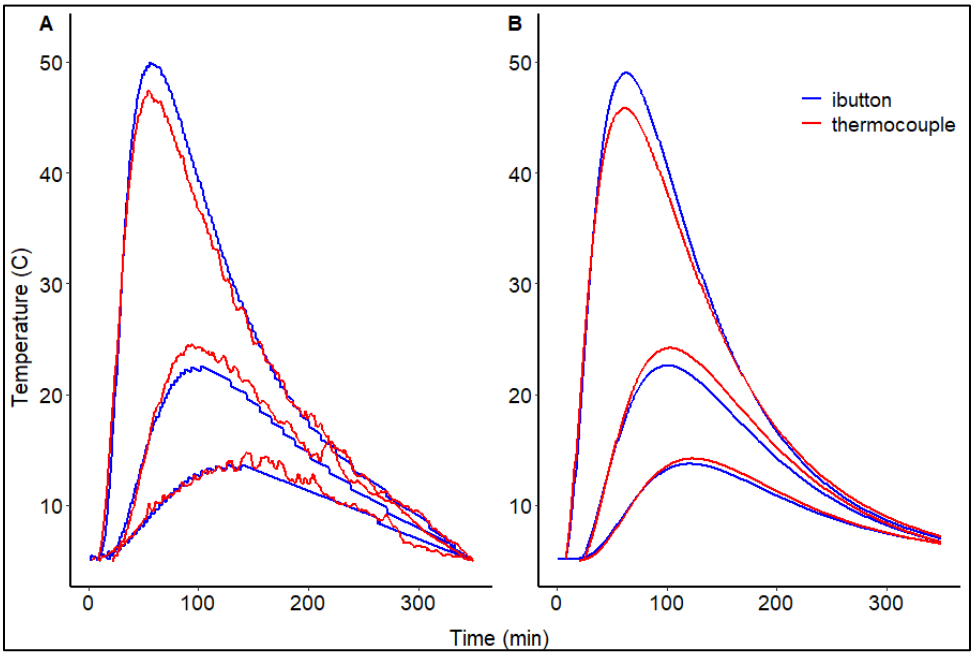

Figure 4. A. Thermocouple (red) and iButton (blue) readings adjusted to shifting temperature baseline for an example replicate. B. BFD equations fit to thermocouple (red) and iButton (blue) readings from the same replicate. The topmost pair of curves are 5 cm, the middle pair are 10 cm, and the bottom pair are 15 cm depth.

Table 5. The mean value and standard error for the BFD parameters fit to thermocouple readings minus the BFD parameters fit to iButton readings within a thermocouple - iButton pair. The values are grouped by the sensor depth of the thermocouple - iButton pairs. A table showing the BFD parameters fit to the data from every sensor, organized by thermocouple - iButton pairs, is included as Appendix S4: Table S3.

iButton Type	InitTemp			MaxTemp			TimeAtMax			Shape		
High Temp.	0.13	+/-	0.29	-4.19	+/-	3.77	7.63	+/-	5.93	-0.09	+/-	0.06
Low Temp.	-0.50	+/-	0.22	1.15	+/-	1.56	3.33	+/-	3.55	0.04	+/-	0.05

4. Case Study

We used data from work done at the Texas A&M Agrilife – Sonora Research Station to demonstrate a simple application of the SheFire framework. This study was originally conducted for other purposes in the summer of 2018. The site is located on the western edge of the Edwards Plateau ecoregion. It is a semi-arid savanna with a bimodal precipitation pattern. The dominant vegetation includes a mix of trees (*Quercus, Juniperus,* and *Prosopis* species) and grasses. The

soils are Tarrant series (Clayey-skeletal, smectitic, thermic Lithic Calciustolls), shallow, and often have limestone bedrock (USDA 2016, Hiers et al. 2019).

In this project, small, controlled burns were conducted with either high or low fuel loads to create different burn conditions. Each burn was 100 m^2 and had an iButton stake installed with sensors at 5, 10, and 15 cm deep in the soil. Here, we present data and the SheFire model from two of the burns: one plot with a high fuel load (HF), and one with a low fuel load (LF). The LF plot received approximately 61 kg of hay as additional fuel, the HF plot received both 61 kg of hay and 201 kg of juniper branches as additional fuel. We fit the SheFire model using default parameter values for both plots. For more information on the design and objectives of the original study, please see Hiers et al. (2019).

For the BFD equations fit to the input data, the HF plot had low RMSE between the fitted BFD equation and the input data with the largest value of 0.55 °C at 5 cm (Table 6). The LF plot also had low RMSE values at all three depths but they were slightly higher than the HF plot with the largest RMSE for LF at 2.25 °C for 5 cm (Table 6). In both plots, the best BFD fits for the input data were at 15 cm, then 10 cm, and 5 cm deep.

Table 6. The model fit information for the LF and HF plots. BFD fit refers to the fit between the input data and the fitted BFD equations. The regression fit measures the fit between the parameters calculated directly by fitting a BFD equation to the input data and the parameters calculated using the parameter-depth regressions.

	Low Fuel (LF)		High Fuel (HF)	
BFD fit	RMSE	Pearson	RMSE	Pearson
5cm	2.25	0.99	0.55	0.98
10cm	1.19	0.98	0.23	0.99
15cm	0.50	0.99	0.15	0.98
Regressions	Statistic	Value	Statistic	Value
MaxTemp	R^2	>0.99	R^2	0.99
InitTemp	Pearson	0.98	Pearson	>0.99
TimeAtMax	R^2	0.99	R^2	>0.99
Shape	Pearson	>0.99	Pearson	>0.99

The parameter-depth regression equations correlated strongly with the BFD parameters that were calculated to fit to input data (Table 6). We assessed the fit for linear relationships (i.e., *MaxTemp* and *TimeAtMax*) using R^2 and non-linear relationships (i.e., *InitTemp* and *Shape*) using Pearson's correlation coefficient. All four BFD terms' regressions had R^2 or Pearson's correlation coefficients at 0.98 or above in both the HF and LF plots (Table 6). The output tables from *shefire* of all fit statistics for each plot can be found in supplementary Table S5 and S6.

To be concise in this case study, we visually compare measured and predicted soil heating for a selection of soil depths across the LF and HF plots (Figure 5). The temperature over time for each depth was calculated using the *temp_over_time* function. The differences in soil temperatures experienced by the two plots were largest in shallow soils: at 3 cm depth in the HF plot, soil temperatures reached over 100 °C but did not even heat to 40 °C at that depth in the LF plot (Figure 5). The duration of heating also differed between the two plots. At 3 cm depth, within 250 minutes, the HF plot cooled to approximately 50 percent of its maximum temperature, while the LF plot had barely begun to cool by 250 minutes (Figure 5).

Although there are many possible fire-effect applications of the SheFire model, we will focus on *survival_percent* for the sake of brevity. Given a sparse literature on thermal tolerance (Dickinson et al. 2005), there are no thermal tolerance data available for the plant present in these plos. Therefore, we demonstrate the utility of this function by showing how contrasting thermal tolerances and variable soil heating affect response for sensitive partridge pea seeds (*Chamaecrista nictitans*, previously *Cassia nictitans*; Martin and Cushwa 1966, Martin et al. 1969), and Douglas fir (*Pseudotsuga menziesii*) and trembling aspen (*Populus tremuloides*) stem vascular cambium cells (Dickinson and Johnson 2004). Sensitive partridge pea (from here on partridge pea) seed survival is based on percent germination after heating treatments (see Martin and Cushwa 1966). Vascular cambium cell survival is based oncounts of dead and live cells based

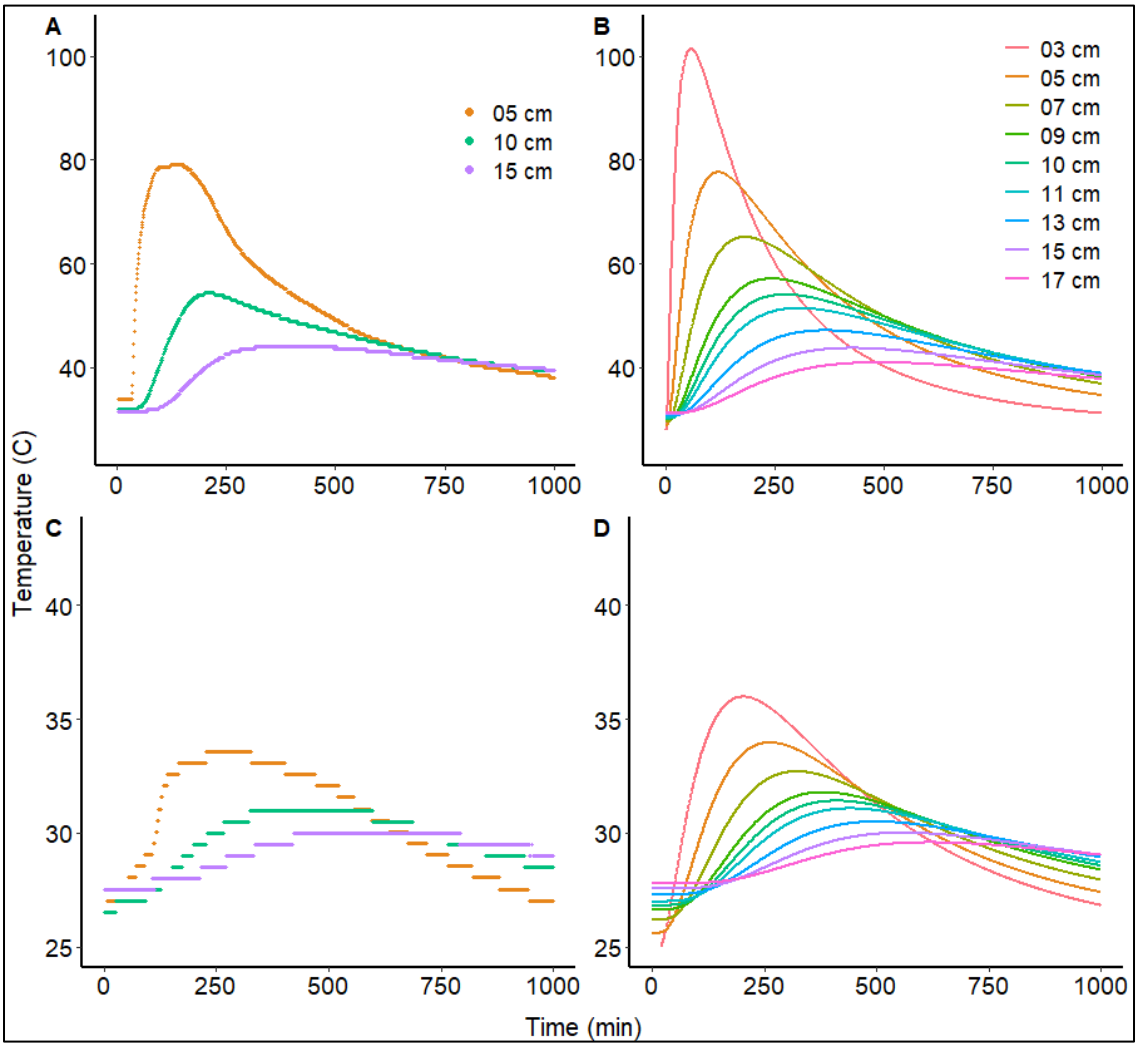

Figure 5. A. Raw temperature data recorded in the HF plot. B. Model predictions for a range of soil depths for the HF plot. C. Raw temperature data recorded in the LF plot. D. Model predictions for a range of soil depths for the LF plot.

on vital staining (Dickinson and Johnson 2004). Because no suitable data on root thermal tolerance exist and to demonstrate the application, we assume that root vascular cambium has a similar heat tolerance to stem vascular cambium. Parameters for the rate process equation (Equation 6) for partridge pea seeds and vascular cambium tissue are in supplementary Table S7.

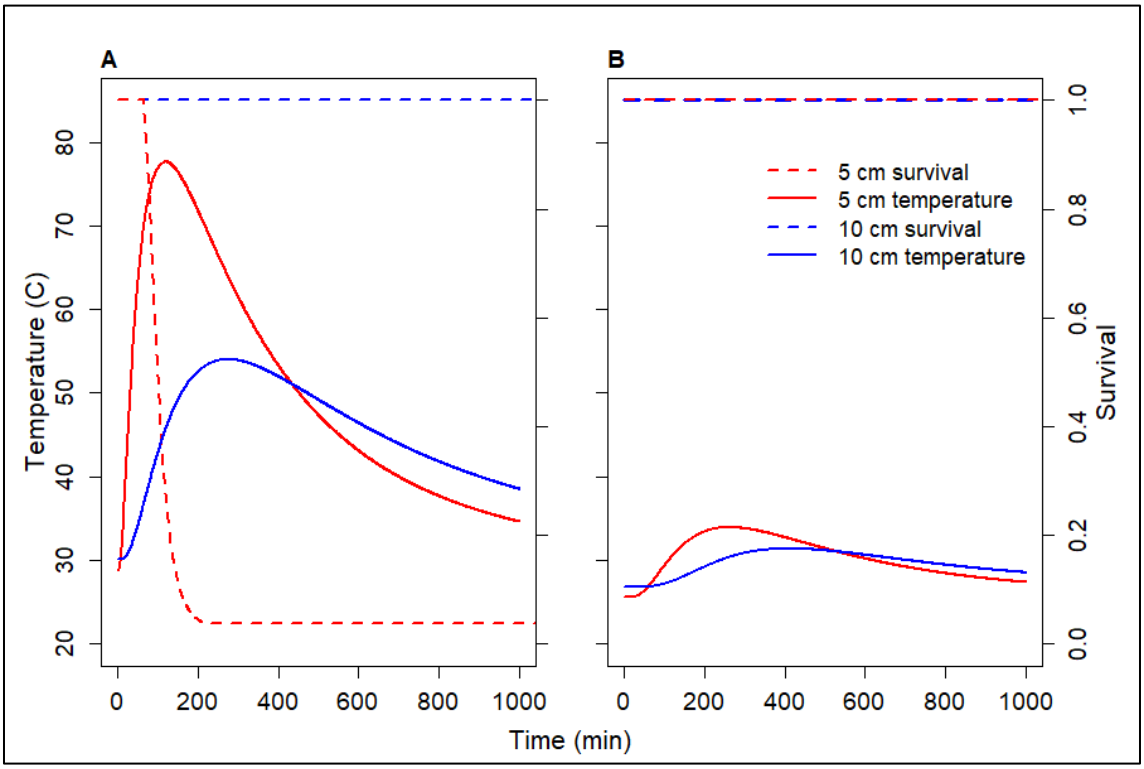

Figure 6. Predicted partridge pea seed survival and soil temperature over time at 5 and 10 cm deep in the soil for A. HF plot and B. LF plot.

Predicted survival for partridge pea seeds was nearly 0 at 5 cm depth in the HF plot but at 10 cm depth, the predicted survival was 100 percent (Figure 6). The seeds had 100 percent predicted survival at both depths in the LF plot which had cooler soil temperatures (Figure 6). Under the same soil heating regimes, different tissues experience vastly different effects (Figure 7). For example, based on modeled soil temperatures at 13 cm depth in the HF plot, the thermal tolerance model predicted that aspen and Douglas fir vascular cambium cell populations would have experienced nearly complete mortality (0.2% and 2.5% survival, respectively) while partridge pea seeds would have 100 percent survival at that depth (Figure 7). Using *survival_depth* run at 0.01 cm increments, the 50% threshold, at which we would predict vascular cambium tissue necrosis (Dickinson and Johnson 2004), was predicted to occur at 14.2 cm depth

for aspen and at 14.1 cm for fir, in the HF plot. In contrast, the 50% threshold for partridge pea seed survival was predicted at 5.9 cm depth.

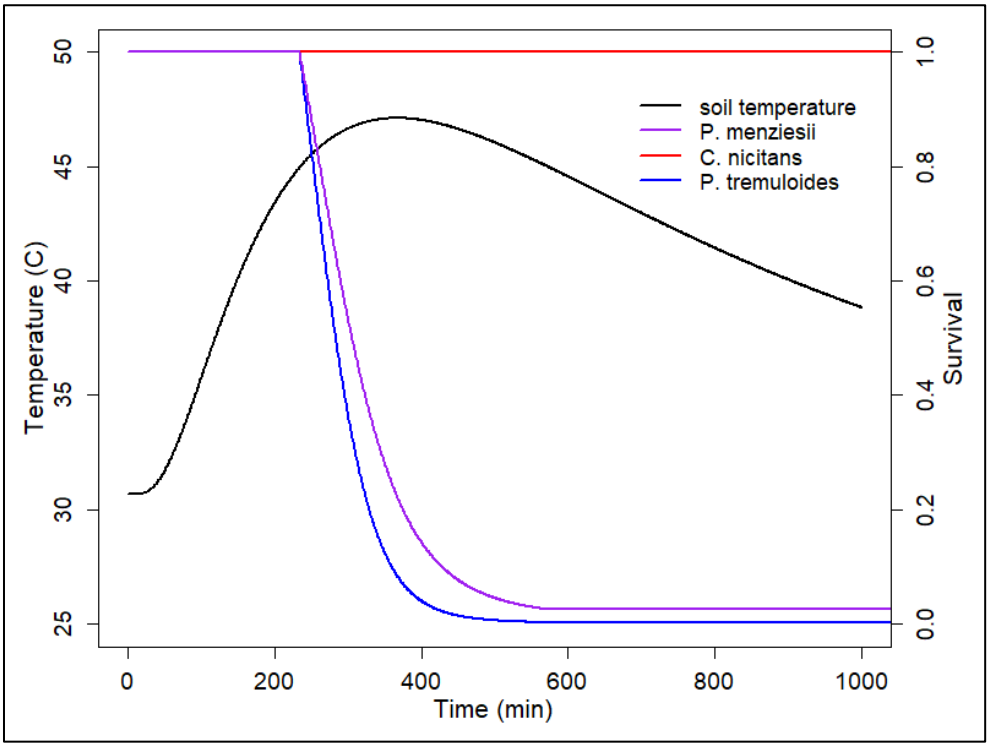

Figure 7. Predicted root vascular tissue survival for aspen and Douglas fir, predicted partridge pea seed survival, and soil temperature at 13 cm deep in the HF plot.

5. Discussion

5.1. SheFire

Fire is a key reorganizing force in terrestrial soils – soil heating can kill plant roots, seeds, and microbes which in turn transform biogeochemical processes, including carbon and nitrogen cycling (Smith et al. 2008, Varner et al. 2009, Swezy and Agee 2011, Hanan et al. 2016a, 2016b), and the frequency of severe wildfires is increasing (Schoennagel et al. 2017, Goss et al. 2020, Hanan et al. 2021). However heating is often perceived as minimal in most surface fires (Hartford and Frandsen 1992), and as a result, has not been studied as extensively as fire effects aboveground. The SheFire modeling framework is a first step towards collecting, extrapolating,

and applying soil temperature data more broadly. The model is a powerful tool for understanding the effects of fires on temperature across soil depths and over time, and how heating directly affects soil biological, chemical, and physical processes. SheFire and iStakes offer a means of describing, understanding, and predicting fire effects on soils in a more mechanistic and accessible way than has been available to date.

Keeley (2009) describes a set of remotely sensed and ground-based measurements termed fire or burn severity that, although easy to obtain, can be indirectly or poorly related to both fire characteristics (i.e., energy rates, totals, and transport that we will term fire energy) and ecosystem responses of interest. In response to limitations of these severity measurements, the dose-response paradigm proposed by Smith et al. (2016a) relates quantitative measures of fire energy to biological outcomes. In situations where fire characteristics can be measured or simulated, the dose-response approach has great potential to elucidate the connections between fires and their effects on ecosystems and to better understand how severity measurements are related to fire energy (Miquelajauregui et al. 2016). A limitation of the dose-response approach is that the mechanism by which a dose causes a response is not specified. As such, dose-response relationships have uncertain generality across varying conditions, species, and ecosystems. A more mechanistic option would be to begin elucidating the processes by which the characteristics of fires cause effects of interest, a general methodology called the process-response approach (Johnson 1985). An increasing number of studies are using process-response approaches to understand fire effects (e.g., Balfour and Midgley 2006, Dickinson and Ryan 2010, Battipaglia et al. 2016, Michaletz 2018, Sparks et al. 2018) though few have focused on soil effects (Choczynska and Johnson 2009, Stephan et al. 2010).

SheFire expands our ability to study fire effects on belowground dynamics in a process-based manner. Using the SheFire modeling framework, researchers can explore both soil heating

through the temperature summary functions, and belowground effects through the thermal tolerance model that can be used to describe biochemical, organismal, and tissue responses to heating. When used in conjunction with easily deployable iStakes, SheFire is primed to enable laboratory and field measurement of soil heating and biotic effects. We hope that SheFire will lead to studies that better describe relationships between fire characteristics and soil heating and encourage more studies that estimate parameters of thermal tolerance models for soil organisms (e.g., Dickinson and Johnson 2004, Dickinson et al. 2005).

5.1.1. Temperature, "dose", estimates

We found that SheFire demonstrated skill in estimating temperature over time at unmeasured soil depths (Table 3; Figure 3). However, because SheFire is based on soil temperatures, in its current form it cannot be used to characterize temperatures at the mineral soil surface. We found that SheFire can be used to predict soil temperatures at depths shallower than the shallowest sensor, but predictions become less accurate as the surface is approached (Table 3). While there are situations where fire and soil conditions allow the model to make estimates for soil temperature at depths < 0.1 cm from the surface, these estimates should be interpreted with caution and resulting conclusions about the soil surface temperature have not been tested. Until more work is done to improve shallow predictions, researchers should be mindful when calculating temperature over time at shallow depths. More soil surface temperature measurements and a better ability to model the physical processes that determine soil surface heat fluxes during fires are needed.

5.1.2. Survival, "response", estimates

There has been significant pushback against the once-dogmatic lethal temperature threshold of 60°C, the proposed threshold temperature at which live tissues and cells are killed (Dickinson and Johnson 2004, Dickinson et al. 2005, Pingree and Kobziar 2019). We demonstrate the application of a thermal tolerance model that shows how variable the response to heating can be, with large

differences between highly tolerant seeds and relatively intolerant vascular cambium (Figures 6 and 7). Nonetheless, the exponential dependence between rates of injury and temperature (Equation 6) and the corresponding rapid fall-off in survival as temperatures increase (Figures 6 and 7) explain why lethal effects of heating appear to be threshold phenomena and can often be approximated as such. These relationships underline both the importance of soil as an insulator and also the thin edge at which organisms in the soil survive or perish during a fire.

There are few studies that investigate thermal tolerance and survival during fires but they show that survival can be highly variable among species, tissue types, and heating regimes (Dickinson and Johnson 2004, Michaletz and Johnson 2007, 2008, Pingree and Kobziar 2019). We need more research to augment the current literature on biological responses to fire-induced heating, particularly estimates of thermal tolerance model parameters (Table S7) across a range of soil microbial taxa (e.g., archaea, bacteria, fungi), life-stages (e.g., vegetative cells, spores) as well as for plant seeds and root tissue across a range of species.

Just as the survival response functions in SheFire reflect a growing understanding of soil organism responses to heating, new response functions can be added to the SheFire framework to model both threshold effects and more complex processes. For instance, the effects of fire on soil organic matter are known to vary with the extent and duration of soil heating (González-Pérez et al. 2004). Therefore, soil heating has major implications for soil carbon storage in fire prone landscapes. Current methods for assessing soil carbon storage and fire interactions are often not mechanistic at the level of soil heating and typically focus on fire frequency, severity, and aboveground fuels (Homann et al. 2011, Pellegrini et al. 2018). SheFire may provide a way to expand that work by linking soil carbon thermal degradation that occurs during fire to the temperatures experienced and the heating duration at different soil depths. Additionally, knowing how deep into the soil profile heating causes organic soil phosphorus to be converted to its more

biologically available form, orthophosphate, can increase our understanding of post-fire plant recovery. Understanding the heat experienced by soil microbial communities is important for predicting microbial community dynamics following fire, which has implications for ecosystem functioning (Whitman et al. 2019). Furthermore, soil temperatures experienced during fires can influence soil NH_4^+ pools after fire, which are a critical component of nitrogen cycling and ecosystem nitrogen budgets (Klopatek et al. 1990). With SheFire, we have established a modeling approach that can be leveraged to fill these knowledge gaps and expand our ability to predict fire effects.

5.2. iStakes

The iButton and thermocouple benchmarking study demonstrates that iButtons provide a comparable alternative to thermocouples. Changing sensor types will not divide the soil temperature literature into two incompatible camps where the data from one sensor type cannot be compared to the data from the other (Table 4 and 5; Figure 5, Bova and Dickinson 2008). While thermocouples are the current standard for measuring soil temperatures during fires (Pereira et al. 2019), iButtons offer many advantages over thermocouples, including lower costs and ease of installation. In terms of ease of use, iStakes are simpler to install in the field than thermocouples because they are merely pushed into the soil and the depth of the top of the stake measured as opposed to thermocouples where the sensors must each be buried and precisely measured with additional work put towards protecting the data loggers from the fire (Pereira et al. 2019). In the growing study of wildfires (Lentile et al. 2007, Miesel et al. 2018, Dickinson et al. 2019) the ability to deploy equipment rapidly allows a team to collect as much data as possible while mitigating risk.

Beyond the logistics of deploying equipment, iStakes offer many advantages in the data they collect. Because an iStake is thin and can simply be pushed into the ground, or in cases of

stony soil inserted into a pilot slot, it causes less disturbance than the hole that must be dug and then filled back in to deploy thermocouples. Disturbed soil heats differently than undisturbed soil so reducing disturbance around the sensors is important for recording temperatures representative of what the soil would experience without sensor installation (Busse et al. 2010). Other researchers have also devised ways to minimize the effects of soil disturbance on the temperature data they record with thermocouples such as Robichaud and Brown who patented a metal canister that is buried and deploys thermocouples that extend into the soil (Robichaud and Brown 2019). However, a risk with this approach is that the metal of the canister will conduct heat down into the soil profile more rapidly than do the surrounding soils, which transfer heat relatively slowly (DeBano 2000, Kreye et al. 2013, Badía-Villas et al. 2014, Aznar et al. 2016). The wood of the iButton stake will not conduct heat like the metal canister would because its thermal diffusivity (determined by the ratio of thermal conductivity to heat capacity) matches that of the soil more closely than does metal (MacLean 1941, Kersten 1949, Bristow 1998).

It is, however, worth noting that iStakes are not ideal in all circumstances due to some logistical and data limitations. First, iButtons do not have replaceable batteries and cannot be recharged, thus battery life is sensor life (Maxim Integrated 2002). Anecdotal evidence suggests that they can record over 500,000 data points before the sensor must be replaced (Maxim Integrated 2002). Thermocouples on the other hand can be used for as long as they remain undamaged. The data loggers need a power source and can eventually break down, but they are considered long lived and have replaceable batteries. The second limitation is that iButtons have lower temperature thresholds than thermocouples. For the high temperature iButtons, that limit is 125 °C. When soil temperatures exceed that limit, but are not high enough to damage the iButton, the sensor will record a timestamp at the appropriate data logging rate, but it will not record a temperature until it cools back to 125 °C and below. Preliminary work indicates that the BFD

fitting portion of the SheFire model can be used to accurately interpolate the missing data when the maximum temperature is above 125 °C. However, soil temperatures as shallow as 5 cm deep rarely exceed 150 °C (DeBano 2000) and decline rapidly with depth (Giovannini and Lucchesi 1997, Badía-Villas et al. 2014, Aznar et al. 2016, Pereira et al. 2019) so outside of the high temperatures in pile burns (Massman et al. 2010) or below deep, smoldering duff (Hartford and Frandsen 1992), iButtons will generally work well.

There are pros and cons to both iStakes and thermocouples, but our data shows strong agreement between iButton and thermocouple readings, indicating that studies using iButton measurements will contribute to the broader body of knowledge. In most cases, iStakes offer an easier alternative to thermocouple installation in the field and decrease soil disturbance.

6. Conclusions

The SheFire framework provides a cutting-edge approach for estimating how fire energy transfers through a soil profile and predicting biological responses. While the current model advances our ability to predict belowground responses to fire, there are many opportunities for future expansion and development. For example, as our understanding of temperature-dependent biological and biogeochemical responses continues to improve, new response functions can be added to the SheFire framework.

In addition to adding new response functions, SheFire could be coupled with other fire models. For example, linking SheFire with aboveground dose-response models, such as the tree mortality model (Michaletz and Johnson 2008), could provide a more complete understanding of how fire affects plants, which can experience heating in both their above and belowground structures. Linking SheFire with models for fire effects on soils, such as those that model thermal conductivity, water content, and soil structure (Massman et al. 2010, Massman 2015, Smits et al.

2016) could strengthen SheFire's predictive ability or even provide additional response functions that focus on those physical effects. Further work could also link SheFire with fire behavior and fire regime models which would enable predictions of soil temperatures and their effects belowground based on the predicted fire characteristics of current and future fire regimes.

SheFire provides a modeling framework that enables researchers to move beyond qualitative and semi-quantitative descriptions of fire severity and explore how soil heating influences specific responses. As we learn to coexist with more frequent wildfire (Schoennagel et al. 2017), SheFire can help researchers and land managers quantify how unplanned wildfires, prescribed fires, and pile burns directly influence soil physical, chemical and biological processes.

Works Cited

Abu-Hamdeh, N. H. 2003. Thermal Properties of Soils as affected by Density and Water Content. Biosystems Engineering 86:97–102.

Abu-Hamdeh, N. H., and R. C. Reeder. 2000. Soil Thermal Conductivity Effects of Density, Moisture, Salt Concentration, and Organic Matter. Soil Science Society of America Journal 64:1285–1290.

Achat, D. L., L. Augusto, M. R. Bakker, A. Gallet-Budynek, and C. Morel. 2012. Microbial processes controlling P availability in forest spodosols as affected by soil depth and soil properties. Soil Biology and Biochemistry 44:39–48.

Adie, H., S. Richert, K. P. Kirkman, and M. J. Lawes. 2011. The heat is on: frequent high intensity fire in bracken (Pteridium aquilinum) drives mortality of the sprouting tree Protea caffra in temperate grasslands. Plant Ecology 212:2013–2022.

Aznar, J. M., J. A. González-Pérez, D. Badía-Villas, and C. Martí Dalmau. 2016. At what depth are the properties of gypseous forest soil affected by fire? Land Degradation and Development 27: 1344–1353

Badía-Villas, D., J. A. González-Pérez, J. M. Aznar, B. Arjona-Gracia, and C. Martí-Dalmau. 2014. Changes in water repellency, aggregation and organic matter of a mollic horizon burned in laboratory: Soil depth affected by fire. Geoderma 213:400–407.

Balesdent, J., I. Basile-Doelsch, J. Chadoeuf, S. Cornu, D. Derrien, Z. Fekiacova, and C. Hatté. 2018. Atmosphere–soil carbon transfer as a function of soil depth. Nature 559:599–602.

Balfour, D. A., and J. J. Midgley. 2006. Fire induced stem death in an African acacia is not caused by canopy scorching. Austral Ecology 31:892–896.

Barnett, C. R. 2002. BFD curve: a new empirical model for fire compartment temperatures. Fire Safety Journal 37:437–463.

Battipaglia, G., T. Savi, D. Ascoli, D. Castagneri, A. Esposito, S. Mayr, and A. Nardini. 2016. Effects of prescribed burning on ecophysiological, anatomical and stem hydraulic properties in Pinus pinea L. Tree Physiology 36:1019–1031.

Bova, A. S., and M. B. Dickinson. 2008. Beyond "fire temperatures": calibrating thermocouple probes and modeling their response to surface fires in hardwood fuels. Canadian Journal of Forest Research 38:1008–1020.

Bristow, K. L. 1998. Measurement of thermal properties and water content of unsaturated sandy soil using dual-probe heat-pulse probes. Agricultural and Forest Meteorology 89:75–84.

Busse, M. D., C. J. Shestak, and K. R. Hubbert. 2013. Soil heating during burning of forest slash piles and wood piles. International Journal of Wildland Fire 22:786–796.

Busse, M. D., C. J. Shestak, K. R. Hubbert, and E. E. Knapp. 2010. Soil Physical Properties Regulate Lethal Heating during Burning of Woody Residues. Soil Science Society of America Journal 74:947–955.

Caldwell, C. R. 1993. Estimation and Analysis of Cucumber (Cucumis sativus L.) Leaf Cellular Heat Sensitivity. Plant Physiology 101:939–945.

Campbell, G. S., Jungbauer Jr, J.D., Bristow, K.L. and Hungerford, R.D., 1995. Soil temperature and water content beneath a surface fire. Soil Science, 159:363–374.

Choczynska, J., and E. A. Johnson. 2009. A soil heat and water transfer model to predict belowground grass rhizome bud death in a grass fire. Journal of Vegetation Science 20:277–287.

DeBano, L. F. 2000. The role of fire and soil heating on water repellency in wildland environments: a review. Journal of Hydrology 231:195–206.

Dickinson, M. B., and E. A. Johnson. 2004. Temperature-dependent rate models of vascular cambium cell mortality. Canadian Journal of Forest Research 34:546–559.

Dickinson, M. B., J. Jolliff, and A. S. Bova. 2005. Vascular cambium necrosis in forest fires: using hyperbolic temperature regimes to estimate parameters of a tissue-response model. Australian Journal of Botany 52:757–763.

Dickinson, M. B., and K. C. Ryan. 2010. Introduction: Strengthening the Foundation of Wildland Fire Effects Prediction for Research and Management. Fire Ecology 6:1–12.

Dickinson, M., L. Loncar, A. Reiner, S. Dailey, J. Bednarczyk, C. Drake, J. Gordon, M. Heckel, B. Kleckler, J. Miesel, and L. Wade. 2019. 2019 Walker Fire, Plumas National Forest, Fire Behavior Assessment Team (FBAT) Report. US Forest Service: AMSET: 34.

Doerr, S., C. Santin, J. Reardon, J. Mataix-Solera, C. Stoof, R. Bryant, J. Miesel, and D. Badia. 2017. Soil heating during wildfires and prescribed burns: a global evaluation based on existing and new data 19:17957.

Giovannini, C., S. Lucchesi, and M. Giachetti. 1990. Effects of Heating on Some Chemical Parameters Related to Soil Fertility and Plant Growth. Soil Science 149:344–350.

Giovannini, G., and S. Lucchesi. 1997. Modification induced in soil physico-chemical parameters by experimental fires at different intensities. Soil Science 162:479–486.

González-Pérez, J. A., F. J. González-Vila, G. Almendros, and H. Knicker. 2004. The effect of fire on soil organic matter—a review. Environment International 30:855–870.

Goss, M., D. L. Swain, J. T. Abatzoglou, A. Sarhadi, C. A. Kolden, A. P. Williams, and N. S. Diffenbaugh. 2020. Climate change is increasing the likelihood of extreme autumn wildfire conditions across California. Environmental Research Letters 15:094016.

Grau-Andrés, R., G. M. Davies, S. Waldron, E. M. Scott, and A. Gray. 2017. Leaving moss and litter layers undisturbed reduces the short-term environmental consequences of heathland managed burns. Journal of Environmental Management 204:102–110.

Hanan, E. J., C. M. D'Antonio, D. A. Roberts, and J. P. Schimel. 2016a. Factors Regulating Nitrogen Retention During the Early Stages of Recovery from Fire in Coastal Chaparral Ecosystems. Ecosystems 19:910–926.

Hanan, E. J., J. Ren, C. L. Tague, C. A. Kolden, J. T. Abatzoglou, R. R. Bart, M. C. Kennedy, M. Liu, and J. C. Adam. 2021. How climate change and fire exclusion drive wildfire regimes at actionable scales. Environmental Research Letters 16:024051.

Hanan, E. J., J. P. Schimel, K. Dowdy, and C. M. D'Antonio. 2016b. Effects of substrate supply, pH, and char on net nitrogen mineralization and nitrification along a wildfire-structured age gradient in chaparral. Soil Biology and Biochemistry 95:87–99.

Hartford, R. A., and W. H. Frandsen. 1992. When It's Hot, It's Hot... Or Maybe It's Not! (Surface Flaming May Not Portend Extensive Soil Heating). International Journal of Wildland Fire 2:139–144.

Hiers, Q. A., M. L. Treadwell, M. B. Dickinson, K. L. Kavanagh, A. G. Lodge, H. D. Starns, D. R. Tolleson, D. Twidwell, C. L. Wonkka, and W. E. Rogers. 2019. Grass Bud bank responses to fire in a semi-arid savanna system. Ecology & Evolution in press.

Homann, P. S., B. T. Bormann, R. L. Darbyshire, and B. A. Morrissette. 2011. Forest Soil Carbon and Nitrogen Losses Associated with Wildfire and Prescribed Fire. Soil Science Society of America Journal 75:1926–1934.

Hudak, A. T., P. Morgan, M. J. Bobbitt, A. M. S. Smith, S. A. Lewis, L. B. Lentile, P. R. Robichaud, J. T. Clark, and R. A. McKinley. 2007. The Relationship of Multispectral Satellite Imagery to Immediate Fire Effects. Fire Ecology 3:64–90.

Ichoku, C., R. Kahn, and M. Chin. 2012. Satellite contributions to the quantitative characterization of biomass burning for climate modeling. Atmospheric Research 111:1–28.

Iverson, L. R., D. A. Yaussy, J. Rebbeck, T. F. Hutchinson, R. P. Long, and A. M. Prasad. 2004. A comparison of thermocouples and temperature paints to monitor spatial and temporal characteristics of landscape-scale prescribed fires. International Journal of Wildland Fire 13:311–322.

Johnson, E. A. 1985. Disturbance: the process and the response. An epilogue. Canadian Journal of Forest Research 15:292–293.

Kennard, D. K., K. W. Outcalt, D. Jones, and J. J. O'Brien. 2005. Comparing Techniques for Estimating Flame Temperature of Prescribed Fires. Fire Ecology 1:75–84.

Kersten, M. S. 1949. Thermal Properties of Soils. University of Minnesota, Institute of Technology 52.

Klopatek, J. M., C. C. Klopatek, and L. F. DeBano. 1990. Potential variation of nitrogen transformations in pinyon-juniper ecosystems resulting from burning. Biology and Fertility of Soils 10:35–44.

Kokaly, R. F., B. W. Rockwell, S. L. Haire, and T. V. V. King. 2007. Characterization of post-fire surface cover, soils, and burn severity at the Cerro Grande Fire, New Mexico, using hyperspectral and multispectral remote sensing. Remote Sensing of Environment 106:305–325.

Kramer, M. G., K. Lajtha, and A. K. Aufdenkampe. 2017. Depth trends of soil organic matter C:N and 15N natural abundance controlled by association with minerals. Biogeochemistry 136:237–248.

Kremens, R. L., A. M. S. Smith, and M. B. Dickinson. 2010. Fire Metrology: Current and Future Directions in Physics-Based Measurements. Fire Ecology 6:13–35.

Kreye, J. K., J. M. Varner, and L. N. Kobziar, 2020. Long-duration soil heating resulting from forest floor duff smoldering in longleaf pine ecosystems. Forest Science 66:291–303.

Kreye, J. K., L. N. Kobziar, and W. C. Zipperer. 2013. Effects of fuel load and moisture content on fire behaviour and heating in masticated litter-dominated fuels. International Journal of Wildland Fire 22:440–445.

Lentile, L. B., P. Morgan, C. Hardy, A. T. Hudak, R. Means, R. Ottmar, P. Robichaud, E. Sutherland, F. Way, and S. Lewis. 2007. Lessons Learned From Rapid Response Research on Wildland Fires. U.S. Department of Agriculture: Forest Service, National Agroforestry Center: 10.

Lorenz, R. W. 1939. High temperature tolerance of forest trees. University of Minnesota: Agricultural Experiment Station. Technical Bulletin 141.

Lutes, D. C. 2017. FOFEM 6.4: First Order Fire Effects Model user guide. Missoula, MT: U.S. Department of Agriculture: Forest Service, Rocky Mountain Research Station, Fire Modeling Institute: 86.

MacLean, J. D. 1941. Thermal conductivity of wood. Forest Products Laboratory: Heating, Piping & Air Conditioning: 12.

Martin, R. E., and C. T. Cushwa. 1966. Effects of heat and moisture on leguminous seed. Proceedings Annual [5th] Tall Timbers Fire Ecology Conference 5:159–175.

Martin, R. E., C. T. Cushwa, and R. L. Miller. 1969. Fire as a physical factor in wildland management. Proceedings Annual [9th] Tall Timbers Fire Ecology Conference 9:271–288.

Massman, W. J. 2015. A non-equilibrium model for soil heating and moisture transport during extreme surface heating: the soil (heat–moisture–vapor) HMV-Model Version 1. Geoscientific Model Development 8:3659–3680.

Massman, W. J. 2021. The challenges of an in situ validation of a nonequilibrium model of soil heat and moisture dynamics during fires. Hydrology and Earth System Sciences 25:685–709.

Massman, W. J., J. M. Frank, and S. J. Mooney. 2010. Advancing Investigation and Physical Modeling of First-Order Fire Effects on Soils. Fire Ecology 6:36–54.

Maxim Integrated. 2002. Book of iButton Standards. Maxim Integrated Products, Inc.

Michaletz, S. T. 2018. Xylem dysfunction in fires: towards a hydraulic theory of plant responses to multiple disturbance stressors. New Phytologist 217:1391–1393.

Michaletz, S. T., and E. A. Johnson. 2007. How forest fires kill trees: A review of the fundamental biophysical processes. Scandinavian Journal of Forest Research 22:500–515.

Michaletz, S. T., and E. A. Johnson. 2008. A biophysical process model of tree mortality in surface fires. Canadian Journal of Forest Research 38:2013–2029.

Miesel, J., A. Reiner, C. Ewell, B. Maestrini, and M. Dickinson. 2018. Quantifying Changes in Total and Pyrogenic Carbon Stocks Across Fire Severity Gradients Using Active Wildfire Incidents. Frontiers in Earth Science 6:41.

Miquelajauregui, Y., S. G. Cumming, and S. Gauthier. 2016. Modelling Variable Fire Severity in Boreal Forests: Effects of Fire Intensity and Stand Structure. PloS One 11:e0150073.

Moran, C. J., C. A. Seielstad, M. R. Cunningham, V. Hoff, R. A. Parsons, Ll. Queen, K. Sauerbrey, and T. Wallace. 2019. Deriving Fire Behavior Metrics from UAS Imagery. Fire 2:36.

Morgan, P., R. E. Keane, G. K. Dillon, T. B. Jain, A. T. Hudak, E. C. Karau, P. G. Sikkink, Z. A. Holden, and E. K. Strand. 2014. Challenges of assessing fire and burn severity using field

measures, remote sensing and modelling. International Journal of Wildland Fire 23:1045–1060.

Murphy, K. A., J. H. Reynolds, and J. M. Koltun. 2008. Evaluating the ability of the differenced Normalized Burn Ratio (dNBR) to predict ecologically significant burn severity in Alaskan boreal forests. International Journal of Wildland Fire 17:490–499.

Neary, D. G., C. C. Klopatek, L. F. DeBano, and P. F. Ffolliott. 1999. Fire effects on belowground sustainability: a review and synthesis. Forest Ecology and Management 122:51–71.

Nelson, R. M. 1952. Observations on heat tolerance of southern pine needles. U.S. U.S. Department of Agriculture, Forest Service, Southeastern Forest Experiment Station, Asheville, NC. 14:1–6.

Ottmar, R. D., J. K. Hiers, B. W. Butler, C. B. Clements, M. B. Dickinson, A. T. Hudak, J. J. O'Brien, B. E. Potter, E. M. Rowell, T. M. Strand, T. J. Zajkowski, R. D. Ottmar, J. K. Hiers, B. W. Butler, C. B. Clements, M. B. Dickinson, A. T. Hudak, J. J. O'Brien, B. E. Potter, E. M. Rowell, T. M. Strand, and T. J. Zajkowski. 2016. Measurements, datasets and preliminary results from the RxCADRE project – 2008, 2011 and 2012. International Journal of Wildland Fire 25:1–9.

Pellegrini, A. F. A., A. Ahlström, S. E. Hobbie, P. B. Reich, L. P. Nieradzik, A. C. Staver, B. C. Scharenbroch, A. Jumpponen, W. R. L. Anderegg, J. T. Randerson, and R. B. Jackson. 2018. Fire frequency drives decadal changes in soil carbon and nitrogen and ecosystem productivity. Nature 553:194–198.

Pereira, P., A. Cerdà, X. Úbeda, J. Mataix-Solera, and G. Rein. 2019. Fire Effects on Soil Properties. Csiro Publishing, Clayton South, Australia.

Pingree, M. R. A., and L. N. Kobziar. 2019. The myth of the biological threshold: A review of biological responses to soil heating associated with wildland fire. Forest Ecology and Management 432:1022–1029.

Quigley, K.M., R. E. Wildt, B. R. Sturtevant, R. K. Kolka, M. B. Dickinson, C. C. Kern, D. M. Donner, and J. R. Miesel, 2019. Fuels, vegetation, and prescribed fire dynamics influence ash production and characteristics in a diverse landscape under active pine barrens restoration. Fire Ecology 15:1–15.

Ramcharan, A., T. Hengl, T. Nauman, C. Brungard, S. Waltman, S. Wills, and J. Thompson. 2018. Soil Property and Class Maps of the Conterminous United States at 100-Meter Spatial Resolution. Soil Science Society of America Journal 82:186–201.

Regan, K., B. Stempfhuber, M. Schloter, F. Rasche, D. Prati, L. Philippot, R. S. Boeddinghaus, E. Kandeler, and S. Marhan. 2017. Spatial and temporal dynamics of nitrogen fixing, nitrifying and denitrifying microbes in an unfertilized grassland soil. Soil Biology and Biochemistry 109:214–226.

Robichaud, P., and R. E. Brown. 2019, March 7. High Temperature Soil Probe. United States of America Patent: US20190072434A1.

Robichaud, P. R. 2000. Fire effects on infiltration rates after prescribed fire in Northern Rocky Mountain forests, USA. Journal of Hydrology 231:220–229.

Rosenberg, B., G. Kemeny, R. C. Switzer, and T. C. Hamilton. 1971. Quantitative Evidence for Protein Denaturation as the Cause of Thermal Death. Nature 232:471–473.

Sándor, R., and N. Fodor. 2012. Simulation of Soil Temperature Dynamics with Models Using Different Concepts. The Scientific World Journal 2012:e590287.

Schoennagel, T., J. K. Balch, H. Brenkert-Smith, P. E. Dennison, B. J. Harvey, M. A. Krawchuk, N. Mietkiewicz, P. Morgan, M. A. Moritz, R. Rasker, M. G. Turner, and C. Whitlock. 2017. Adapt to more wildfire in western North American forests as climate changes. Proceedings of the National Academy of Sciences 114:4582–4590.

Smith, A. M. S., A. M. Sparks, C. A. Kolden, J. T. Abatzoglou, A. F. Talhelm, D. M. Johnson, L. Boschetti, J. A. Lutz, K. G. Apostol, K. M. Yedinak, W. T. Tinkham, and R. J. Kremens. 2016a. Towards a new paradigm in fire severity research using dose–response experiments. International Journal of Wildland Fire 25:158–166.

Smith, J. E., A. D. Cowan, and S. A. Fitzgerald. 2016b. Soil heating during the complete combustion of mega-logs and broadcast burning in central Oregon USA pumice soils. International Journal of Wildland Fire 25:1202–1207.

Smith, N. R., B. E. Kishchuk, and W. W. Mohn. 2008. Effects of Wildfire and Harvest Disturbances on Forest Soil Bacterial Communities. Applied and Environmental Microbiology 74:216–224.

Smits, K. M., E. Kirby, W. J. Massman, and L. S. Baggett. 2016. Experimental and Modeling Study of Forest Fire Effect on Soil Thermal Conductivity. Pedosphere 26:462–473.

Sparks, A. M., C. A. Kolden, A. M. S. Smith, L. Boschetti, D. M. Johnson, and M. A. Cochrane. 2018. Fire intensity impacts on post-fire temperate coniferous forest net primary productivity. Biogeosciences 15:1173–1183.

Stephan, K., M. Miller, and M. B. Dickinson. 2010. First-Order Fire Effects on Herbs and Shrubs: Present Knowledge and Process Modeling Needs. Fire Ecology 6:95–114.

Swezy, D. M., and J. K. Agee. 1991. Prescribed-fire effects on fine-root and tree mortality in old-growth ponderosa pine. Canadian Journal of Forest Research 21:626–634.

USDA. 2016. Official Series Description - TARRANT Series. U.S. Department of Agriculture.

Varner, M. J., F. E. Putz, J. J. O'Brien, J. Kevin Hiers, R. J. Mitchell, and D. R. Gordon. 2009. Post-fire tree stress and growth following smoldering duff fires. Forest Ecology and Management 258:2467–2474.

Whitman, T., E. Whitman, J. Woolet, M. D. Flannigan, D. K. Thompson, and M.-A. Parisien. 2019. Soil bacterial and fungal response to wildfires in the Canadian boreal forest across a burn severity gradient. Soil Biology and Biochemistry 138:107571.

Zhang, Y., H. Shen, Q. Gao, and L. Zhao. 2020. Estimating soil organic carbon and pH in Jilin Province using Landsat and ancillary data. Soil Science Society of America Journal 84:556–567.

Supplementary S1: Model Implementation

The *shefire* function, which fits the model, has thirteen adjustable parameters beyond the input data (supplementary Table S1). The default settings will work in most situations, but they can be adjusted according to the user's needs or to fit a particularly high or low energy fire, which may need a longer cool down period postfire or some data smoothing to identify the start of the fire effects, respectively. A full list of the parameter names and descriptions can be found in supplementary Table S1.

The *time.buffer* parameter warrants a more detailed explanation. Because soil heating begins at the surface and transmits from shallow to deeper depths over time, depending on the exact heating profile of a given fire, extrapolating temperatures for depths shallower than the shallowest sensor may not be mathematically possible if the time when the shallowest sensor begins to warm is set as the starting point for the model (*time.buffer* of 0). The time the maximum temperature is reached (*TimeAtMax*) must be positive, so with a short *time.buffer* there is a smaller window of time when the shallower soil depths can reach their maximum temperature and still fall within the model time range. Thus, by setting the amount of time added prior to the time when the shallow sensor begins to warm as the start point, *time.buffer* also dictates, in conjunction with the exact heating patterns of the specific fire and soil conditions being modeled, how shallow of a depth can be predicted. The default time is 30 minutes, which, based on datasets we have examined (discussed later in the validation experiment and the case study), may be more than is needed to predict up to within 1.0 cm of the soil surface for many fires. In other cases, it may not be enough time and the shallowest depth that can be calculated will be deeper than 1.0 cm. Users can increase the *time.buffer* as needed. However, a tradeoff for increasing the t*ime.buffer* is that it can negatively affect the BFD fits and BFD parameter-depth regressions. In particular, there is a consistent relationship between a longer *time.buffer* and worse regression fit

for the Shape parameter. This is a tradeoff that users must navigate if they want temperature predictions at shallow soil depths.

The shallowest depth that can be predicted by the model is not necessarily the shallowest depth for which the predictions are logically reasonable. The shallowest depth that has reasonable predictions varies with the characteristics of the fire, heating, and the *time.buffer*. If users are estimating heating at shallow depths and using large *time.buffers*, we recommend plotting temperature over time for multiple depths to make sure the estimates are reasonable. Generally, predictions ≥ 0.5 cm deeper than the shallowest depth that can mathematically be calculated are reasonable, but this is not a hard and fast rule. If a user needs to look at shallow depths specifically, they should plot the temperature over time for that depth alongside a few deeper depths and determine if this model is the right tool for them to use. In the future, more data on surface temperatures and physical modeling (e.g., Massman 2021) may guide developments of SheFire that would improve near-surface predictions.

The most challenging parameter-depth regression to fit is for *InitTemp*. Due to diurnal heating, the relationship between soil depth and temperature is variable depending on the time of day and weather preceding the fire induced heating (Sándor and Fodor 2012). Therefore, if the correlation between the *InitTemp* regression and the initial temperatures from the BFD equations fit to the input data falls below the correlation threshold (*corr.threshold*; see supplementary Table S1 for parameter details), the model reverts to a secondary option. The secondary option uses the initial temperature from the sensor closest to the soil depth of interest as the *InitTemp* term for that depth. If any of the other three parameter-depth regressions (*MaxTemp, TimeAtMax*, or *Shape*) fall below the correlation threshold, the model construction will abort and present an error message explaining what occurred.

The *shefire* function output is slightly different when the parameter-depth regression equations are calculated versus when they are not (*regression* parameter set to True and False, respectively; see supplementary Table S1 for parameter details). Without the parameter-depth regressions, the model is incomplete and cannot be used to estimate temperature over time at any depth other than the three sensor depths. The function output is restricted to a list containing the BFD equations that were fit to the input data, their fit evaluation, the temperature values from those equations at the temporal resolution selected in the *res* parameter (see supplementary Table S1 for parameter details), and information about the beginning and end of the time range used to fit the equations. The full model, with the parameter-depth regressions, has an output list containing all the equations and data necessary to calculate temperature over time for a range of soil depths and run the summary and response functions (Table 2). Information about all the fit evaluations for the BFD equations fit to the input data as well as the parameter-depth regressions is in the summary tables and can be printed or saved with the *print.plots.tables* and *save.plots.tables* parameters (see supplementary Table S1 for parameter details).

Table S1. Table of the *shefire* function parameters. The parameter name, description, and possible reasons to adjust the parameter are included. All parameters have default values except for the input data.

Parameter Name	Description	Potential Adjustments
input	Data frame of formatted input temperature data	Data unique to each location
sensor.depths	List of the temperature sensor depths in cm	Default is 5, 10, and 15 cm because those are the recommended sensor depths when using iStakes
cutoff	The time (min) after the shallow sensor's maximum temperature (*TimeAtMax*) that the code will cut off the data set for fitting unless temperatures rise again (i.e., diurnal heating) or the data set ends first	The default is 24 hours (1440 min), but soils heated by high energy or smoldering fires may be cooling for more than 24 hours

override.clip	Prevents the function from clipping the beginning or end of the data set. Default is False	Set to True if the input data have been manually clipped to exactly the desired time frame for fitting
moving.window	Smooths the data (mean value across the window) when locating the starting point for heating in the shallow sensor. The default is False	This can be useful in low energy fires in particular, when the fire heating may not be faster than diurnal heating on a point-to-point basis
window.size	Only needed if moving.window is True. The size (in time steps) of the window that used for smoothing with moving.window. Default is 3	Window size can be increased for particularly noisy data or slow warming
regression	This will have the function calculate the parameter-depth regressions which can be used to extrapolate or interpolate to other soil depths. This is needed to use any summary or response functions. Default is True	Set to False to calculate only the BFD equations that are fit to the input data
res	Only needed when *regression* is False. Sets the temporal resolution (in min) for the output temperatures from the equations fit to the sensor data. The temperature values (at every time point based on the temporal resolution) are returned in the return list at the end of the function. Default is 1 minute	Change temporal resolution to output the temperatures from the fitted parameter equations at timesteps other than one minute, i.e., temperature at every 30 seconds would be *res* = 0.5 minutes
corr.threshold	Threshold for accepted level of correlation between the input temperatures and the fitted temperatures as well as between the parameter-depth regressions and the BFD parameters calculated to fit the input data. Correlations less than the threshold will cause the model construction to abort. Default is 0.8	Adjust for a higher or lower level of acceptable correlation
time.buffer	The time (min) added before the temperature begins to rise for the shallow sensor. The buffer is often needed to be able to extrapolate to depths shallower than the shallowest sensor. However, keep the *time.buffer* as short as possible because longer buffers can worsen the fits for equations and regressions. The default is set to 30 minutes	If you do not need extrapolations to depths shallower than your shallowest sensor or if you are not calculating the regressions, users can set *time.buffer* to 0. Depending on the rate of heating for a given fire, a shorter buffer can work or in a few cases it may need to be extended if the model cannot make realistic predictions at a shallow depth of interest
print.plots.tables	If True, prints a standard set of plots (plotted at the temporal resolution of	Set to True to print the plots and tables

	the input data, not "res") to visualize BFD equation fits and prints summary tables containing equation details and fit information. Default is False	
save.plots.tables	If True, saves a standard set of plots (plotted at the temporal resolution of the input data, not "res") to visualize BFD equation fits as jpeg images and saves the summary tables containing equation details and fit information as CSV files. Default is False	Set to True to save the plots and tables
save.name	Only needed if save.plots.tables is True. The name that will be used for saving the plots and tables. Default is "SheFire"	Set the name that will be used in saved file names
save.directory	Only needed if save.plots.tables is True. The file path for where to save the plots and tables, if different from current working directory	Set to change the location the files be saved

Supplementary S2. iStake construction and field deployment

S2.1. iStake construction

The iStakes are made of 0.5 cm thick softwood. The purpose of using wood is that its thermal properties and drying and wetting behavior (which influence thermal properties) better match soil than other materials, particularly metals. As such, the stake itself will have limited impact on soil heating and temperature measurements. A width of 2.5 cm works well to drill the holes for the iButtons without cracking the wood. The holes for the iButtons should be 1.5 cm in diameter for a snug fit. The stakes can be any length depending on the number of sensors and depths needed for a particular project. For example, in a pile burn that is expected to reach high temperatures, either placing the full stake deeper into the soil profile or shifting the sensors holes deeper along the stake may make sense. For general application, the following dimensions are recommended: 16 cm long with 2 cm of taper at the end with the iButton centers at 3, 8, and 13 cm from the top of the stake (Figure 1). This placement means that, when installing the stake so that the top is 2 cm deep in the soil, the iButton centers will be at 5, 10, and 15cm deep. An

additional piece that can make stake retrieval faster is to drill a small hole in the top of the stake to attach a piece of wire or other non-combustible flagging that will stay above the soil surface. That flagging makes it easier to locate the stake post fire. A small piece of foil attached to the top of the stake can help prevent any charring or other heat damage to the stake, increasing longevity. We encourage users to experiment with a range of woods and milling techniques that may result in improved iStake function both thermally and in ease of use.

Depending on the depths to be measured, the stake will need either the high temperature or the low temperature iButtons. With the standard stake that places iButtons at 5, 10, and 15cm depth, using a high temperature iButton in the top position and low temperature iButtons in the bottom two is recommended. If particularly high temperatures are expected, such as in a pile burn or high fuel loading, it would be advisable to use high temperature iButtons in the deeper positions as well or simply place the stake deeper into the ground to measure cooler soil depths. Based on the precise goals of the project, varying numbers of sensors can be used, and they can be placed at different soil depths. For use with the SheFire model, three depths must be measured. So far, the model has been validated using sensor depths at 5, 10, and 15 cm but further work may show other depth combinations to be equally effective.

S2.2. Field deployment

Field deployment of the iStakes is straightforward. First, the sensors must be launched from a laptop or other computer using a software application such as OneWireViewer by Maxim Integrated. Launching the sensors requires setting a logging rate and start time which should be chosen depending on the specifics of the situation. Setting the iButtons to start at the same time will meet that SheFire requirement for the three datasets to start at the same time. Minimal data trimming by hand can also achieve the same result. The SheFire model does not have specific data logging rate requirements but the three sensors need to have the same rate. Using the

quickest data logging rate possible will provide the most information but will reduce the length of time that the iButtons can be deployed. We generally recommend using a 10 min logging rate as a compromise between temporal resolution and the need or desire to have the iStakes deployed for multiple days. It is often helpful to deploy the stakes a day or days prior to the fire and to leave them in the ground a day or more after the fire to discern diurnal heating and to fully characterize soil cooling. Being able to deploy iStakes well ahead of the fire also allows for data capture in the face of uncertainty as to when the fire will reach the iStake or if a prescribed burn will be conducted on a particular day.

Once launched, the iButtons are ready to snap into the wooden stakes and can be placed in the ground. If the soil is especially rocky or compacted, it may be necessary to use a metal bar, with the same dimensions as the stake, and a hammer to create the space in the soil for the stake but in many cases, simply pressing the stake into the soil will be adequate. For the stakes described above, the top of the stake should be two cm below the surface of the mineral soil. That buffer space, accounted for in the sensor placement along the stake, ensures the stake will not char during the fire. See Figure 2A for a deployment diagram. After the fire and cooling period, the stakes can simply be pulled out of the ground. The data from the iButtons are then downloaded to a laptop or other computer and the iButtons stopped or redeployed.

Supplementary S3. Methods

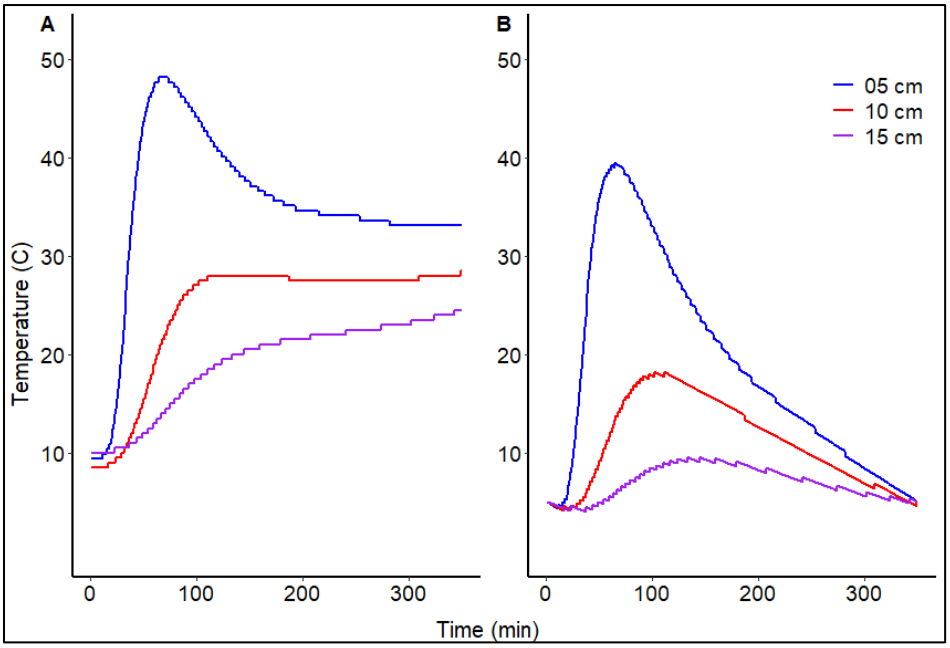

Figure S1. The temperatures over time at 5, 10, and 15 cm deep from an example replicate. A. The unadjusted temperatures B. The adjusted temperatures. The temperatures were adjusted for a shifting baseline temperature.

Supplementary S4. Results

Table S2. SheFire validation results with both the adjusted and unadjusted temperatures. Each replicate is a pair of model building (5, 10, and 15 cm) and model testing (4, 7, and 12 cm) iStakes. The statistics show the comparison between the model predictions and measured temperatures for 4, 7, and 12 cm deep. The "adjusted" statistics are from temperatures adjusted to a shifting temperature baseline before building or running the model. The "not adjusted" statistics are from the raw temperature values with no adjustment.

Adjusted	12cm			7cm			4cm		
replicate id	Pearson	R^2	RMSE	Pearson	R^2	RMSE	Pearson	R^2	RMSE
1016T2C1	0.98	0.97	0.56	0.98	0.97	1.28	no sensor data		
1016T2C3	0.99	0.98	0.52	0.99	0.99	0.94	no sensor data		
1017T2C1	0.99	0.98	0.46	0.98	0.95	1.79	0.95	0.91	4.36
1017T2C2	0.98	0.96	1.29	0.99	0.99	1.71	no sensor data		
1017T2C3	0.99	0.98	0.47	0.99	0.98	0.95	no sensor data		
1018T1C1	0.99	0.98	0.52	0.98	0.97	1.69	0.97	0.93	3.95
1018T1C2	0.98	0.97	0.72	0.99	0.97	1.62	no sensor data		
1018T1C4	0.98	0.96	0.56	0.99	0.97	1.15	0.98	0.97	2.07
1018T2C1	0.96	0.93	0.81	0.94	0.89	2.34	0.94	0.89	3.88
Mean	0.98	0.97	0.66	0.98	0.96	1.50	0.96	0.92	3.56
Stnd Error	<0.01	0.01	0.09	0.01	0.01	0.15	0.01	0.01	0.51
Not Adjusted									
1016T2C1	0.99	0.98	0.54	0.94	0.87	2.09	no sensor data		
1016T2C3	model could not run						no sensor data		
1017T2C1	model could not run								
1017T2C2	model could not run						no sensor data		
1017T2C3	model could not run						no sensor data		
1018T1C1	model could not run								
1018T1C2	0.99	0.98	0.67	0.93	0.87	2.78	no sensor data		
1018T1C4	model could not run								
1018T2C1	0.99	0.98	0.58	0.88	0.78	2.92	0.63	0.40	7.24
Mean	0.99	0.98	0.60	0.92	0.84	2.60	NA	NA	NA
Stnd Error	<0.01	<0.01	0.04	0.02	0.03	0.26	NA	NA	NA

Table S3. Detailed comparison of unadjusted iButton and thermocouple readings. Each replicate is comprised of an iButton stake and three thermocouples. The paired thermocouples and iButtons are at the same soil depth. Each iButton thermocouple pair is compared separately from the other two paired sets of sensors within the replicate. In replicate 1018T1C4, the thermocouple at 5 cm malfunctioned.

	15cm			10cm			5cm		
Replicate id	Pearson	R^2	RMSE	Pearson	R^2	RMSE	Pearson	R^2	RMSE
1016T1C1	0.98	0.96	0.82	0.99	0.99	0.65	>0.99	>0.99	0.65
1016T1C2	0.99	0.98	0.69	>0.99	>0.99	0.29	0.98	0.96	1.72
1016T1C3	0.99	0.98	0.64	0.99	0.99	0.65	0.99	0.97	1.51
1016T1C4	0.99	0.99	0.43	>0.99	0.99	0.45	0.97	0.94	1.53
1016T2C1	0.97	0.94	0.73	0.95	0.89	1.21	0.93	0.87	3.15
1017T1C1	>0.99	0.99	0.48	0.99	0.97	1.11	0.99	0.97	2.13
1017T1C2	0.99	0.99	0.50	0.98	0.96	1.83	>0.99	0.99	1.60
1017T1C3	>0.99	>0.99	0.30	0.98	0.96	1.31	0.99	0.98	1.50
1017T1C4	0.98	0.95	1.35	0.98	0.97	1.31	>0.99	0.99	1.13
1017T2C1	0.99	0.99	0.42	0.93	0.86	1.73	0.99	0.99	0.94
1018T1C1	0.98	0.95	0.92	0.98	0.96	1.35	0.96	0.93	2.73
1018T2C2	0.99	0.98	0.53	0.99	0.97	1.02	0.92	0.84	5.04
1018T1C3	0.99	0.97	0.79	0.98	0.96	1.11	0.97	0.94	2.01
1018T1C4	0.96	0.92	1.31	0.99	0.98	0.76	sensor malfunction		
1018T2C1	0.99	0.98	0.45	0.97	0.95	1.11	0.91	0.83	3.84
Mean	0.99	0.97	0.69	0.98	0.96	1.06	0.97	0.94	2.11
Stnd Error	<0.01	0.01	0.08	0.01	0.01	0.11	0.01	0.02	0.32

Table S4. The BFD parameters fit to paired thermocouple and iButton sensors using adjusted data. Each row is a different sensor pair. One thermocouple at 5 cm deep malfunctioned.

	InitTemp		MaxTemp		TimeAtMax		Shape	
Depth	Thermoc.	iButton	Thermoc.	iButton	Thermoc.	iButton	Thermoc.	iButton
5 cm	3.78	4.36	45.82	49.02	61.14	62.49	1.21	1.05
5 cm	5.38	5.08	44.10	39.18	49.65	55.27	1.19	1.08
5 cm	4.76	4.80	44.75	43.03	57.90	54.36	1.07	1.07
5 cm	4.64	5.10	30.21	27.44	64.83	74.12	1.02	0.93
5 cm	4.35	4.63	38.16	40.51	71.70	59.46	0.88	1.12
5 cm	3.65	5.32	50.22	56.16	80.17	74.05	0.81	0.72
5 cm	2.24	1.66	65.07	56.95	74.25	71.07	0.95	1.10
5 cm	3.93	2.62	42.85	38.84	79.87	75.82	0.89	1.10
5 cm	4.19	2.48	12.71	63.42	147.69	67.73	0.43	1.07
5 cm	4.78	4.74	37.80	38.24	78.08	75.06	0.73	0.82
5 cm	5.65	6.27	39.61	45.40	82.56	72.85	0.73	0.79
5 cm	8.76	6.35	51.10	52.27	57.18	70.15	0.72	0.82
5 cm	4.14	5.27	28.44	35.53	91.45	91.26	0.72	0.66
5 cm	NA	3.89	NA	32.17	NA	94.90	NA	0.65
5 cm	5.35	5.12	40.97	44.47	70.31	56.24	0.88	1.11
10 cm	3.73	4.08	24.19	22.60	102.45	100.32	0.78	0.80
10 cm	3.82	3.97	17.84	18.00	89.25	88.10	0.95	1.03
10 cm	3.63	4.21	18.49	17.95	100.00	92.36	0.79	0.90
10 cm	4.57	4.46	15.04	13.59	111.15	112.45	0.88	0.85
10 cm	2.34	3.86	18.86	18.91	71.30	91.16	1.79	0.98
10 cm	2.87	3.95	21.20	25.22	119.31	109.68	0.58	0.63
10 cm	3.58	3.91	27.96	28.09	120.49	107.86	0.59	0.71
10 cm	3.57	4.11	18.03	20.39	119.79	110.16	0.63	0.72
10 cm	3.20	3.64	28.20	29.12	97.07	104.48	1.01	0.73
10 cm	3.18	4.27	19.03	19.29	85.76	106.76	1.36	0.70
10 cm	2.24	4.36	22.64	22.25	106.73	104.63	0.80	0.72
10 cm	3.48	4.02	24.98	23.56	98.41	102.98	0.84	0.76
10 cm	4.36	4.53	17.87	17.40	106.88	120.85	0.87	0.62
10 cm	4.71	1.33	16.69	14.66	128.57	135.06	0.57	0.69
10 cm	4.08	4.16	22.19	20.08	86.95	92.47	0.97	0.95
15 cm	4.97	5.16	14.21	13.73	123.37	120.72	0.61	0.63
15 cm	5.24	4.95	12.03	12.14	114.04	103.89	0.59	0.87
15 cm	4.56	4.47	8.92	9.76	125.54	113.31	0.41	0.56
15 cm	4.36	5.12	7.56	8.94	123.48	127.85	0.45	0.61
15 cm	5.07	4.56	10.09	11.12	126.82	116.22	0.59	0.78
15 cm	4.46	4.69	11.85	13.19	144.39	137.93	0.48	0.49
15 cm	4.83	4.84	12.59	14.42	144.79	135.04	0.50	0.52
15 cm	4.53	4.28	10.78	10.74	142.34	136.85	0.43	0.53

15 cm	3.03	4.22	60.34	14.54	65.86	131.87	1.08	0.57
15 cm	4.12	5.06	10.33	11.41	139.67	130.23	0.58	0.57
15 cm	4.07	5.15	10.75	12.36	154.25	129.64	0.48	0.56
15 cm	0.45	5.02	9.62	13.08	156.92	125.42	0.96	0.60
15 cm	3.89	5.10	8.83	10.15	168.47	140.88	0.55	0.48
15 cm	3.04	3.87	9.21	9.61	199.74	151.61	0.42	0.56
15 cm	5.27	4.74	11.49	10.90	133.02	126.15	0.52	0.66

Supplementary S5. Case Study

Table S5. The BFD fit information from the SheFire model for A. the low fuel plot and B the high fuel plot. The table shows the BFD terms, root mean square error, and Pearson correlation coefficient for each soil depth measured. It also gives information about the time points to which the data set was trimmed, and the subsequent duration of the data set used to build the model.

A – low fuel (LF)	Depth	InitTemp	MaxTemp	TimeAtMax	Shape	RMSE	Pears.
Shallow - 5cm	5	25.63	34.03	259.82	1.16	0.55	0.98
Middle - 10cm	10	26.73	31.24	411.83	0.84	0.23	0.99
Deep - 15cm	15	27.60	30.10	556.60	0.65	0.15	0.98
Formula: Temp = InitTemp + (MaxTemp - InitTemp)e^(-z)							
z = (log(time) - log(TimeAtMax))^2 / ShapeConstant							
Real time conversion							
Start of data set used	08-02-18 15:53						
End of data set used	08-03-18 11:43		Time elapsed (min): 1190				
B – high fuel (HF)	Depth	InitTemp	MaxTemp	TimeAtMax	Shape	RMSE	Pears.
Shallow - 5cm	5	28.74	78.29	126.34	2.11	2.25	0.99
Middle - 10cm	10	30.38	52.81	260.11	1.62	1.19	0.98
Deep - 15cm	15	30.81	44.36	434.63	1.35	0.50	0.99
Formula: Temp = InitTemp + (MaxTemp - InitTemp)*e^(-z)							
z = (log(time) - log(TimeAtMax))^2 / ShapeConstant							
Real time conversion							
Start of data set used	7-30-18 17:29						
End of data set used	7-31-18 16:11		Time elapsed (min): 1362				

Table S6. The parameter-depth regression for A. the LF plot and B. the HF plot. The table shows the fit statistic (either R^2 or Pearson correlation coefficient) and its value, the regression equation, the shallowest soil depth that can be extrapolated by the model, and the time range covered by the model. The regression equations give the BFD parameter for soil depth x.

A – Low fuel plot (LF)			
Parameter	Statistic	Value	Equation
MaxTemp	R^2	0.99	e^(3.71+(-0.11*log(x)))
InitTemp	Pearson	>0.99	22.99*(x^--0.07)
TimeAtMax	R^2	>0.99	112.63+29.68*x

Shape	Pearson	>0.99	2.65*(x^-0.51)
Shallowest	0.001 cm	cannot extrapolate shallower	
StartTime	08-02-18 15:53	beginning of model time range	
EndTime	08-03-18 11:43	end of model time range	FullTime: 1190 min
B – High fuel plot (HF)			
Parameter	Statistic	Value	Equation
MaxTemp	R^2	>0.99	e^(5.19+(-0.52*log(x)))
InitTemp	Pearson	0.98	25.99*(x^--0.06)
TimeAtMax	R^2	0.99	-34.59+30.83*x
Shape	Pearson	>0.99	4.04*(x^-0.40)
Shallowest	1.1545 cm	cannot extrapolate shallower	
StartTime	7/30/18 17:29	beginning of model time range	
EndTime	7/31/18 16:11	end of model time range	FullTime: 1362 min

Table S7. Parameters of the rate process equation (Equation 7) for *C. nictitans* seeds and vascular cambium tissue. We extracted the *C. nictitans* thermal tolerance data from Martin et al. (1969) Figure 8 and fit the first-order rate process equation to them to estimate parameter values. Martin et al's data are times at fixed, elevated temperatures at which 100% seed mortality was first reached during heating trials. Vascular cambium cell survival is based on counts of dead and live cells based on vital staining (Dickinson and Johnson 2004). We assume that root vascular cambium has a similar heat tolerance to stem vascular cambium.

Example	Activation entropy - deltaS (J/mol*K)	Activation enthalpy - deltaH (J/mol)	Lower limit of relevant temperature range (C)	Source
Cassia seeds	112	147741	70	Martin, Cushwa, Miller (1969)
Aspen	665	312522	45	Dickinson and Johnson (2004)
Douglas fir	528	270036	45	Dickinson and Johnson (2004)

Supplementary Works Cited

Dickinson, M. B., and E. A. Johnson. 2004. Temperature-dependent rate models of vascular cambium cell mortality. Canadian Journal of Forest Research 34:546–559.

Martin, R. E., C. T. Cushwa, and R. L. Miller. 1969. Fire as a physical factor in wildland management. Proceedings Annual [9th] Tall Timbers Fire Ecology Conference. Tallahassee, FL. Tall Timbers Research, Inc., Tallahassee, FL.:271–288.

IV. Conclusions and future directions

Wildfires are a driving force shaping our landscapes. They can affect everything from plant community composition to soil characteristics and biogeochemical cycling (e.g., Giovannini et al. 1990, Neary et al. 2005, Knelman et al. 2015, Doerr et al. 2017, Alcañiz et al. 2018). Fires directly affect soils through the extent and duration of heating but also have indirect effects through processes including ash and char deposition. In this work I developed a new approach for measuring and modeling the direct effects of fires using SheFire and iStakes. I used an experimental setup to validate the model and to benchmark ibuttons against thermocouples. I also explored how N cycling is transformed by the combination of direct and indirect fire effects in the field. Using a novel dataset that included immediate pre- and postfire samples, I measured nitrogen availability and cycling through time across a range of fire severities.

I found that fire severity alone was not fully responsible for changes in soil N cycling after the fire. High soil water content and fire severity interacted to produce increased levels of N availability and cycling in the soil sampling location that burned compared to control locations. Additionally, the length of time that the soils had high water content was an important factor contributing to N cycling, which furthered the divergence between the fire severity categories: high and extreme severity sampling locations experienced increased N availability and cycling when soils were wet but could not sustain those rates with prolonged soil wetting unlike low severity sampling locations which had moderate rate increases but could sustain them. These results suggest that, in this system, N availability and cycling is driven by rain events and seasonal soil wetting after fires.

Although I found these intriguing patterns with N availability and cycling with soil moisture across varying levels of fire severity, there is room for expansion. This case study focused on a single fire and did not have extensive replication within fire severity. While the

patterns I found are strong in this situation, the data are not sufficient to generalize to other fires. Fire effects are variable both spatially and temporally (e.g., Neary et al. 2005, Certini 2005, Hanan et al. 2016, Alcañiz et al. 2018). It remains difficult to generalize all but the broadest strokes patterns from one fire to another.

1. Sampling design for unplanned wildfires

The sampling design employed in this study is promising. It provides a framework for measuring ephemeral shifts postfire as well as long term changes to N cycling. Including unburned control sites can enable researchers to tease seasonal effects apart from fire by season interactions—in other words, what would the temporal patterns be in the absence of fire. Although the fire behavior is uncontrolled, this study shows how prefire measurements and control areas enable researchers to study unplanned wildfires as effectively as they can study prescribed burns. Research has shown that unplanned wildfires and prescribed fires are not readily comparable (e.g., Alba et al. 2015, Price et al. 2018) so it is crucial that we find ways to study both as wildfire activity increases. Furthermore, because soil contains the largest terrestrial carbon (C) pool (Scharlemann et al. 2014), understanding how fire can influence soil biogeochemical processes, such as coupled C and N cycles, is critically important as fires become more frequent and/or more severe (Westerling et al. 2006, Schoennagel et al. 2017).

2. Modeling framework for soil temperatures and direct responses

SheFire is a modeling framework that successfully predicts temperatures over time for unmeasured soil depths. The survival response functions provide a valuable tool for quantifying the biological impacts of fire on soils. They also serve as an example for how we can model direct fire effects using temperature data. As our understanding of soil processes and fire induced soil transformations expands, SheFire provides a foundation for how to model these processes.

Traditionally, fire severity, either assessed on the ground or remotely from satellite imagery, has been used to categorize burned areas. However, using changes to aboveground vegetation and the soil surface to categorize fire effects is problematic (Smith et al. 2016). This is particularly true when studying soils because aboveground changes do not always scale linearly with belowground effects. But using soil temperatures offers a quantitative alternative. Although not a strictly controlled dose-response experiment, using soil temperatures, as opposed to fire severity, would address many of the concerns raised in (Smith et al. 2016) and other syntheses concerning how we measure fire intensity and fire effects. Although instrumenting large areas before fire is not currently feasible, shifting to categorizing fires by temperatures when it possible would be a good first step.

In this research, I originally planned to use soil temperatures, as opposed fire severity, to categorize and group sampling locations in the Walker Fire. Unfortunately, due to a few failed and missing sensors, there were not enough data. However, there is great potential for future work to describe soil heating using quantitative temperature estimates rather than more qualitative, less mechanistic assessments of fire severity. Currently, there are no consistent relationships between fire severity estimates and soil physical, chemical, and biological changes following fire. Moving from indirect, qualitative fire severity estimates to quantitative fire temperature/energy measurements will enable us to more mechanistically represent the processes that lead to such wide variation. Future work may find that, while soil effects do not closely follow aboveground fire severity, they may be tightly correlated with the soil temperatures during the fire. Any increase in our understanding of these processes helps us better predict fire effects and sustainably manage our fire-prone landscapes.

Works Cited

Alba, C., H. Skálová, K. F. McGregor, C. D'Antonio, and P. Pyšek. 2015. Native and exotic plant species respond differently to wildfire and prescribed fire as revealed by meta-analysis. Journal of Vegetation Science 26:102–113.

Alcañiz, M., L. Outeiro, M. Francos, and X. Úbeda. 2018. Effects of prescribed fires on soil properties: A review. Science of The Total Environment 613–614:944–957.

Certini, G. 2005. Effects of fire on properties of forest soils: a review. Oecologia 143:1–10.

Doerr, S., C. Santin, J. Reardon, J. Mataix-Solera, C. Stoof, R. Bryant, J. Miesel, and D. Badia. 2017. Soil heating during wildfires and prescribed burns: a global evaluation based on existing and new data 19:17957.

Giovannini, C., S. Lucchesi, and M. Giachetti. 1990. Effects of Heating on Some Chemical Parameters Related to Soil Fertility and Plant Growth. Soil Science 149:344–350.

Hanan, E. J., J. P. Schimel, K. Dowdy, and C. M. D'Antonio. 2016. Effects of substrate supply, pH, and char on net nitrogen mineralization and nitrification along a wildfire-structured age gradient in chaparral. Soil Biology and Biochemistry 95:87–99.

Knelman, J. E., E. B. Graham, N. A. Trahan, S. K. Schmidt, and D. R. Nemergut. 2015. Fire severity shapes plant colonization effects on bacterial community structure, microbial biomass, and soil enzyme activity in secondary succession of a burned forest. Soil Biology and Biochemistry 90:161–168.

Neary, D. G., K. C. Ryan, and L. F. DeBano. 2005. Wildland fire in ecosystems: effects of fire on soils and water. Gen. Tech. Rep. RMRS-GTR-42-vol.4. Ogden, UT: U.S. Department of Agriculture, Forest Service, Rocky Mountain Research Station. 250 p. 042.

Price, O. F., P. J. Purdam, G. J. Williamson, and D. M. J. S. Bowman. 2018. Comparing the height and area of wild and prescribed fire particle plumes in south-east Australia using weather radar. International Journal of Wildland Fire 27:525–537.

Scharlemann, J. P., E. V. Tanner, R. Hiederer, and V. Kapos. 2014. Global soil carbon: understanding and managing the largest terrestrial carbon pool. Carbon Management 5:81–91.

Schoennagel, T., J. K. Balch, H. Brenkert-Smith, P. E. Dennison, B. J. Harvey, M. A. Krawchuk, N. Mietkiewicz, P. Morgan, M. A. Moritz, R. Rasker, M. G. Turner, and C. Whitlock. 2017. Adapt to more wildfire in western North American forests as climate changes. Proceedings of the National Academy of Sciences 114:4582–4590.

Smith, A. M. S., A. M. Sparks, C. A. Kolden, J. T. Abatzoglou, A. F. Talhelm, D. M. Johnson, L. Boschetti, J. A. Lutz, K. G. Apostol, K. M. Yedinak, W. T. Tinkham, and R. J. Kremens. 2016. Towards a new paradigm in fire severity research using dose–response experiments. International Journal of Wildland Fire 25:158.

Westerling, A. L., H. G. Hidalgo, D. R. Cayan, and T. W. Swetnam. 2006. Warming and Earlier Spring Increase Western U.S. Forest Wildfire Activity. Science 313:940–943.